NUMERICAL STUDY OF GEOMETRY AND ROTATION DEPENDENCE ON THE FLOW IN LABYRINTH SEALS

A Thesis

by

VAMSHI KRISHNA YAMSANI

Submitted to the Office of Graduate Studies of
Texas A&M University
in partial fulfillment of the requirements for the degree of

MASTER OF SCIENCE

August 2011

Major Subject: Mechanical Engineering

NUMERICAL STUDY OF GEOMETRY AND ROTATION DEPENDENCE ON THE FLOW IN LABYRINTH SEALS

A Thesis

by

VAMSHI KRISHNA YAMSANI

Submitted to the Office of Graduate Studies of
Texas A&M University
in partial fulfillment of the requirements for the degree of

MASTER OF SCIENCE

Approved by:

Chair of Committee,	Gerald Morrison
Committee Members,	Je C. Han
	Hamn-Ching Chen
Head of Department,	Dennis O' Neal

August 2011

Major Subject: Mechanical Engineering

ABSTRACT

Numerical Study of Geometry and Rotation Dependence on the Flow in Labyrinth Seals.

(August 2011)

Vamshi Krishna Yamsani, B.Tech., Indian Institute of Technology Guwahati

Chair of Advisory Committee: Dr. Gerald Morrison

A computational study was conducted on the flow, both compressible and incompressible, in a labyrinth seal at various geometries and rotation rates. The computations were performed using the commercial software Fluent®, which solves the k-ε model to predict the flow field in the seal. Various clearance-pitch ratios were used to study the effect of clearance on the flow. The aspect ratio, which is defined as the pitch-height ratio was varied to study the influence of the depth of the cavity on the flow as a whole. These studies span a range of Taylor's number that is defined accordingly, while fixing the Reynolds number at 1000.

The effects of clearance, aspect ratio and rotational rates were studied using carry-over coefficient and discharge coefficient. It was observed that a secondary recirculation zone (SRZ) occurs inside a seal cavity above certain Taylor's number. This significantly changes the flow field in the seal and the cavity, which results in an increase in pressure drop across the seal for a given flow boundary condition. This formation of SRZ's was more evident in incompressible flow (water) and occurred at prohibitively high rotational speeds in case of air (compressible flow). It was also

observed that flow with teeth on rotor was characterized by SRZ's, while it is not the case with teeth on stator. A flow map which shows the onset and presence of SRZ's is presented.

The ratio of tangential velocity of the shaft to the average of the swirl velocity in a cavity at various geometries of the cavities is presented. They seemed to be decreasing with decreasing depth and followed a linear pattern with the aspect ratios of the cavity.

DEDICATION

Dedicated unto the feet of supreme Lord Krishna

ACKNOWLEDGEMENTS

My sincerest thanks go to Professor Gerald Morrison for his valuable time and suggestions during my association with him. As a guide and advisor, he has been exceptionally patient at times of need. I highly appreciate his suggestions about my future and career prospects.

My heart and soul are always with my parents, whose love has been of the highest motivation for my studies in the United States and India.

Never would this appreciation be meaningful without His blessings and I have no words to thank Lord Almighty, for His perennial shower of grace. I thank Lord Krishna.

I have inexplicable gratitude for the motivation this one person has provided without her words. Her intentions, all of them towards my best cause, I believe have guided me towards finishing this manuscript on time. I thank Lakshmi Srinivasan and will treasure her friendship for years to come.

NOMENCLATURE

c - Radial clearance, m

C_d-Discharge coefficient for a given tooth of a multi tooth labyrinth seal

D - Shaft diameter, m

h - Tooth height, m

s -Tooth pitch, m

w -Tooth width, m

x - Axial distance along seal, m

β -Divergence angle of jet, radians

γ - Kinetic energy carry over coefficient

ε - Dissipation of turbulent kinetic energy

κ -Turbulent kinetic energy

μ -Dynamic viscosity, Pa/s

ρ_i-Fluid density at seal inlet, kg/m^3

ρ_i-Fluid density at tooth inlet, kg/m^3

χ- Percentage of kinetic energy carried over

τ -Shear at the rotor-fluid interacting wall

TABLE OF CONTENTS

Page

LIST OF FIGURES

Page

Page

Page

LIST OF TABLES

1. INTRODUCTION

The labyrinth seal as described by Sneck [1], consists of a tortuous flow path between high and low pressure regions by means of a series of non-contacting restrictors (referred to as teeth) and separating chambers (referred to as cavities). This geometry produces flow frictions and turbulence which tend to dissipate the pressure energy of the fluid as it flows through the seal, thereby reducing the leakage. Mechanisms of leakage reduction in labyrinth seals include turbulence induced viscous losses, chamber vortex generation, flow stagnation losses, and flow streamline curvature. CFD simulations provide useful insight into the flow field details to help facilitate better physical understanding and improved seal design.

Labyrinth seals offer robust yet relatively simple design for manufacturing and are durable. A few other interesting seal types include the viscoseal (for relatively high viscous fluids) and the brush seal (limited by material properties). But, labyrinth seals offer superior usability in terms of low maintenance, negligible running torque, and reduced particle contamination. They are often used in high performance turbomachinery to seal shafts in pumps and between compressor or turbine stages in gas turbine engines. More importantly, they are used to control flow leakage between the turbine blade tips and the stator. The thermodynamics of labyrinth seals is quite well understood, but much remains to be learned about the basic fluid mechanics of seals.

_____

This thesis follows the style of Journal of Turbomachinery.

This is particularly true of the dissipative processes which convert kinetic energy to thermal energy within the labyrinth's chambers. Until this gap is filled, decisions regarding sizing of the chamber depth and width or pitch of the seal will continue to be made based upon rules of thumb or from an engineer's experience.

Leakage across labyrinth seals has a pronounced influence on the efficiency of high pressure centrifugal compressors. A proper evaluation of leakage in the design step is of key importance for predicting compressor overall efficiency and for achieving proper stage aerodynamic matching. Erroneous prediction of leakages produces a corresponding error in predicting absorbed power and leads to improper selection of the stage design flow coefficients. This in turn results in stage aerodynamic mismatching with further reduction of efficiency and surge margin. Thus the ability to predict leakage through labyrinth seals of a known geometry and also to aid the development of new seal designs with lower leakage rate is of inevitable importance for high performance turbomachinery.

Typical flow field in a straight-through labyrinth seal is shown in **Figure 1**. For a seal with teeth on stator, the lower part acts as a rotor that rotates with a certain frequency. For a seal operating with teeth on rotor, the geometry would look like a reflection about the horizontal. As can be observed from the figure, a certain portion of the jet entering each cavity impinges onto the side wall of the next tooth thereby recirculating that part of the fluid stream within the cavity. Flow in seals is characterized by the amount of recirculation, which is desirable from a designer's standpoint.

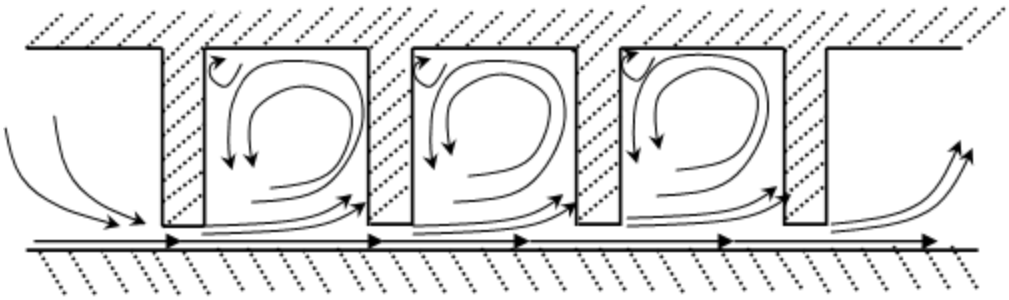

Figure 1. Typical flow in a straight-through labyrinth seal.

Most common types of labyrinth seals are straight-through, stepped, staggered, and radial. They are shown in **Figure 2**.

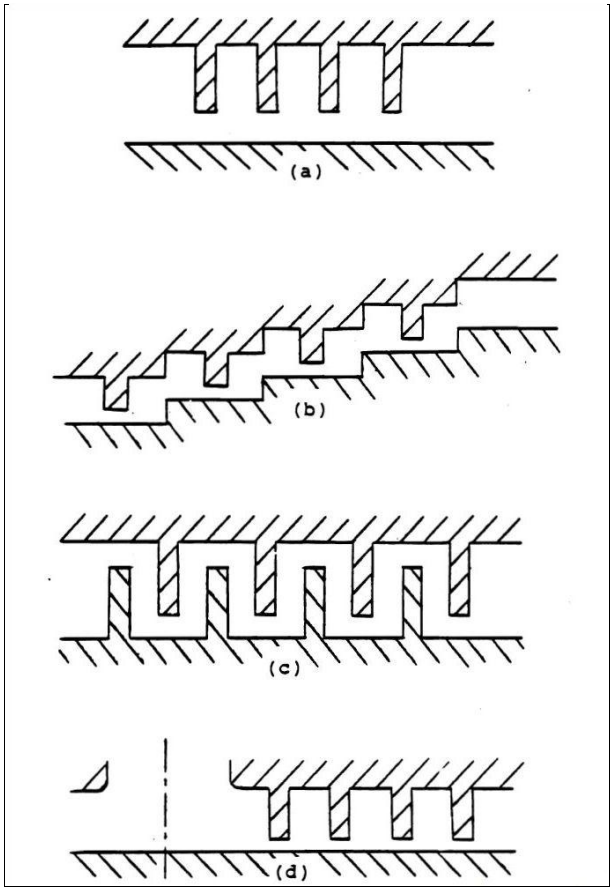

Figure 2. Types of labyrinth seals.

a) Straight-through, b) Stepped, c) Staggered, d) Radial

2. REVIEW OF PREVIOUS ANALYSES

This present work is an extension of the efforts performed before now for estimation of leakage flow in labyrinths. Leakage flow rate is dependent on the flow field in the seal, which are characterized by the flow coefficients. The flow coefficients essentially describe the kinetic energy dissipation through turbulent mixing in the seal cavity. The flow coefficients were first determined by Professor Martin [2] at the turn of 19th century. Although he did not recognize the need to determine the degree to which the kinetic energy is dissipated between the teeth, subsequent work by Egli [3], Hodkinson [4], Heffner [5] and Vermes [6] considered this very important phenomenon. This kinetic energy carry over is quantized in terms of a flow parameter commonly called Kinetic Energy Carry-Over Coefficient, γ.

The effect of flow parameters for labyrinth seals was studied in windback seals by G. L. Morrison and Adnan Al-Ghasem [7] and by G. L. Morrison and Saikishan [8]. They found that the carry over coefficient, γ, varied with flow parameters as well as geometry for labyrinth seals. This work proposes to further their study within a larger matrix of flow parameters and geometry specifications for straight-through labyrinth seals. It is also proposed to validate the existing results against a broader spectrum of sizes for labyrinth seals. In the present study, it is planned to do no analytical treatment of the flow pattern, but the idea is to derive flow parameters through the already existing CFD model (k-ε model) on Fluent and enable designers to have an idea of geometry effects for their design.

The carry-over coefficient is commonly represented as a function of clearance-pitch ratio [8] and in some cases also as a function of the seal's width-pitch ratio [6]. Heffner [5] and Jeri [9] thought that the optimum depth-pitch ratio is approximately unity although it has not been scientifically established. Benvenuti [10] deducted that an optimum number of throttlings exists for an imposed seal length and for given upstream conditions and the required expansion ratio. He proposed possible flow patterns for different throttling pitches and reasoned his explanation of reduction in flow resistance on the same. This present work also tries to establish solid results scientifically in this aspect. Various simulations will be performed to come to an optimum depth-pitch ratio.

A particularly useful quantification of the leakage in a seal is the discharge coefficient, C_d. This coefficient describes the ratio of the leakage mass flow rate to an ideal mass flow rate:

$$C_d = \frac{\dot{m}}{\dot{m}_{ideal}} \tag{1}$$

According to Waschka and Wittig [11], ideal mass flow is calculated for the compressible sub-critical flow using equation (2). The labyrinth clearance area is used as the cross sectional area of a hypothetical nozzle, and the seal overall pressure ratio as the nozzle pressure ratio.

$$\dot{m}_{ideal} = A_{cl}\left\{\frac{2k}{(k-1)} P_i \rho_i \left(\frac{P_e}{P_i}\right)^{\frac{2}{k}} \left[1 - \left(\frac{P_e}{P_i}\right)^{\frac{k-1}{k}}\right]\right\}^{1/2} \tag{2}$$

In the present study, C_d is defined as per equation (3)

$$C_d = \frac{\dot{m}}{A\sqrt{2\rho(P_i - P_e)}} \tag{3}$$

where P_i and P_e are the inlet and exit pressures. Hence, total pressure loss can be calculated if the discharge coefficient of each individual cavity in the seal is known and vice versa. Waschka and Wittig [12] studied the influence of rotational speeds on the discharge coefficients as a function of the Reynolds number. A large decrease of the discharge coefficient (by as much as 25%) toward higher rotational speeds is evident at low Reynolds number for seals with teeth on stator.

Most of the data collected for labyrinth seals and also the CFD studies involved pressure ratios close to 1.0 and lower Mach numbers. The present study aims at establishing the usability of the labyrinth seals at especially high rotational shaft speeds (until 350 m/s). Tangential speeds close to Mach number of 1.0 have never been tested [13], but promise a significant applicability in high performance turbomachinery. Previous studies by Rao and Narayanamurthi [14] were performed at rotational speeds from 0 to 1425 rpm. It is further shown by Benvenuti [10] that rotation affects leakage rates by as much as 10%.

A particular type of instability arises at high tangential speeds, which leads to a coupled system of vortices within the cavity. Such phenomenon was studied numerically by Demko[15] and experimentally verified by Johnson [16] for seals with tooth on rotor. The relative importance of swirl to axial momentum ratio was studied with various Taylor's numbers and Reynold's numbers. A flow map indicating the onset of this secondary recirculation zone (SRZ) was developed and it was found that the SRZ developed at very high ratios of Taylor number to Reynold's number. While Taylor vortices in annular gaps are caused by hydrodynamic instabilities, the origin of a secondary recirculation zone in the labyrinth cavity is due to the boundary conditions at

the rotor. Hence, the rotational effects are strongly dependent on seal geometry, especially the cavity design. The formation of SRZs is a desirable phenomenon, for it increases the pressure drop across a seal for a given leakage flow rate, and hence is a focus in the present study. It could be possible that the formation of SRZs at lower axial Reynold's number for various clearances might help significantly shed light on the physics of combined effects of axial inertia and viscous effects.

Since the design of a labyrinth seals is almost always a compromise between placing the greatest number of teeth in a given space and at the same time having the pitch distance between the teeth large enough to reduce the kinetic energy carry-over to a minimum, an efficient configuration can be attained only through the proper proportioning of all the dimensions at various rotational speeds. This effect should also be coupled with compressibility effects of the gas flowing through the seal. These effects do not seem to be considered together previously and this work presently attempts to do so. Until the chamber dissipation process is better understood, it is not possible to develop a rational basis for optimizing seal performance subject to the above discussed geometric and flow constraints.

3. RESEARCH OBJECTIVES

The objective of this work is to establish trends in the flow field of various labyrinth seals using CFD simulations in Fluent®. Since performing experiments on seals with such small clearances as in the present study is not only time consuming but also expensive, this work focuses on predictions based on CFD. Effect of change in aspect ratios with considerations to allow for more design options are of prime objective. This objective will be realized through the following:

1. Perform simulations of the flow field through a labyrinth seal of various geometries and rotational speeds.
2. Establish trends in the carry-over coefficients and discharge coefficients which describe the flow in the seal as a whole and the cavity in particular.
3. Study the effect of clearance that ranges from a 0.10 mm. to 1mm. on the flow parameters and give a design parameter for engineers.
4. Change the depth of the cavity to look at the formation of secondary recirculation zone, which is a desirable phenomenon in terms of decreasing the leakage across the seal.
5. Establish the significant improvement in performance in terms of increasing the pressure drop across a seal for a given flow leakage flow rate while running a shaft with teeth as compared to cases where there are teeth on stator.

6. Look at the ratios of shaft tangential speeds and the averaged swirl velocity of the fluid in the cavity for both tooth on stator and rotor. To study the differences in a compressible and incompressible flow.
7. Have a comparative study of flow in a labyrinth seal with teeth on rotor and a seal with teeth on stator by looking at the effects of rotational speeds of the rotor.
8. To look at the effect of the body force in driving the fluid to form secondary recirculation zone at various Taylor numbers.

4. COMPUTATIONAL METHOD

Turbulent flows are characterized by fluctuating velocity fields. These fluctuations mix transported quantities such as momentum and energy causing them to fluctuate as well. Since these fluctuations can be of small scale and high frequency, they are too computationally expensive to simulate directly in practical engineering calculations. Instead, the instantaneous (exact) governing equations can be time-averaged or otherwise modified to remove the small scales, resulting in a modified set of equations that are computationally less expensive to solve. However, the modified equations contain additional unknown variables, and turbulence models are needed to determine these variables in terms of known quantities. Here, standard k- ε turbulence model has been used because of its widespread applicability and simplicity in computing complex problems. Also, this model has been previously used to study the flow in labyrinth seals with established accuracy [8]. A further discussion on k- εmodel is given in appendix A and is explained in Fluent® manual [17].

ANSYS 12.0.16 version of Fluent is used to solve the model. A pressure based Navier-Stokes equation solver with finite volume discretization is used. The grid was adapted for resolving pressure gradients as shown in **Figure 3**.

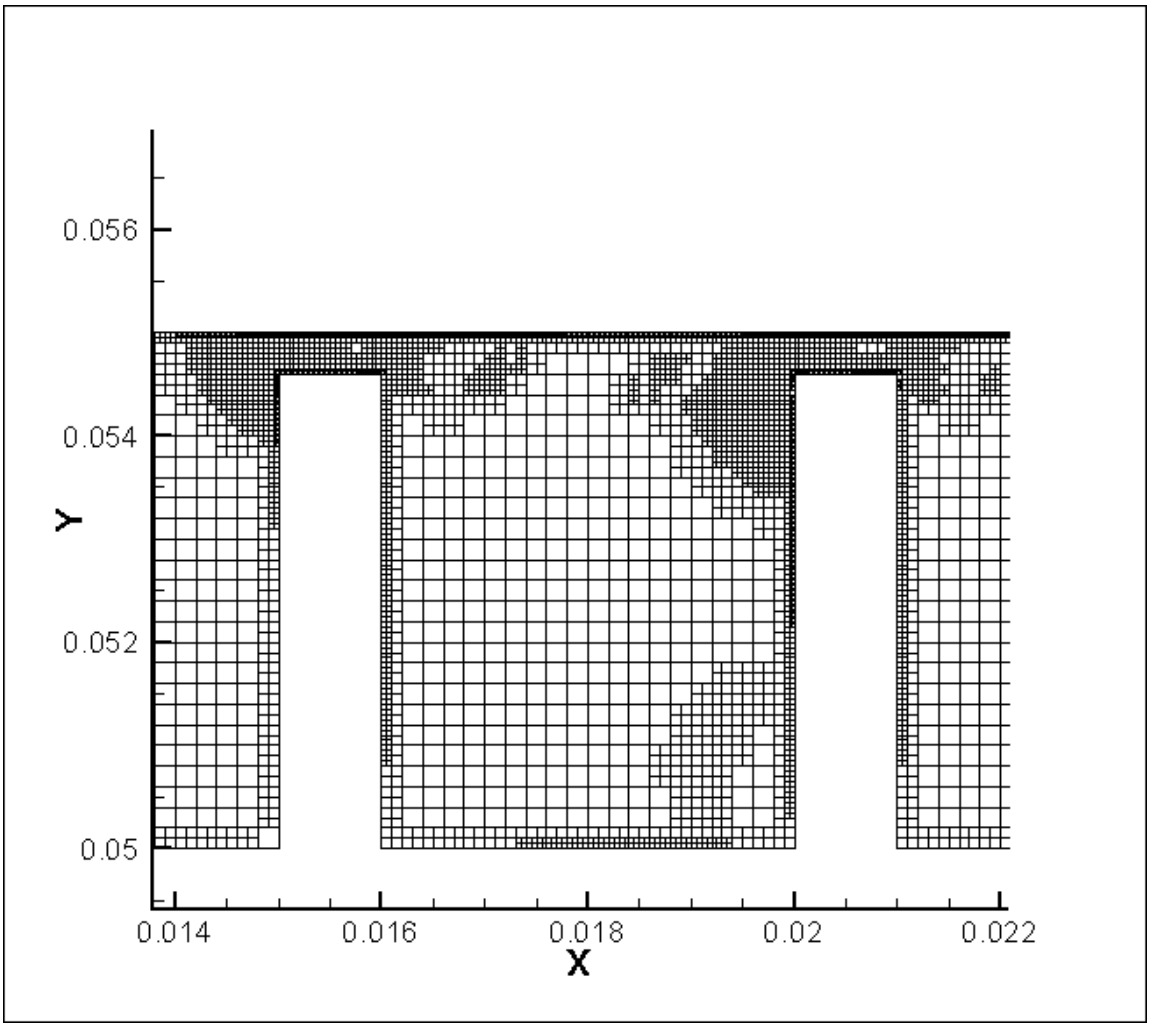

Figure 3. Mesh adaptation based on pressure gradient.

Morrison and Al-Ghasem [7] showed that for seal analyses, the enhanced wall treatment that is available in Fluent must be used to obtain accurate prediction of the flow field. Nodes have to be close to the walls at y^+ values less than 5 to resolve the laminar sublayer as shown in **Figure 4**. The entire grid was created in Gambit 2.4.6 using quad cells. The final mesh based on both pressure gradient adaptation and y^+ adaptation is finer under the tooth and near the walls, while it is coarser inside the seal cavity and in the long stretches of inlet and exit. The long entrance and exit regions

before and after the seal are present to allow the inlet and exit conditions to equilibrate before the flow enters the first cavity. In this present study, the inlet and exit lengths are taken to be 3 times and 6 times the height of the seal cavity respectively.

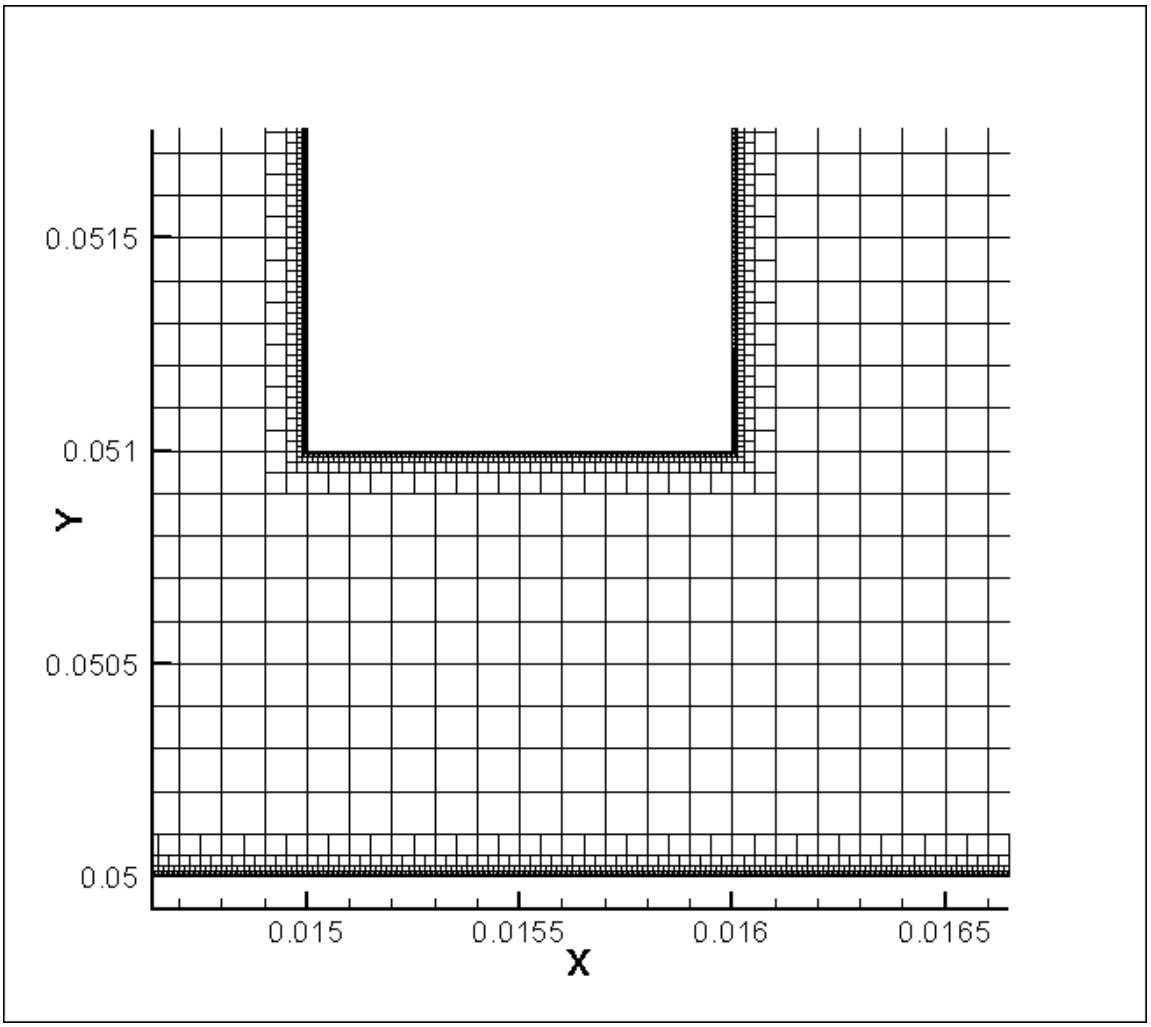

Figure 4. Mesh adaptation based on y^+ less than 5.

The geometry of the seal has dimensions whose diameter is 50 mm. with clearance of 0.1, 0.15, 0.2, 0.4, 0.6, 0.8 and 1 mm. The pitch of each seal is maintained at 5 mm, with the heights changing such that the pitch-height ratio is 0.5, 0.75, 1, 1.25,

1.5 and 2. The geometry and flow are assumed to by axisymmetric and hence a two dimensional simulation is used, along axial and radial directions. A sample flow domain for a case with teeth on rotor is shown in **Figure 5**.

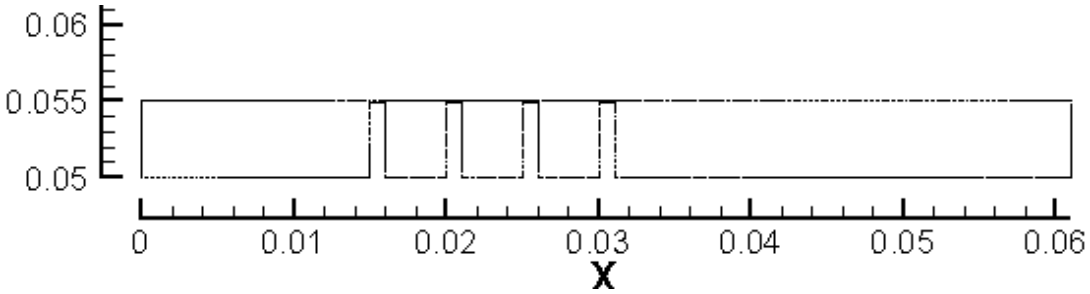

Figure 5. A typical labyrinth seal with teeth on rotor.

A grid independence study was performed by adapting the mesh with a suitable pressure gradient and also by refining the mesh close to the walls using the wall function adaptation with y^+ less than 5. Different pressure gradients were used and the pressure distribution on the surface of stator is plotted. When the pressure distribution did not change sufficiently with further refinement in the mesh, it is assumed that grid independence has been achieved. The results of this study are shown in **Figure 6**. From the figure, a pressure gradient of 10 is assumed best in terms of keeping the number of nodes low while achieving computation accuracy. Hence, for this study, a pressure gradient of 10 is adopted.

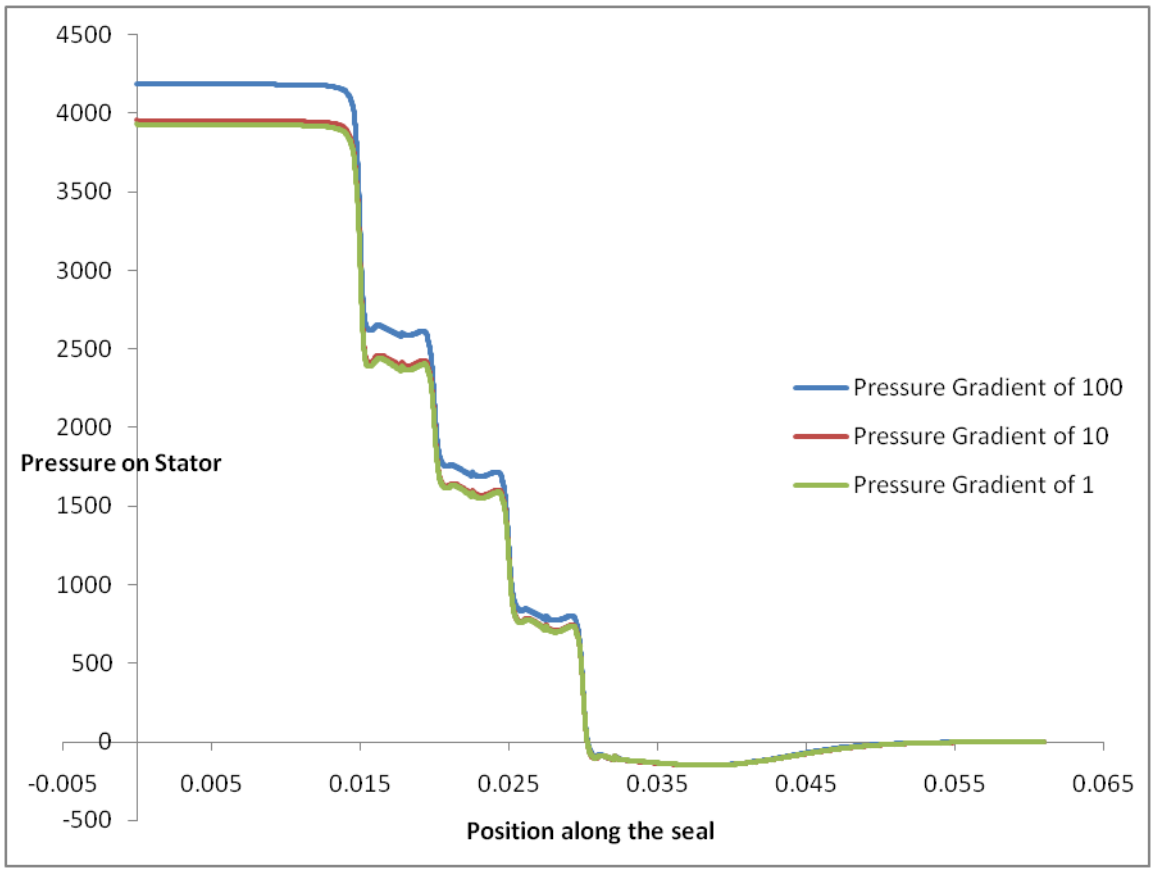

Figure 6. Pressure distribution on stator with various pressure gradients.

5. FLOW IN A SEAL WITH TEETH ON STATOR

Fluid flow in a labyrinth seal is characterized by axial and tangential velocity components. When a shaft rotates, it carries the fluid bound within a seal along with it imparting swirl to the fluid. The magnitude of swirl imparted to the fluid depends on its viscous nature together with its axial inertia. The fluid circulates within the cavity while moving forward as a whole causing dissipation of the energy and axial displacement of the fluid along when there is a favorable pressure gradient.

A typical labyrinth seal with teeth on stator is shown in **Figure 1**. Flow in a seal can be both compressible and incompressible depending on the fluid. In the present study, water is used to characterize an incompressible fluid and air is representative of a compressible fluid as discussed in further sections.

Hodkinson [4] defined the flow parameter carry-over coefficient, γ, which is a measure of a cavity's ability to dissipate energy. His definition is based on the divergence of the flow exiting from under the tooth into the cavity. The angle of divergence of the streamline, β, is obtained using the streamline that separates the flow in the cavity and the flow under the tooth. From this streamline, the carry-over coefficient, γ can be estimated as illustrated in **Figure 7**. Hodkinson provided the following relationships to calculate γ.

$$\gamma^2 = \frac{1}{1-\chi} \tag{4}$$

$$\tan\beta = \frac{1-\chi}{s\,\chi} \tag{5}$$

where, χ is the percentage of kinetic energy carried over. For 100% kinetic energy dissipation, $\gamma = 1$. It increases as the percentage of kinetic energy dissipated decreases.

Hodkinson's definition of γ assumed one major recirculation zone in the cavity as shown in **Figure 7**. This assumption is valid until rotor shaft speeds impart significant tangential velocities. This produces a body force which introduces a secondary recirculation zone as seen in **Figure 8**. This makes Hodkinson's definition of γ invalid. By this definition, carry-over coefficient cannot be less than unity. Since, it is difficult to define γ when there is no dividing streamline that separates the flow in the cavity from the flow under the tooth, γ is assumed as unity when the streamline is carried into the cavity due to centrifugal effects. For example, γ for each cavity in **Figure 8** is taken to be unity.

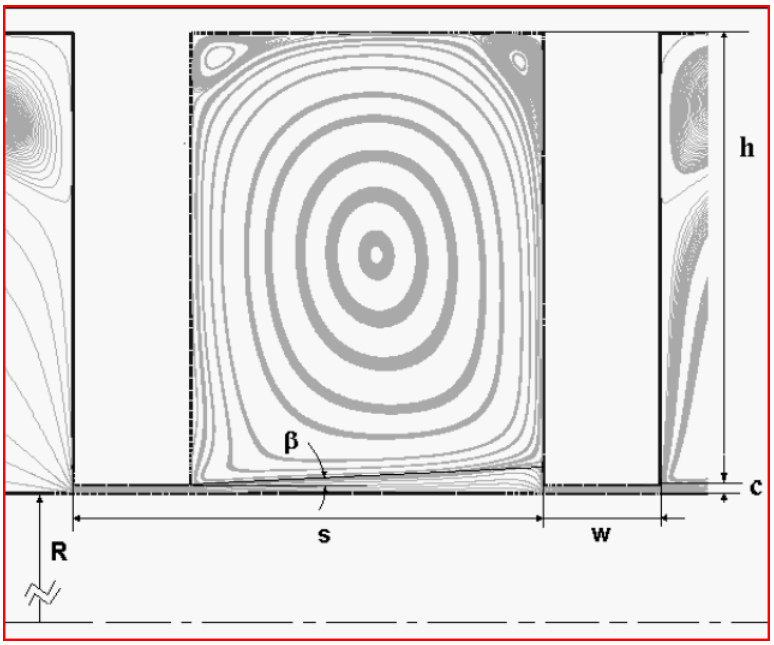

Figure 7. Determination of the angle β.

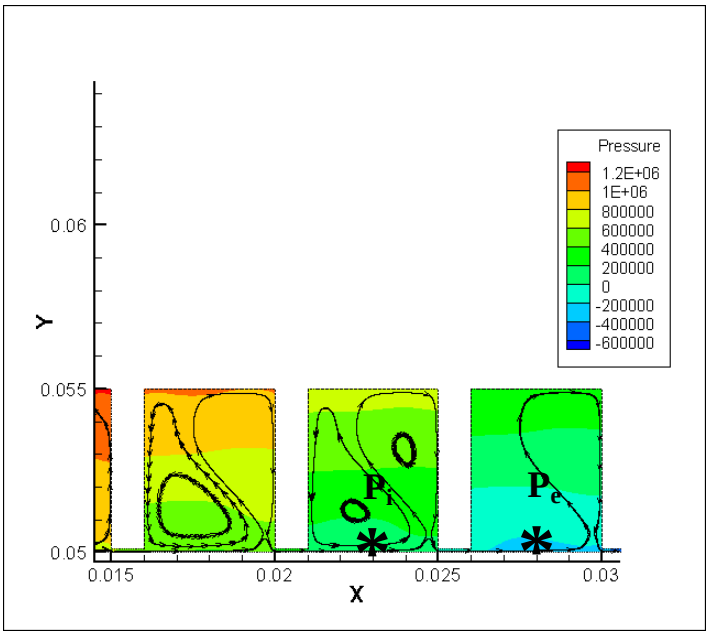

Figure 8. Typical flow in a seal with water as working fluid.

Another flow parameter, discharge coefficient (C_d), is a measure of the seal efficiency. The discharge coefficient describes the total losses that occur as the fluid flows through the cavity and under the tooth. It represents the combined effects of the dissipation in the cavity and the frictional losses that occur under the tooth and is defined as:

$$C_d = \frac{\dot{m}}{A\sqrt{2\rho(P_i - P_e)}} \tag{6}$$

where p_i and p_e are inlet and exit pressures across a tooth as shown in **Figure 8**. Therefore, by knowing the discharge coefficients of all the teeth in a seal one can calculate the leakage mass flow rate based on the overall pressure difference across the seal. It is also possible to calculate the pressure distribution across the seal. The smaller the value of C_d the more effective the seal is.

5.1 Incompressible Flow

This section emphasizes using an incompressible fluid such as water as the working fluid. The flow field in a seal is significantly different for the case of an incompressible fluid compared to a compressible fluid. Viscous forces are higher in this case compared to a compressible flow and its effect is pronounced in the streamline curvature and circulating zones in the cavity. The flow through the seal with water as working medium is shown in **Figure 8**.

5.1.1 Effect of clearance on flow parameters

The flow in a seal is understood by measuring the values of C_d and γ. To study the effect of clearance, the pitch and the tooth width of the seal are fixed at 5 mm. and 1 mm. respectively, while varying the clearance from 0.10 mm. to 1.0 mm. The shaft speeds were varied from 0 to 350 m/s in multiples of 50 m/s. **Figure 9** summarizes the effect of clearance and shaft speed on the streamline curvature in the cavity of a seal with teeth on stator.

Figure 9. Different streamlines with varying clearance for tooth on stator.

At low shaft speeds (until 150 m/s), it is observed that by increasing the c/s ratio from 0.02 to 0.2, there is transition from one recirculation zone to the formation of small secondary recirculation zone (SRZ) in the seal cavity. This transition to small SRZ's occurs at a c/s ratio of 0.04. Increasing the c/s ratio greater than 0.08 leads to larger SRZ's and subsequently to diverted flow SRZ's at very high c/s ratios (close to 0.20). The formation of vortices under the teeth is a significant observation with increasing clearance. Vortex formation under the teeth occurs at a critical c/s ratio of 0.08 for high shaft speeds. For clearances greater than this value, vortices under the teeth become stronger and decrease the effective clearance for the flow under the tooth. They also help the formation of diverted flow SRZ within the cavity by routing the flow into the cavity.

The effect of shaft speed on the streamline curvature is seen through the formation of SRZ's. At lower clearances, (c/s less than 0.04), increasing shaft speeds from 50 to 350 m/s causes a steady transition from one recirculation zone to smaller SRZ's and subsequently resulting in diverted flow SRZ's. For a medium range clearance (c/s = 0.04), the flow transition is unique with increasing shaft speed. The through flow is completely routed down into the cavity before a secondary recirculation zone can even be formed. This anomaly is seen in **Figure 10** with the difference in axial and swirl velocity being substantial. The clearance is large enough for the axial velocity to be low, while small enough to cause enough wall shear to rotate the fluid along with the rotor and imparting enough swirl to overcome axial momentum. At large clearances (c/s greater than 0.08), increasing shaft speed causes vortices under the teeth and hence leads to diverted flow secondary recirculation zones with a total split in the cavity.

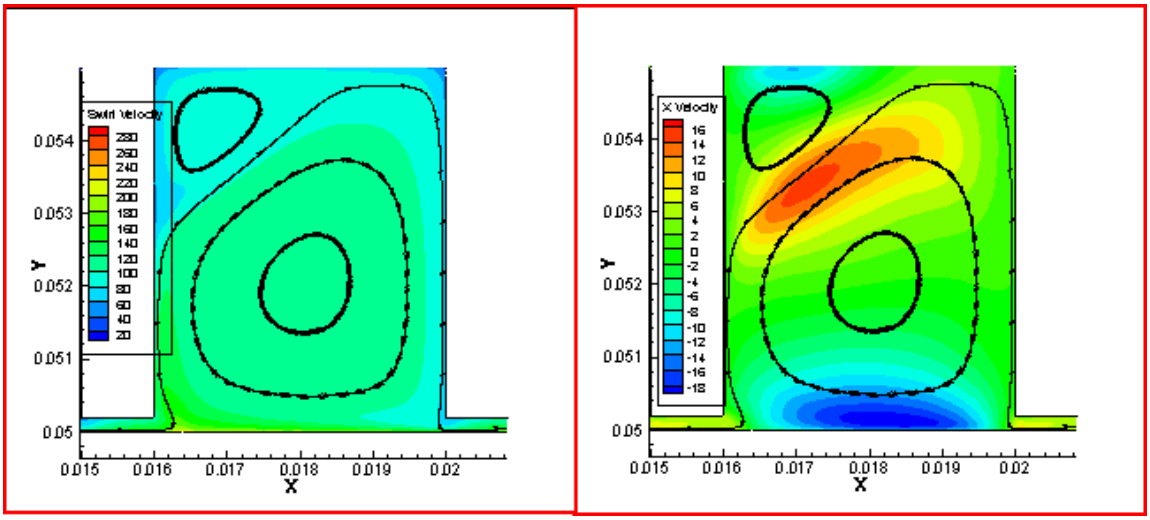

Figure 10. Unique flow structure at c/s ratio of 0.04; W_{sh} = 250 m/s.

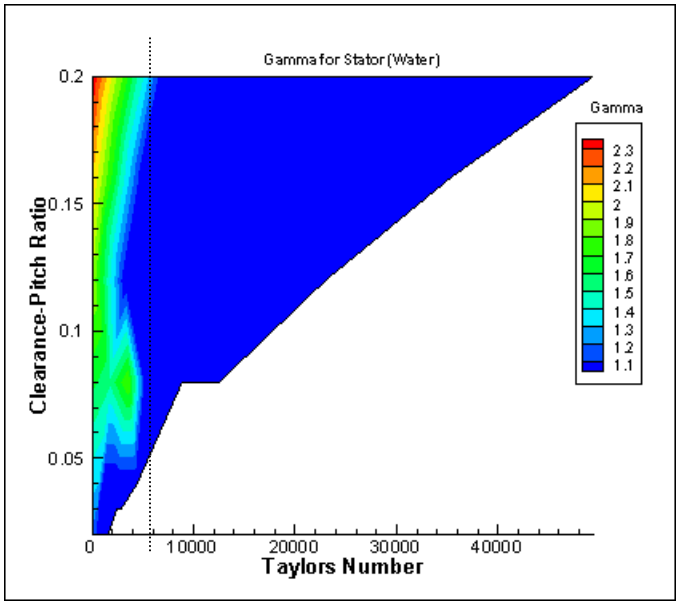

Figure 11. γ for various clearances and **Ta** for stator; incompressible flow.

Figure 53 in Appendix D shows the trends in carry-over coefficient of each cavity in a seal with increasing clearance which can be summarized in **Figure 11**. The figure shows that there are secondary recirculation zones at a Taylor number greater than

Table 1. Presence of SRZ's with tooth on stator for water at various clearances.

Clearance /height (mm)	**Shaft Speed (m/s)**							
	0	50	100	150	200	250	300	350
0.02	No	No	***S***	***L***	***L***	***L***	***L***	***D***
0.03	No	No	***L***	***L***	***L***	***L***	***D***	***D***
0.04	No	No	***L***	***L***	***R***	***R***	***R***	***D***
0.08	No	No	***L***	***D***	***D***	***D***	***D***	***D***
0.12	No	***L***	***L***	***D***	***D***	***D***	***D***	***D***
0.16	No	***D***	***D***	***D***	***D***	***D***	***D***	***D***
0.20	No	***D***	***D***	***D***	***D***	***D***	***D***	***D***

S - small SRZ; L - large SRZ; R-Reverse Pressure Gradient; D - Diverted Flow SRZ

600 regardless of the c/s ratio as indicated by $\gamma = 1$. For the regions where Hodkinson's definition for γ holds true, γ increases with c/s showing the turbulence dissipation inside the seal cavity decreases with increasing c/s. Increasing the shaft speed decreases γ for all values of c/s.

Table 1 summarizes the formation of SRZ's at various shaft speeds with varying clearance. These SRZ's can be either small, large or completely diverted into the cavity depending on the clearance and Taylor number as explained before. While there are no secondary recirculation zones with stationary shafts, increasing shaft speed causes vortex formation. At higher shaft speeds, the fluid gains swirl momentum and is routed into the cavity causing a diverted flow recirculation. It is observed that at higher clearances ($c/s > 0.12$), diverted flow is seen at even lower shaft speeds. For $c/s \leq 0.12$, a large vortex formation eventually leads to a diverted flow. At a critical clearance-pitch ratio of 0.04, large vortices lead to a reverse pressure gradient before forming a diverted flow and at lower clearances lower than $c/s = 0.04$, small vortices are formed before forming large vortices.

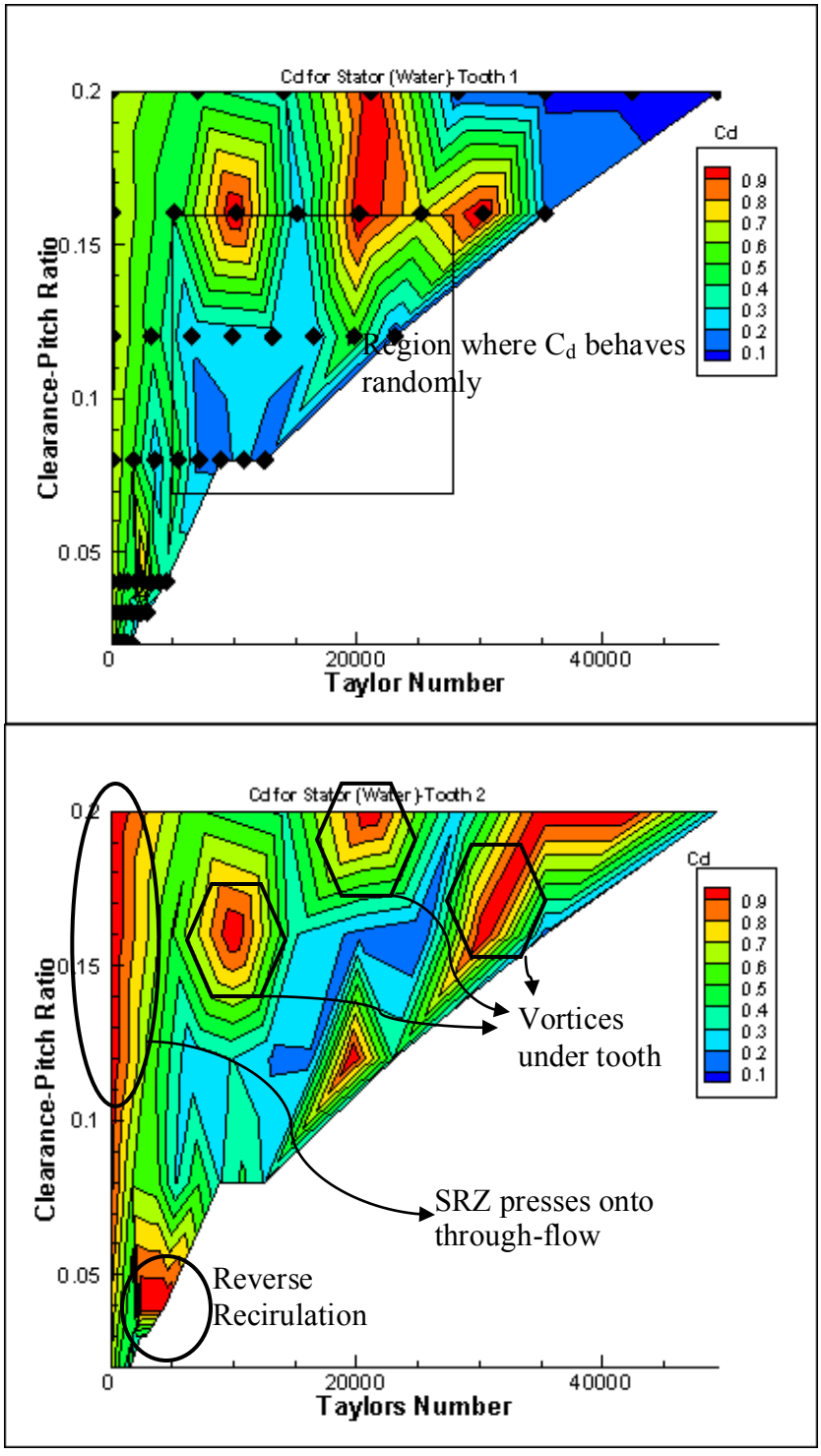

Figure 12. C_d in a stator for various clearances and **Ta**; incompressible flow; w = 1 mm, s = 5 mm, h = 5 mm.

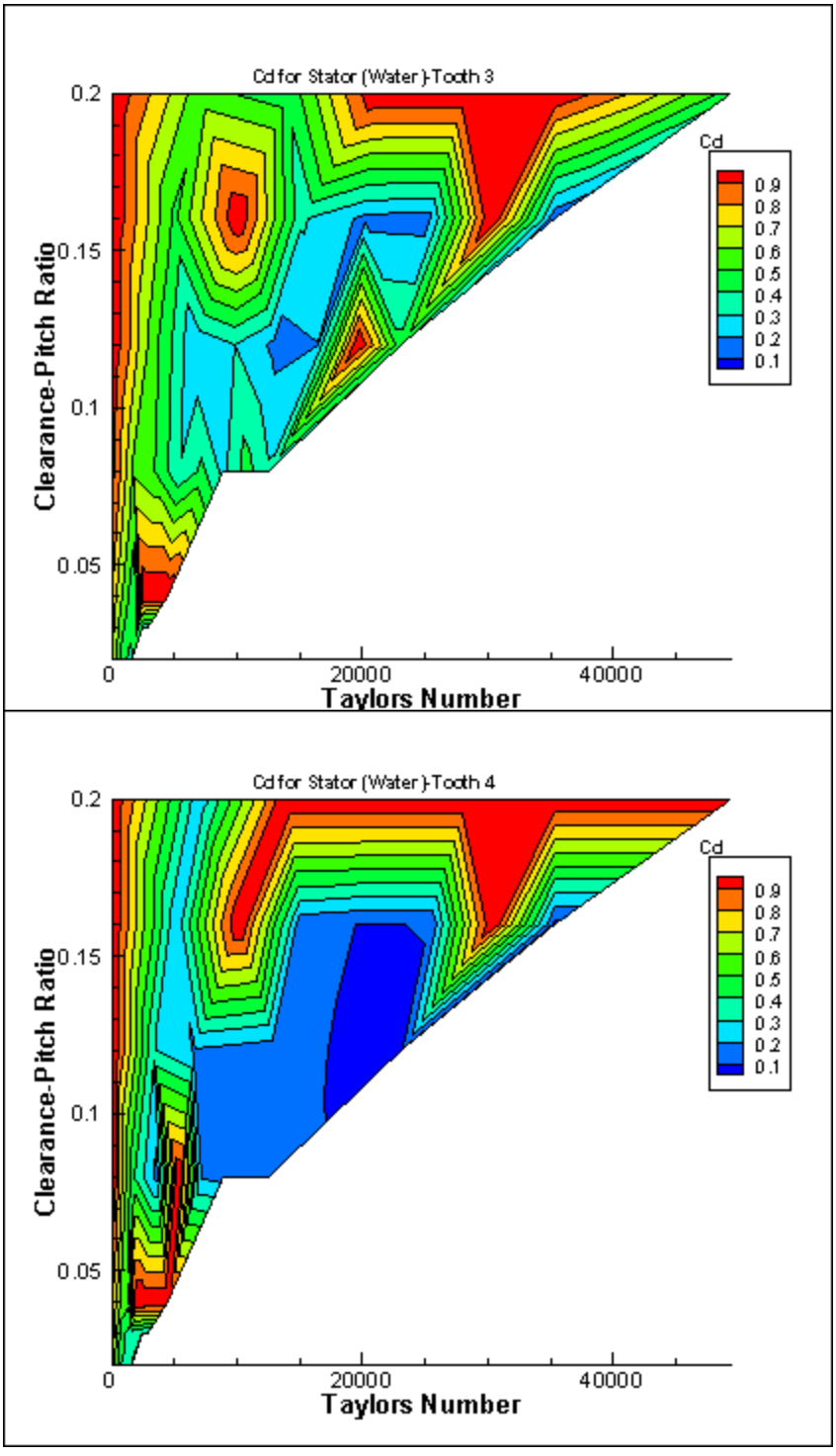

Figure 12. Continued.

The values of discharge coefficients are calculated for each tooth by measuring the inlet and exit pressure to the tooth. Appendix E contains **Figure 55** that relates the change in discharge coefficients with the change in clearance of the seal and are summarized as 2D contour plots in **Figure 12** for various teeth. The discharge coefficient values for the first tooth are different from the second and subsequent teeth values, as observed by Saikishan and others [8].

At zero shaft speed, the discharge coefficient increases from about 0.6 to 0.7 as c/s increases. The C_d value for the second, third and fourth teeth increases from 0.6 to 0.9 as c/s increases. Hence, the first tooth does more sealing than subsequent teeth for larger c/s. For really large c/s, flow is almost unaffected by subsequent teeth. This is due to the similarity in the flow structure at larger clearances at which, diverted recirculation zones are formed. These diverted SRZ's create a similar flow pattern for higher clearances leading to similar Cd values. With increasing clearance, in general, Cd increases although a clear relation between Cd and clearance does not seem to exist. A clearance of above 0.40 mm (c/s ratio of 0.08) results in the discharge coefficients behaving in a random manner. This fact is illustrated by the values of discharge coefficients in **Figure 12**. This result holds true even for air (to be observed in the next section) and has been predicted by Saikishan [8]. For this reason, he did not look at seals with a c/s ratio of greater than 0.04.

Figure 12 also sheds some light on the behavior of fluid flow at higher clearances and higher Taylors numbers. The C_d values are greatly influenced by the type of flow. A Taylors number of 500-600 is found to be the region where secondary recirculation zones occur regardless of c/s ratio. This is true for cases where c/s ratio is

less than 0.08. Such observation is backed by the γ values in **Figure 11**. But the same cannot be said in case of higher clearances, where there is formation of vortices under teeth and the flow pattern is completely different from that in lower clearance. At lower $c/s \leq 0.08$, for the first tooth, C_d decreases with increasing shaft speed. At higher c/s, C_d changes randomly with various shaft speeds. For $c/s \leq 0.08$, vortices under the tooth largely affect C_d values which are dependent on shaft speed. This can be understood with the formation of vortices under tooth as seen from **Figure 13** where areas demarking the formation of vortices under teeth have undesirably high values of C_d (shown with hexagonal demarcation). Incoherent behavior in C_d is also explained by the presence of these vortices.

The seal behaves inefficiently at higher clearances for smaller Taylor numbers. At smaller clearances, large Taylor numbers are seen to be adversely affecting the seal performance. While, there is a reverse pressure gradient within a seal at lower clearance (**Figure 10**), the recirculation zone presses onto the through flow at higher clearances. This protruding secondary flow reduces the effective clearance in a seal cavity and generates swirl momentum to cause diverted SRZ's (**Figure 13**).

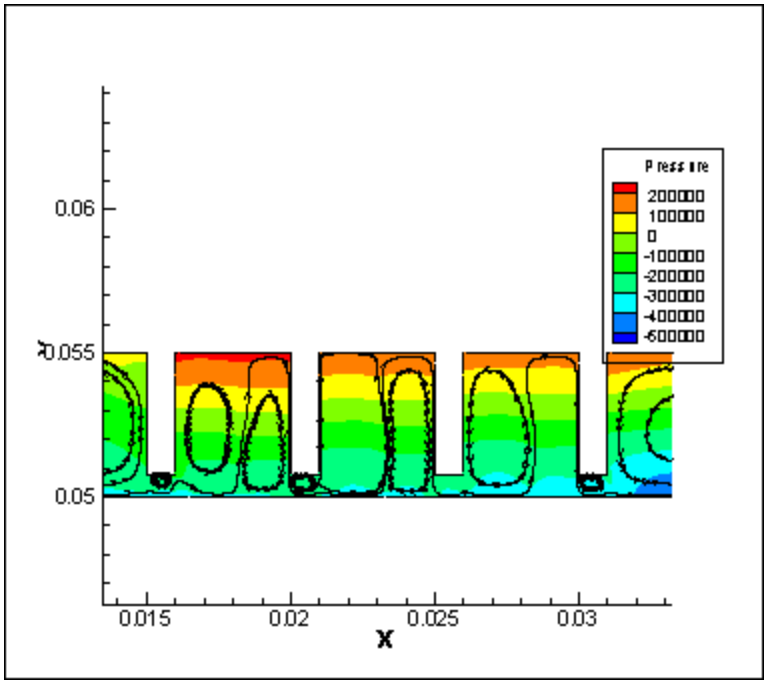

Figure 13. Formation of vortices under tooth for large clearance.

5.1.2 Effect of cavity depth on flow parameters

The influence of cavity depth is more pronounced in the case of incompressible fluid. **Figure 14** summarizes the effect of changing cavity depth on the streamline curvature in the cavity of the seal with teeth on stator.

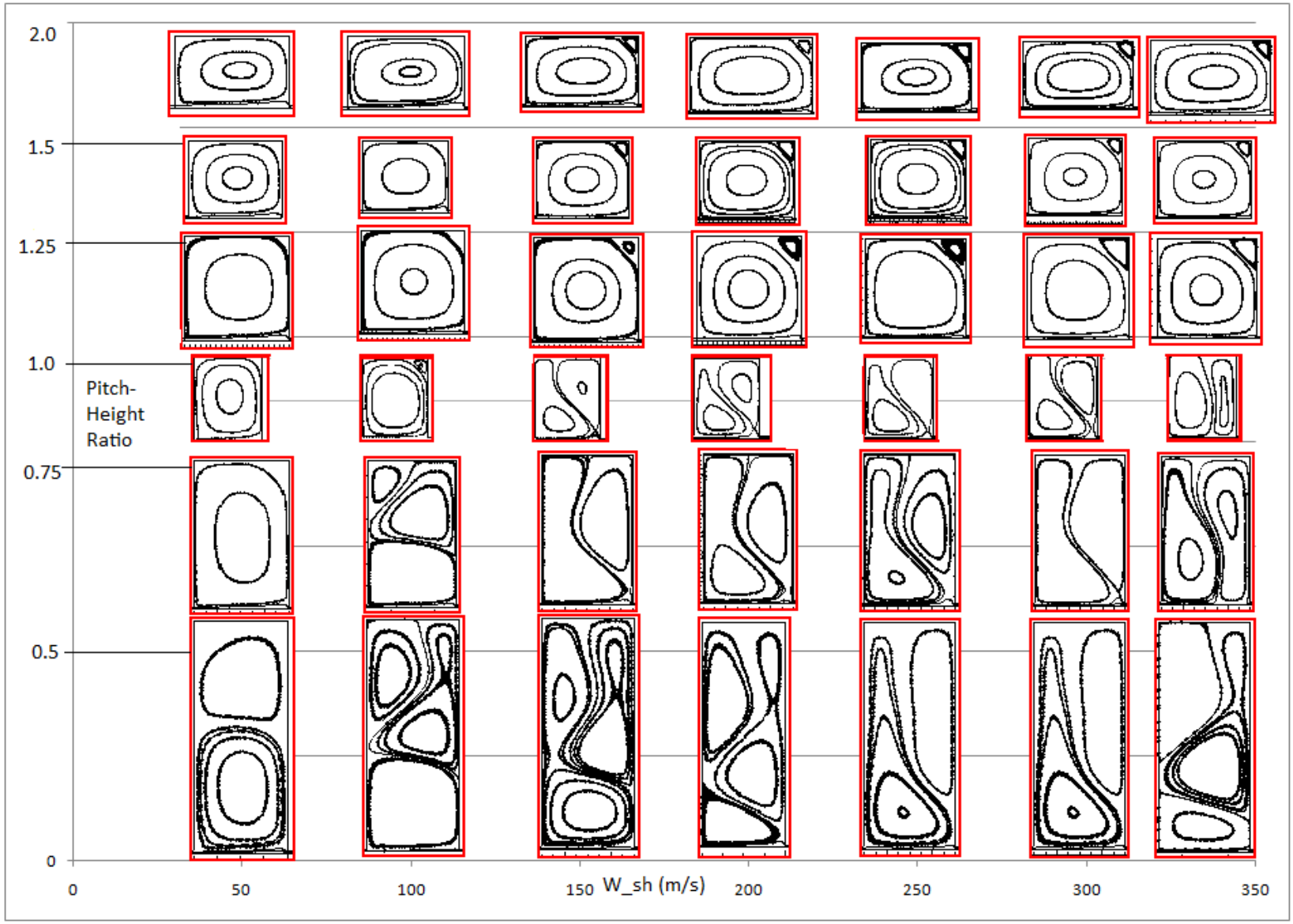

Figure 14. Streamlines with varying cavity depth for teeth on stator.

Figure 15 shows the carry over coefficients while **Figure 16** shows the discharge coefficients. **Figure 16** shows the values of C_d change from 0.65 at lower Taylor numbers to a lower value of 0.28 at higher Taylors numbers for all four teeth. This suggests better seal performance with increased shaft speed. This low C_d is caused by the large centrifugal body force generated at the higher shaft speeds which cause the through flow to be routed down into the cavity. Although the discharge coefficient, C_d, does not change with increasing cavity depth at a particular Taylors number (along the Y-axis of **Figure 16**), the contours of carry-over give some interesting results (**Figure 15**). At shallow cavities, the formation of SRZ's is not common and occurs with relatively high difficulty.

By increasing the cavity depth to a geometry where the cavity depth and pitch are nearly the same, there is a transition to the diverted secondary recirculation zones at Taylors numbers close to 500-600. Such formation is not observed for pitch-height > 1. As this pitch-height becomes lower than 1, the critical Taylors number at which large secondary vortices are formed is seen to be around 500 to 700. Hence, for deeper cavities, there is a total split for Ta ~ 500 to 700, while a transition to secondary vortices at slightly shallower cavities is observed. If the cavity is even shallower, then such **Ta** does not exist implying no such vortices. **Table 2** summarizes these effects while showing small, large and diverted flow SRZ's.

Table 2. Presence of SRZ's with tooth on stator for water at various cavity depths.

Pitch /height	Shaft Speed (m/s)							
	0	50	100	150	200	250	300	350
0.50	No	***S***	***L***	***L***	***L***	***L***	***L***	***L***
0.75	No	***S***	***L***	***L***	***L***	***L***	***D***	***D***
1.00	No	No	No	***L***	***L***	***L***	***L***	***D***
1.25	No	No	No	No	No	No	No	No
1.50	No	No	No	No	No	No	No	No
2.00	No	No	No	No	No	No	No	No

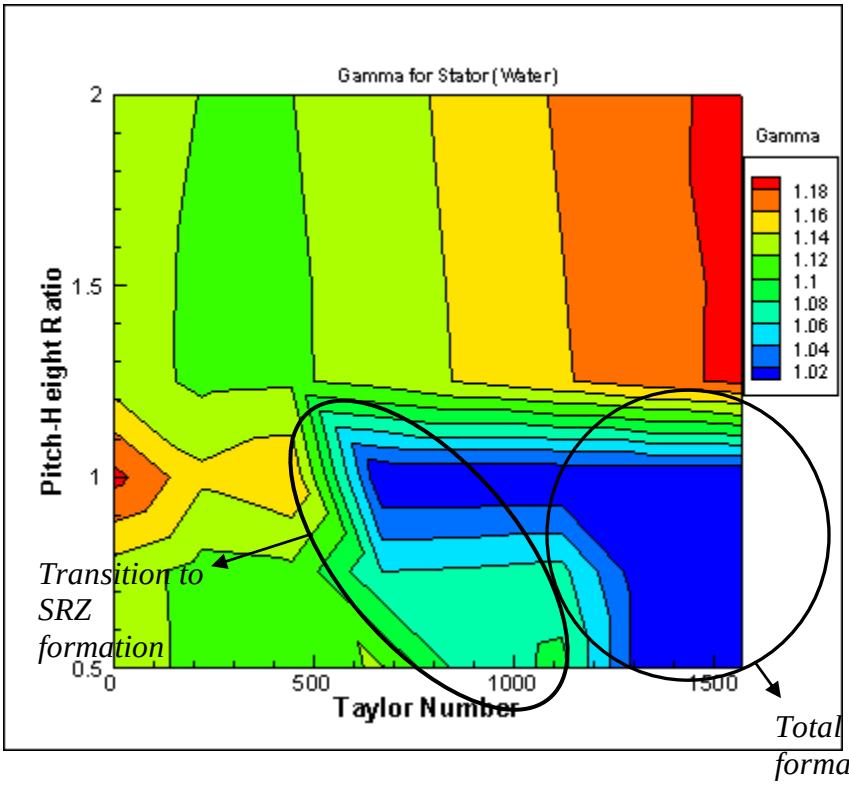

Figure 15. γ for various cavity depths and **Ta** for a stator; incompressible flow. c = 0.1 mm, s = 5mm, w = 1mm.

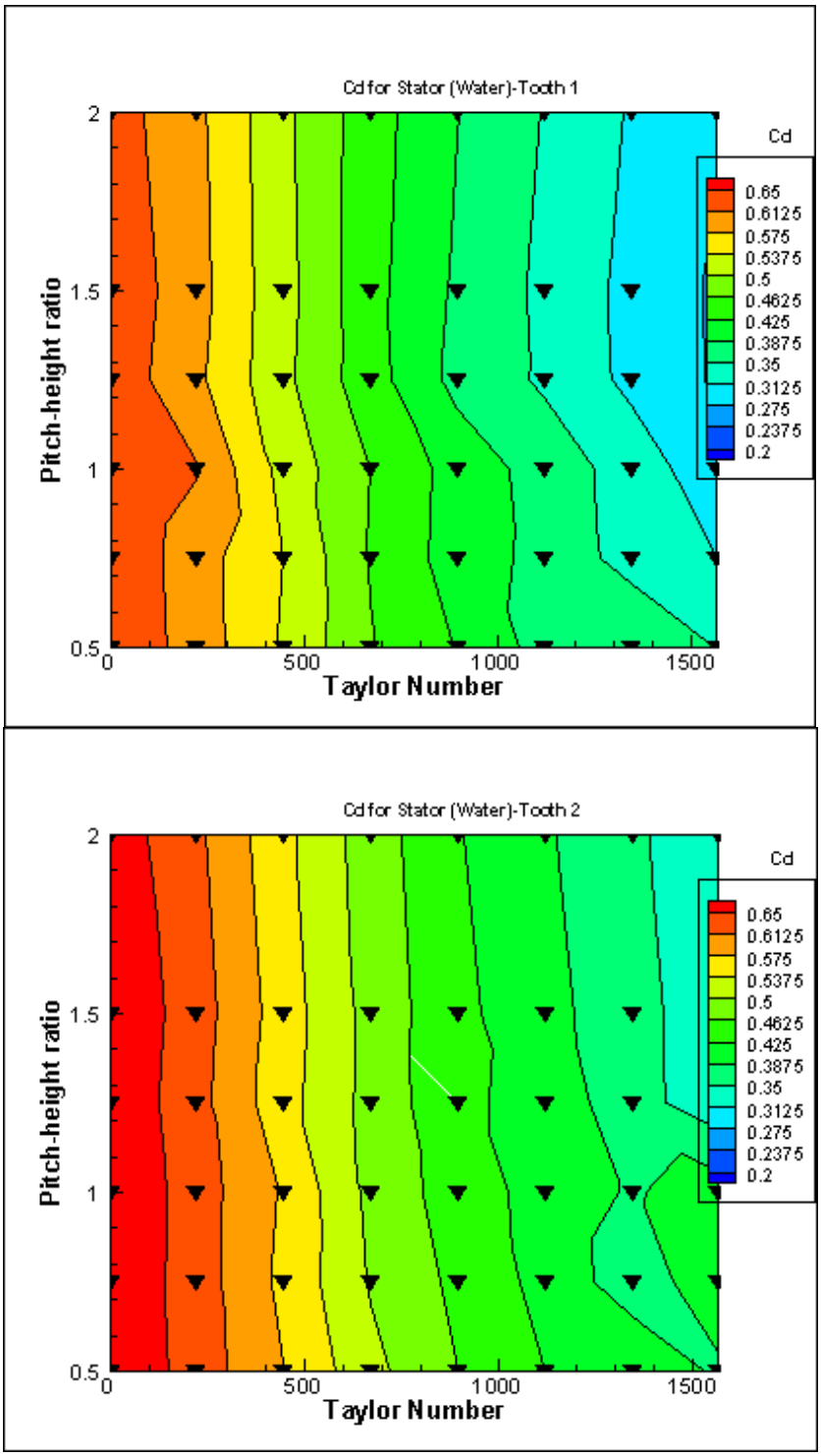

Figure 16. C_d for various cavity depths and **Ta** for stator; incompressible flow. c = 0.1 mm, w = 1 mm, s = 5mm.

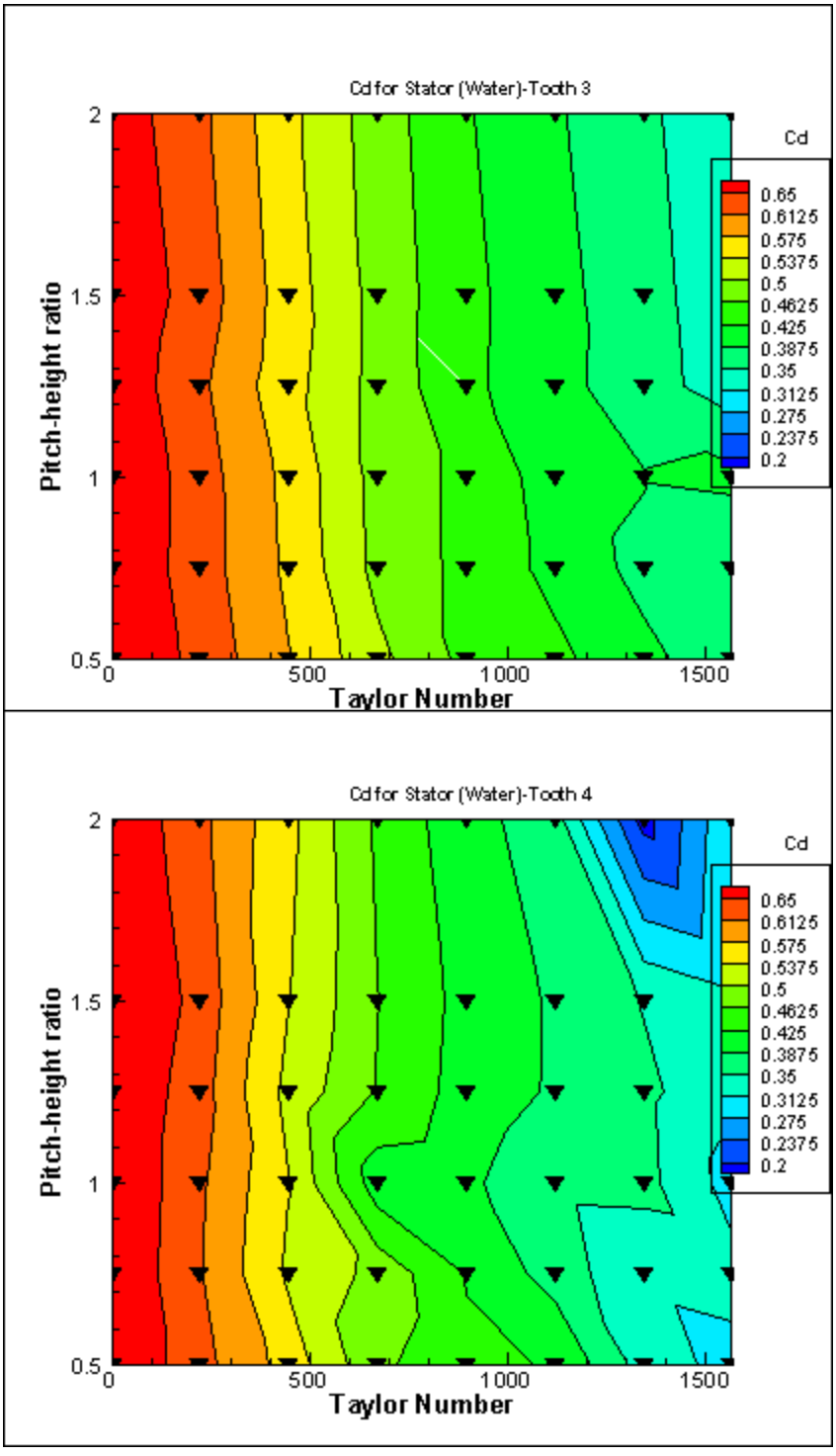

Figure 16. Continued.

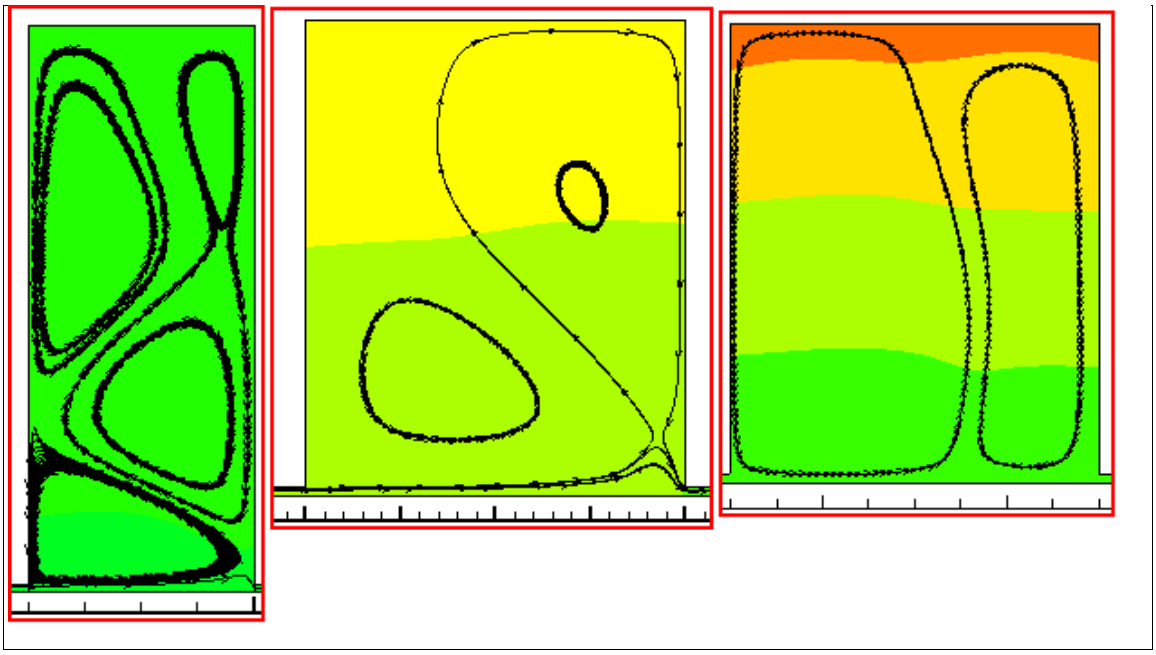

Figure 17. Different stages of SRZ's formation; No SRZ, large SRZ, diverted flow SRZ.

The difference in the formation of SRZ's is depicted in the **Figure 17**, where the secondary vortex does not exist in the first diagram, and is in the incipient stages in the second one, while it is completely formed in the last one. **Figure 16** shows that the discharge coefficient is not affected by any increase in cavity depth. This observation is similar to that observed for carry-over coefficient. For incompressible fluid with teeth on stator, cavity depth does not seem to be a critical design parameter. Though the formation of SRZ's is guided primarily by shaft speed, there is a difference in the way it is formed for a deeper cavity compared to a shallow cavity. The difference is pointed out in **Figure 18**.

For reference, **Table 3** shows the Taylors number values of the simulations performed and are taken to plot the 3D contour plots discussed earlier.

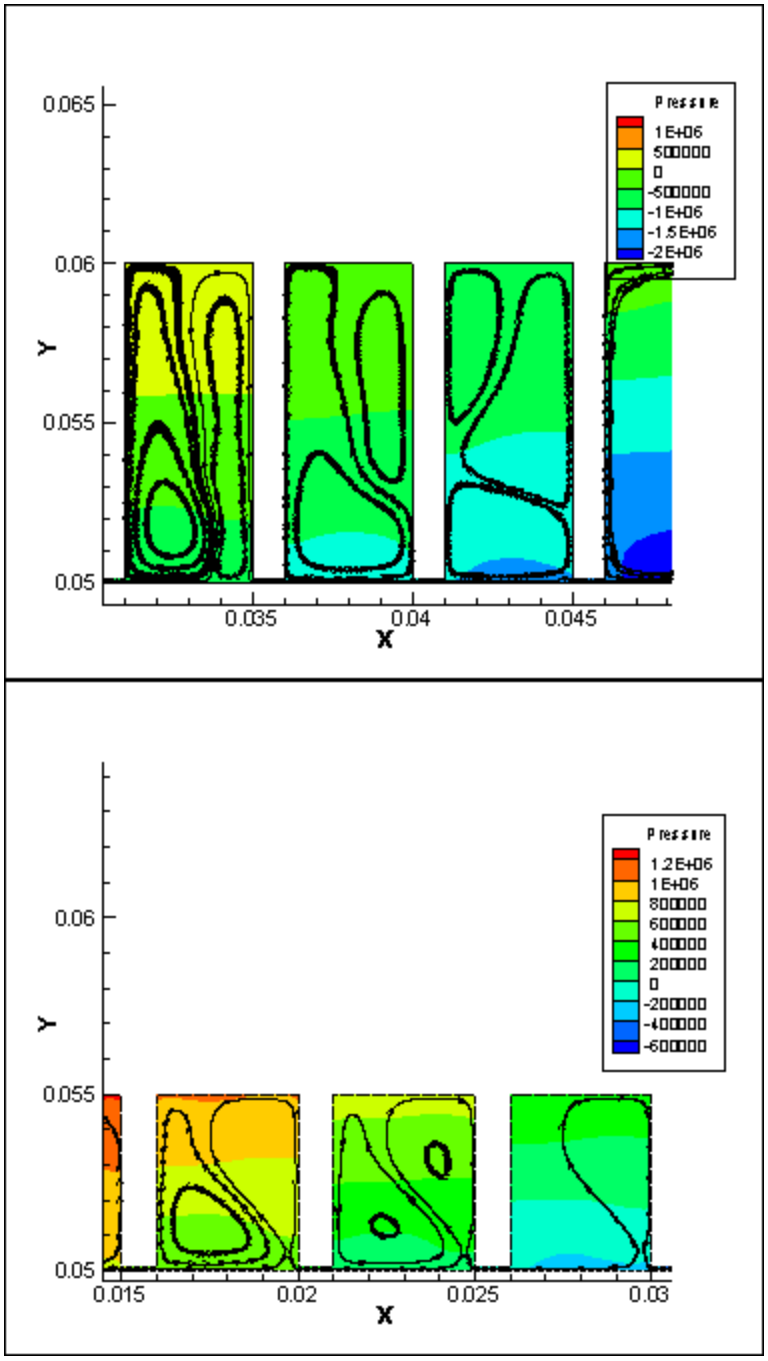

Figure 18. Difference in SRZ's for a deep and shallow cavity.

Table 3. Taylors numbers of the simulations performed for water.

Shaft Speed (m/s)	Clearance (mm)						
	0.1	**0.15**	**0.2**	**0.4**	**0.6**	**0.8**	**1**
0	0	0	0	0	0	0	0
50	224	411	632	1789	3286	5060	7071
100	447	822	1265	3578	6573	10119	14142
150	671	1232	1897	5367	9859	15179	21213
200	894	1643	2530	7155	13145	20239	28284
250	1118	2054	3162	8944	16432	25298	35355
300	1342	2465	3795	10733	19718	30358	42426
350	1565	2876	4427	12522	23004	35418	49497

5.2 Compressible Flow

This section emphasizes using a compressible fluid such as air as the working fluid. Flow through the seal with air as the working medium is shown in **Figure 19**. The effects of compressibility become evident at high rotational speeds of the shaft as evidenced by pressure difference across the seal. The centrifugal force of the fluid builds up as the flow moves downstream into the third cavity where the flow profile is different from that in the first cavity. This can be understood from **Figure 19** where the distribution of swirl velocity is different from that in the first cavity. The distribution of swirl velocity in the final cavity is more uniform since the fluid at this point in the seal has been subjected to more centrifugal forces than the fluid upstream the seal.

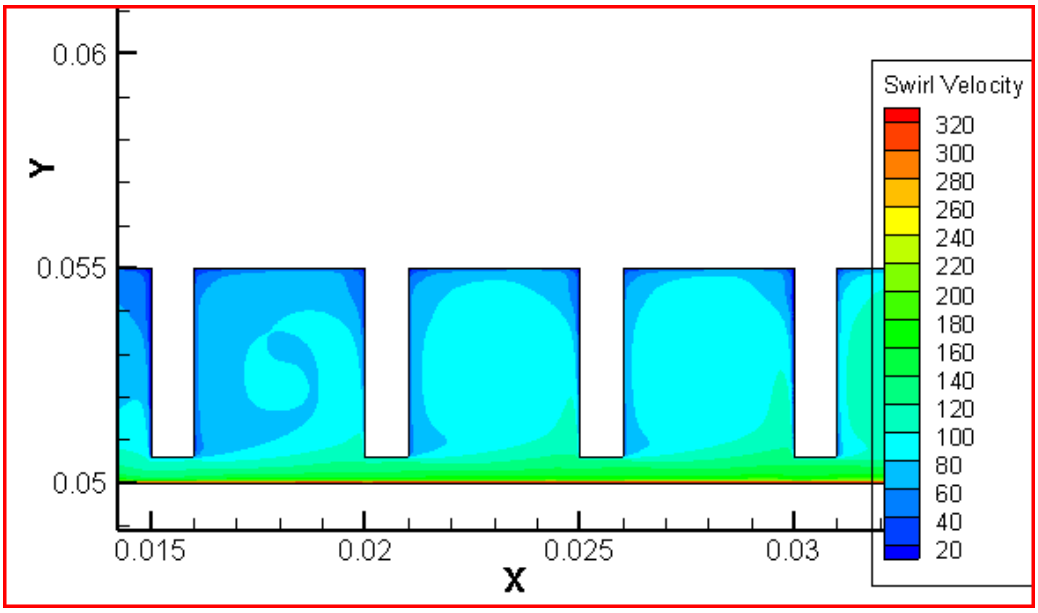

Figure 19. Compressible flow showing swirl velocity in seal with teeth on stator, c = 0.6 mm, w = 1mm, s = 5mm, h = 5mm; W_{sh} =200 m/s.

The Taylor number relates swirl inertia and viscous effects as well as geometrical parameters dealing with the flow curvature. For flow in labyrinth seals, the Taylor number is defined as:

$$Ta = \frac{W_{sh} c}{\gamma} \left(\frac{c}{r_{sh}}\right)^{1/2} \tag{7}$$

A particular type of flow instability arises at high Taylor numbers which is characterized by a system of torroidal eddies, commonly referred to as Taylor vortices, that circulate between the shaft and rotor. Taylor vortices are found in both laminar and turbulent flows, with or without an imposed axial flow[18]. It was found that when swirl was large compared to the axial flow, a second vortex develops in the cavity. In the case of a labyrinth seal, this is a desirable phenomenon since it significantly increases the pressure drop across a cavity. **Table 4** shows that there are no secondary recirculation zones while the fluid is compressible even at shaft speeds as high as 350 m/s. It is to be

noted that this shaft speed corresponds to a Mach number close to 1. Hence, in terms of eddy dissipation within a cavity, a compressible fluid does not fare well. This behavior is contrasted with that of an incompressible fluid, water, where SRZs are more common. This is due to the fact that the viscosity of air, μ_{air} is ~$2x10^{-5}$ Pa.s. while μ_{water} is ~10^{-3} Pa.s. Water is 100 times more viscous than air, which leads to higher viscous dissipation for a seal with water as the working medium. The absence of SRZ's for air can be explained by comparing the scales of the body forces generated for water and air. Air is 1000 times less dense than water. Hence the body force generated within the cavity of a seal, $\frac{\rho u_\theta^2}{r}$ is a 1000 times lesser in the case of a seal with air compared to that of a seal with water. **Table 3** and **Table 5** show the Taylor numbers of the various Taylors numbers at which simulations were performed.

Table 4. Absence of Secondary Recirculation Zones (SRZ) with tooth on stator and air.

Pitch/height	Shaft Speed (m/s)							
	0	**50**	**100**	**150**	**200**	**250**	**300**	**350**
0.5	No	No	No	No	No	No	No	No
0.75	No	No	No	No	No	No	No	No
1	No	No	No	No	No	No	No	No
1.25	No	No	No	No	No	No	No	No
1.5	No	No	No	No	No	No	No	No
2	No	No	No	No	No	No	No	No

Clearance (mm)	Shaft Speed (m/s)							
	0	**50**	**100**	**150**	**200**	**250**	**300**	**350**
0.10	No	No	No	No	No	No	No	No
0.15	No	No	No	No	No	No	No	No
0.2	No	No	No	No	No	No	No	No
0.4	No	No	No	No	No	No	No	No
0.6	No	No	No	No	No	No	No	No
0.8	No	No	No	No	No	No	No	No
1	No	No	No	No	No	No	No	No

Table 5. Taylors numbers of the simulations performed for air.

Shaft Speed (m/s)	Clearance (mm)						
	0.1	**0.15**	**0.2**	**0.4**	**0.6**	**0.8**	**1**
0	0	0	0	0	0	0	0
50	11	21	32	89	164	253	354
100	22	41	63	179	329	506	707
150	34	62	95	268	493	759	1061
200	45	82	126	358	657	1012	1414
250	56	103	158	447	822	1265	1768
300	67	123	190	537	986	1518	2121
350	78	144	221	626	1150	1771	2475

5.2.1 Effect of clearance on flow parameters

A number of simulations have been performed with a seal whose pitch is fixed at 5mm. To study the effect of clearance, other geometric parameters such as tooth height (of 5mm.) and width (of 1mm.) are fixed. Appendix B to F present the CFD results for γ and C_d as a series of 2D plots. These data are presented in 3D graphs in this section which present the overall results more clearly. The nomenclature of **Figure 49** in Appendix B as [5s1h1w0.40c] represents a seal with pitch of 5 mm, pitch-height ratio of 1, width of 1 mm and a clearance of 0.40 mm. The clearance is varied from 0.1 mm to 1mm while considering various rotational speeds of the shaft ranging from 0 to 350 m/s for a fixed Reynolds number of 1,000. **Figure 51** in Appendix C shows the trends in the change in discharge coefficients with change in clearance. The flow field in a seal and its cavities can be understood better by analyzing both the flow parameters (γ and C_d) simultaneously.

All the X-Y plots in **Figure 49** (Appendix B) that show variation of γ can be summarized in a 3-D contour plot in **Figure 20**. The plot systematically shows how the fluid flow is influenced with increase in clearance-pitch ratio for a fixed Reynolds number of 1,000.

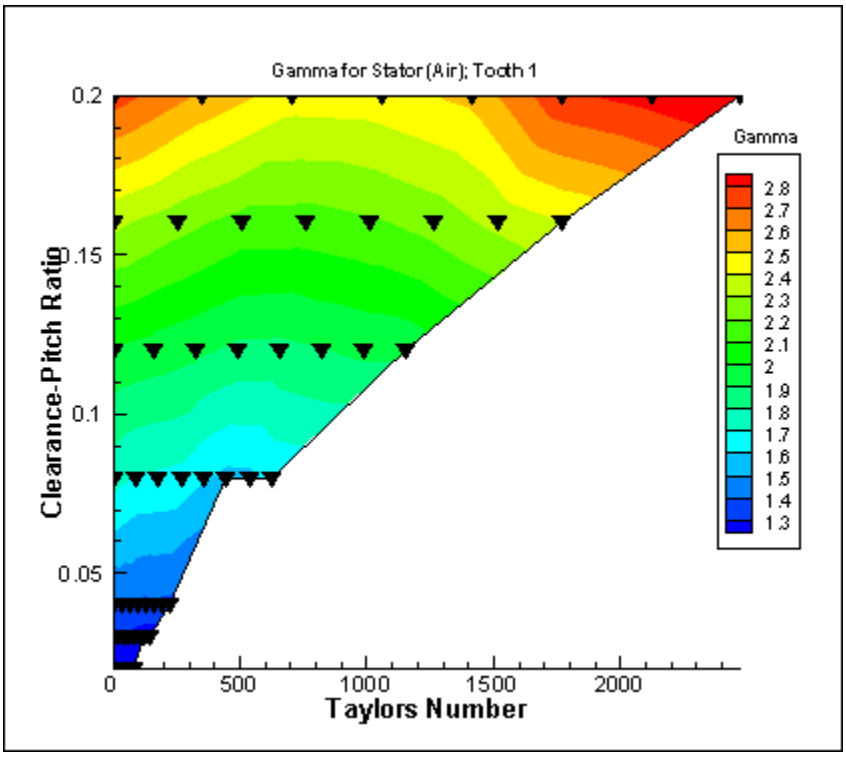

Figure 20. γ in a stator for various clearances and **Ta** in compressible flow. s = 5 mm, w = 1 mm, h = 5 mm,

The carry over coefficient increases as the clearance is increased, changing from $\gamma = 1.3$ for a c/s ratio of 0.02 to $\gamma = 2.9$ for c/s = 0.2. There is minimal Taylor number dependence for this tooth on stator seal. Thus, the energy dissipated in the seal decreases with increasing c/s. **Figure 21** presents streamlines with axial velocity (u_x) and swirl velocity (u_θ) contours for a large clearance. The flow tends to pass straight through the seal as indicated by the large values of γ. The axial velocity is of the order of 25 m/s while the swirl velocity is significantly higher at 320 m/s. This large difference causes the vortex in the cavity to press down on the fluid flow under the tooth causing the fluid to pass over without being pulled into the cavity. This behavior is responsible for the increase in carry-over coefficients (values greater than 2.5).

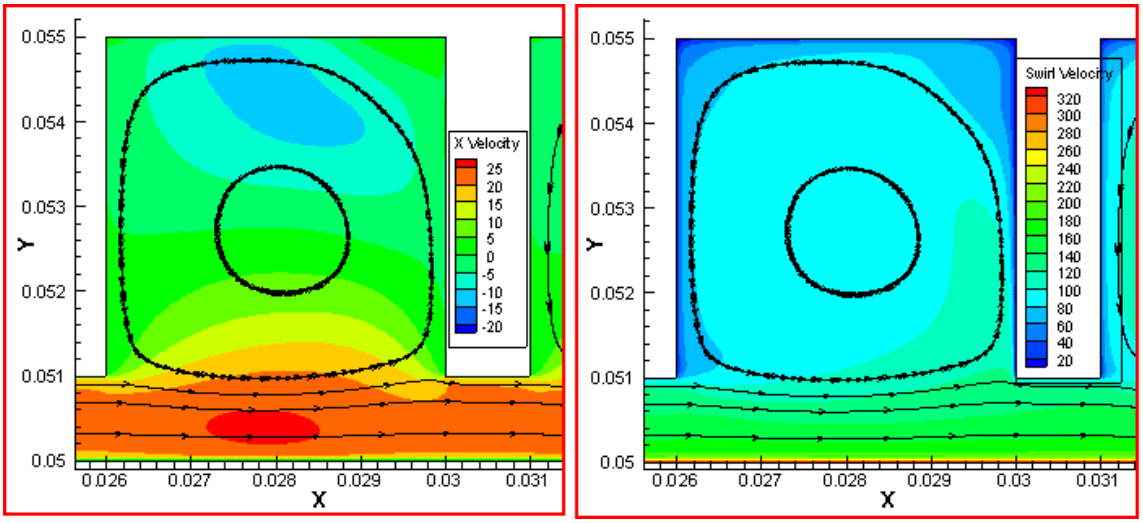

Figure 21. Axial and swirl velocity distribution in a seal with W_{sh} = 350 m/s; c/s = 0.20.

The discharge coefficient values, C_d is different for the first tooth compared to the subsequent teeth (**Figure 22**). These results are plotted in 2D plots in **Figure 51** in Appendix C which are represented in a 3D plot in **Figure 23**. For the first tooth, C_d increases from 0.6 to 0.74 as clearance increases from c/s of 0.02 to 0.20, showing that its sealing efficiency decreases with increasing clearance. The first tooth has lower C_d values compared to the subsequent teeth at all clearances suggesting that the first tooth does more sealing than the rest of the teeth. Also, the dependence of the first tooth C_d values on the Taylors number is minimal compared to that of teeth 2, 3 and 4 implying that the seal performance remains the same at all shaft speeds.

The sealing performance of teeth 2, 3 and 4 is very similar and is evident from similar values of C_d. These teeth have larger values of C_d (~1) at c/s $\geq$ 0.08. This is a critical clearance-pitch ratio as observed by Saikishan and others [8]. These teeth perform better at higher Taylors numbers regardless of the c/s ratio as suggested from the decreasing values of C_d. This holds true for even larger c/s values ($\geq$ 0.08) where C_d decreases to lower than 1 at higher shaft speeds greater than 250 m/s. Such behavior is in contrast with the first tooth performance which performs the same at all shaft speeds.

Hence, it is not desirable to use a seal with teeth on stator for a clearance-pitch ratio greater than 0.08 for compressible flow at lower Taylors number. This critical c/s ratio is in close agreement with Saikishan's work [8] which predicts inefficient design of seal with c/s greater than 0.04. Low clearances perform relatively better at even higher Taylors numbers as seen from the contour plots where there is uniform C_d and γ distribution.

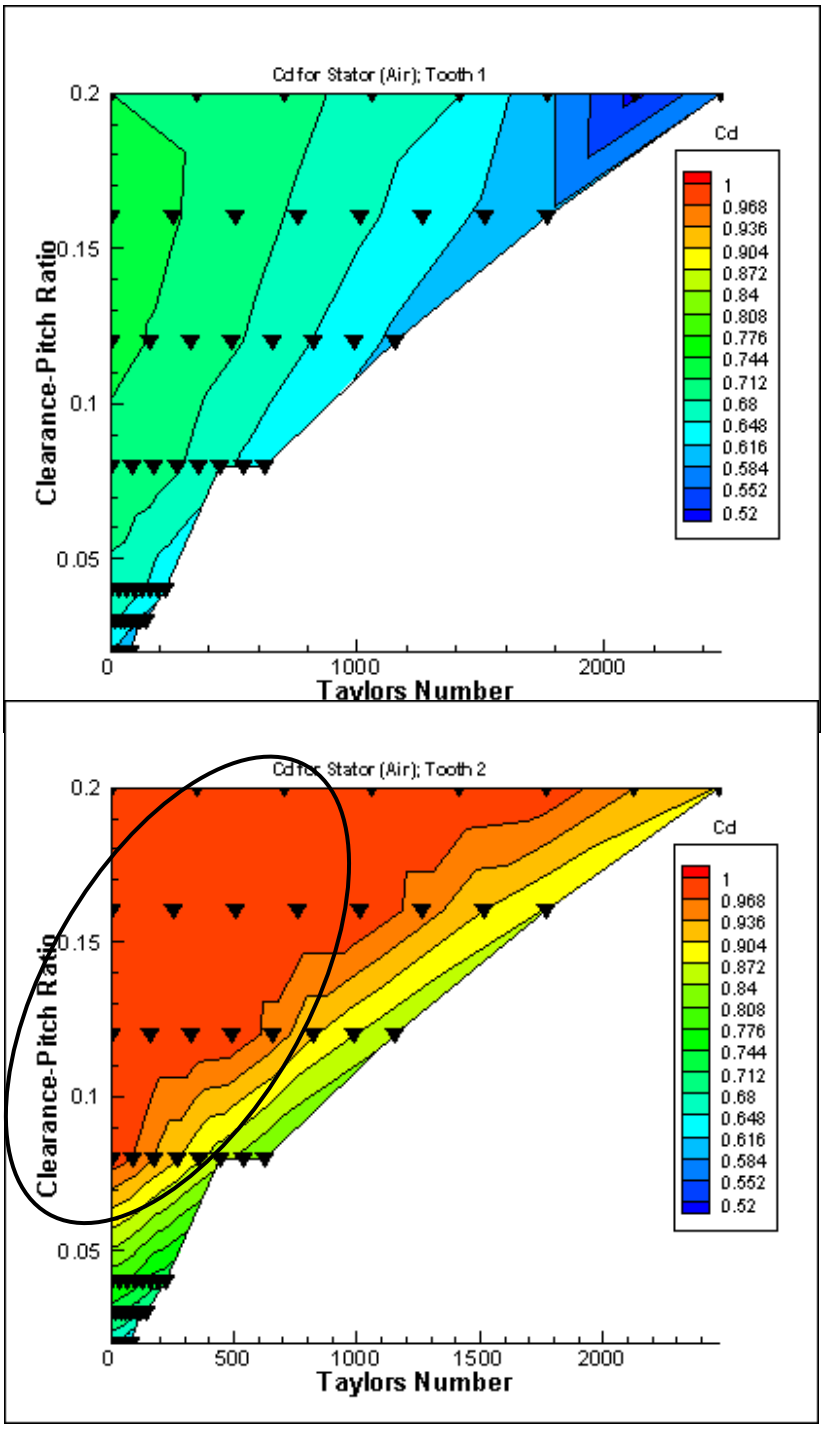

Figure 22. C_d in a stator for various clearances and **Ta** in compressible flow. s = 5 mm, w = 1 mm, h = 5 mm.

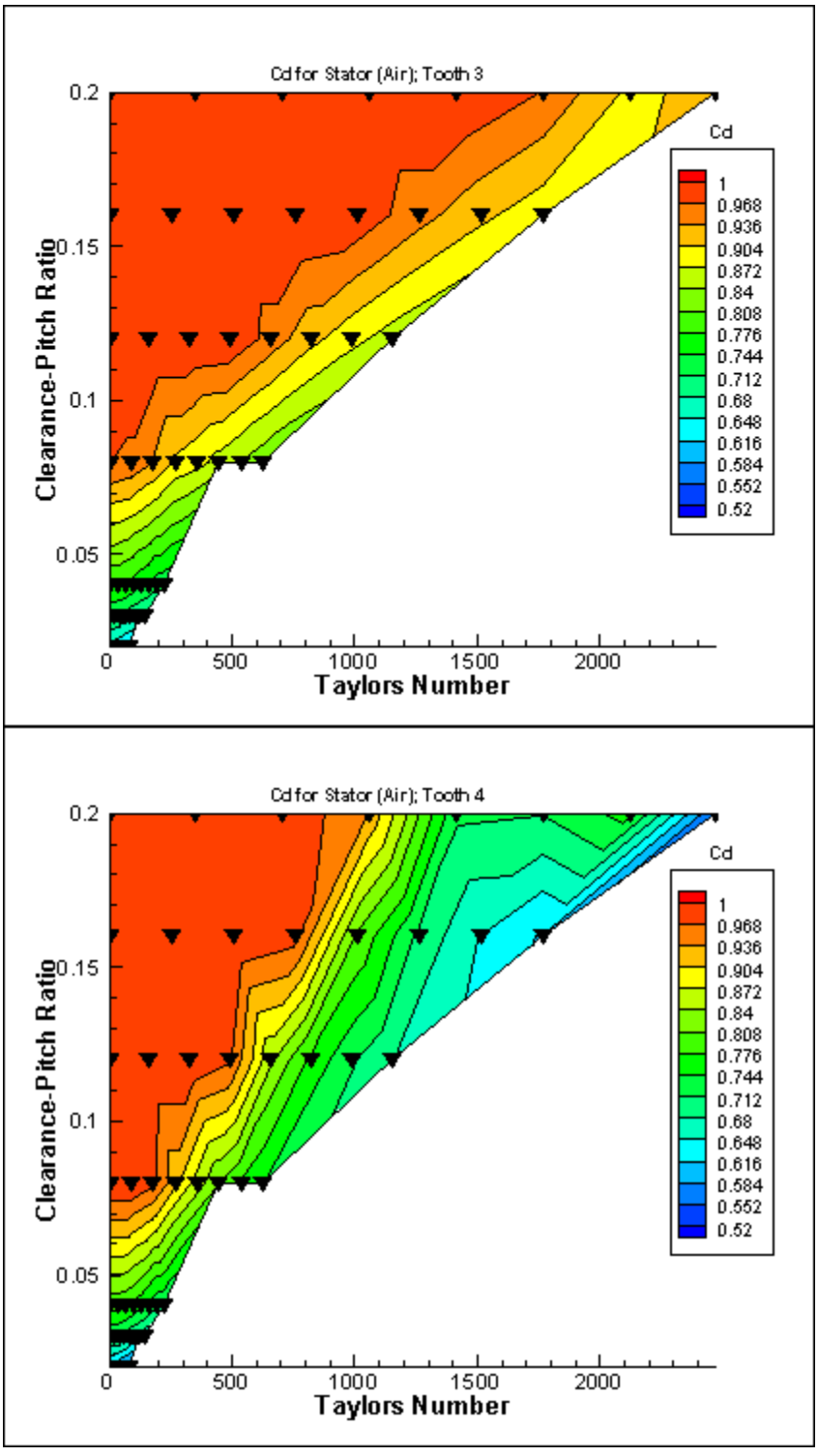

Figure 22. Continued.

5.2.2 Effect of cavity depth on flow parameters

A previous study by Saikishan and Morrison [8] did not look broadly into the effects of the cavity depths on the carry-over coefficients and discharge coefficients. Simulations were performed at varying depths of the cavity by fixing the pitch at 5 mm, and the width of the tooth at 1 mm. It is interesting to find that γ is independent of the depth of the cavity in a compressible flow. To understand the effect of changing cavity depths, **Figure 50** that shows the variation of γ with various cavity depths is summarized in **Figure 23**.

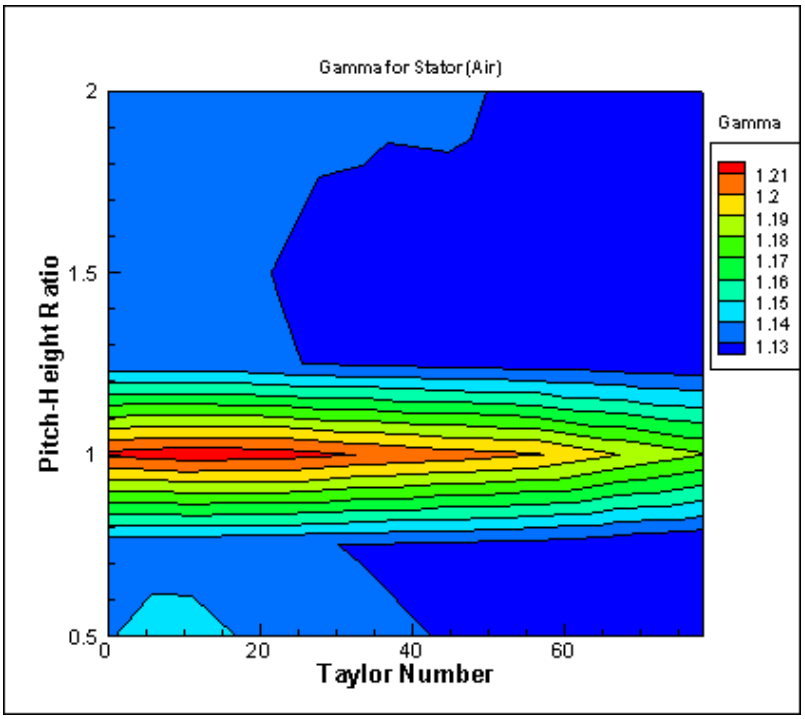

Figure 23. Contour plot for γ in a stator for various depths and **Ta**; compressible flow.

The above figure illustrates how the carry-over coefficient essentially remains the same with a deviation of less than 7% while changing the pitch-height ratio of the

cavity. The values of γ change from 1.13 to 1.21 only. It is to be noted that, within the context of the accuracy of CFD, a 7% deviation does not mean anything significant. Very similar behavior is observed for discharge coefficients in a seal suggesting the flow to be unchanged with respect to changing cavity depth in terms of energy dissipation. Hence, for designing seals with teeth on stator, tooth depth can be assumed to be the last design parameter to look into if the working fluid is compressible.

As can be seen from **Figure 20** and **Figure 23**, the carry-over coefficient, γ is independent of the rotational speed of the shaft at lower clearance of less than 0.20 mm. (c/s ratio of 0.04). Such behavior can be attributed to the axial inertia of the fluid coming out from under the tooth. The axial velocity of fluid under a 0.20 mm clearance tooth is about 3 times that of a 0.60 mm clearance tooth. Hence, it is that much more difficult for the fluid to be pushed into the cavity and circulate within the cavity. **Figure 24** explains it with contours of axial velocity profiles in the first tooth of the seal.

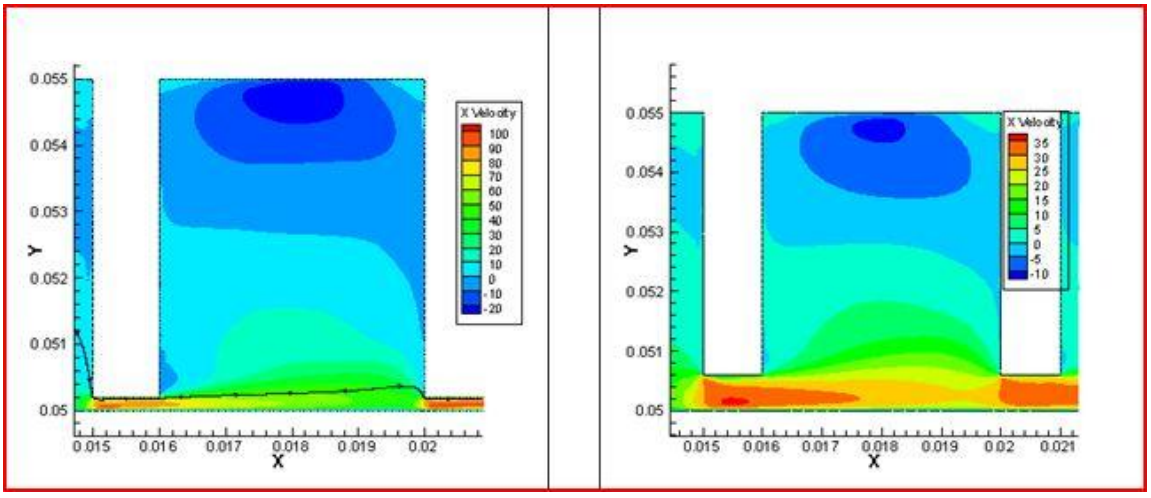

Figure 24. Axial velocity variation under the tooth; c = 0.20 & 0.60 mm, W_{sh} = 350 m/s.

Figure 48 that shows the variation of C_d with cavity depth is summarized in **Figure 25**. The C_d for the first three teeth are essentially independent of seal depth. The fourth tooth shows a decrease in C_d with decreasing cavity depth. The discharge coefficient decreases with increase in shaft speed (or Taylors number). The effect of shaft speed is more pronounced in the case when the seal clearance is changing (**Figure 22**). It shows that higher Taylors numbers in wider clearances cause lower discharge coefficients and this information can be important if the design does not allow higher clearances. Essentially, the disadvantage of using higher clearance is outweighed by the advantage (fact) of using a higher shaft speed, which can offer relief to engineers designing tightly constrained clearance specifications.

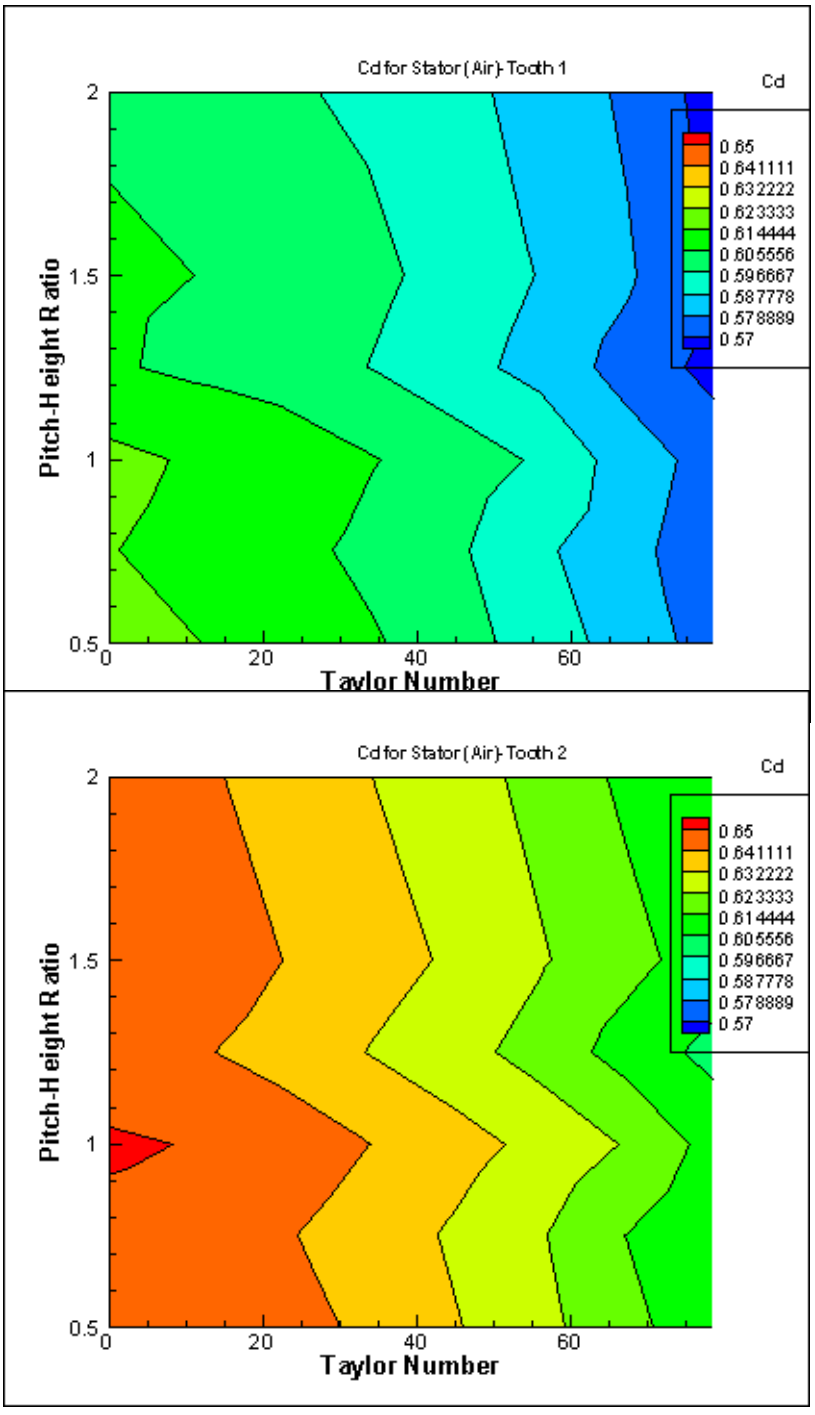

Figure 25. Contour plot for C_d in a stator for various depths and **Ta**; compressible flow. c = 0.1 mm, s = 5 mm, w = 1 mm.

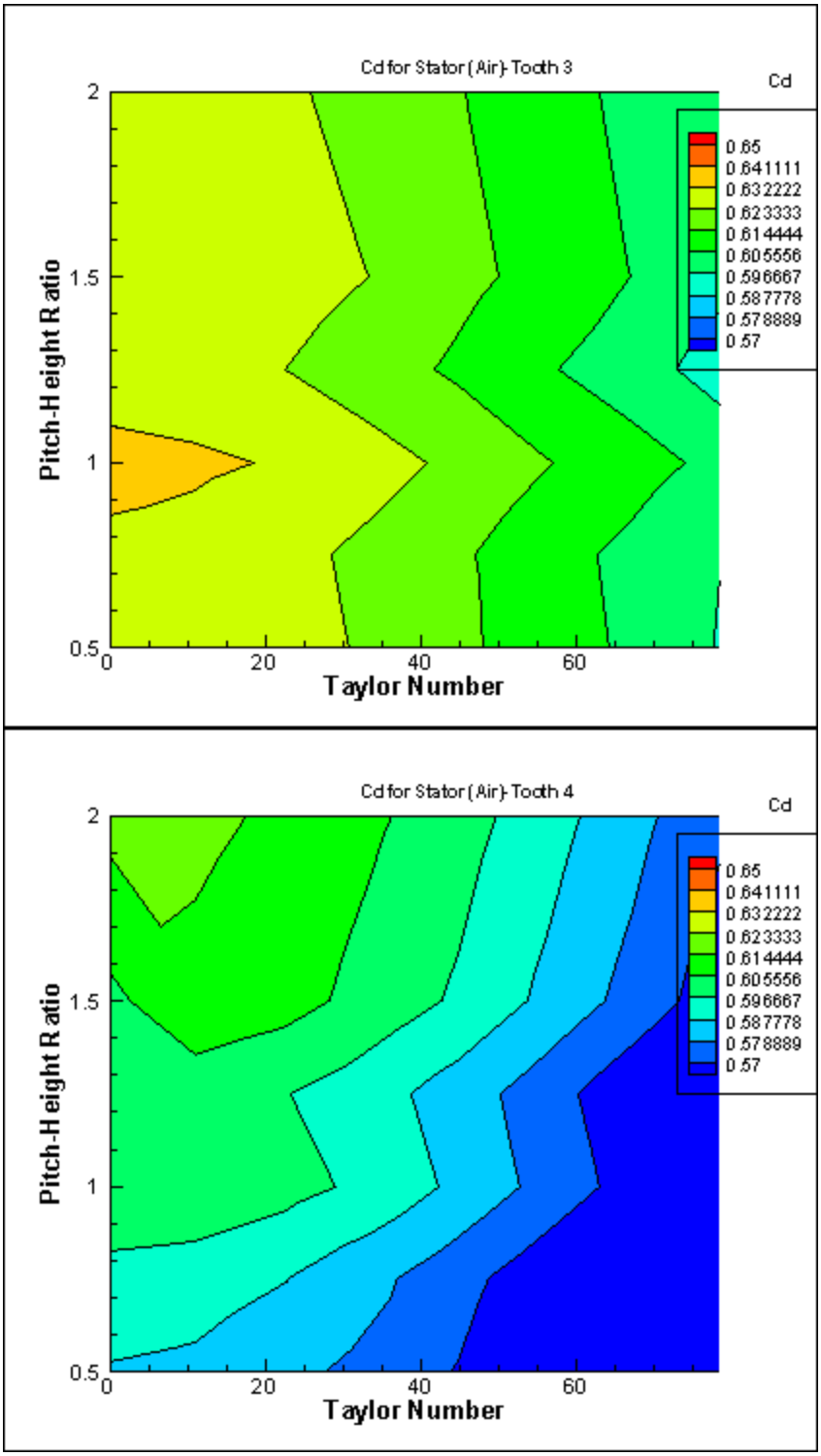

Figure 25. Continued.

6. FLOW IN A SEAL WITH TEETH ON ROTOR

Figure 26 shows a typical flow field in a labyrinth seal with teeth on rotor. A characteristic difference between the flow in a seal with teeth on rotor and those with teeth on stator is the area of contact that rotates the fluid. It is as much as three times larger than for the tooth on a stator case. This has a large impact on γ and C_d as seen further due to the significantly larger tangential velocities imparted to the fluid.

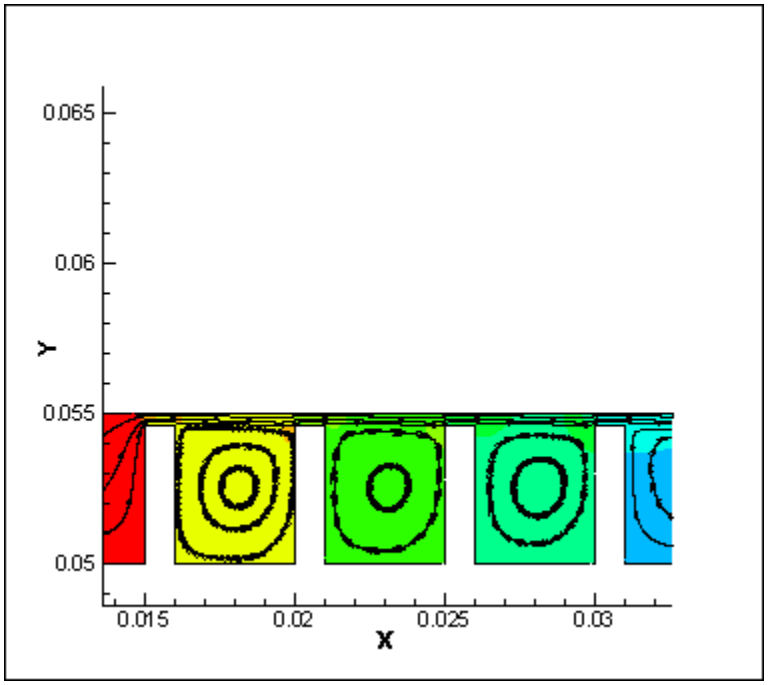

Figure 26. Flow field in a seal with teeth on the shaft, $W_{sh} = 0$.

6.1 Incompressible Flow

The effects of flow in a seal with teeth on rotor are accentuated with the presence of an incompressible working fluid as discussed in further sections. The flow in such cases is shown in **Figure 27**.

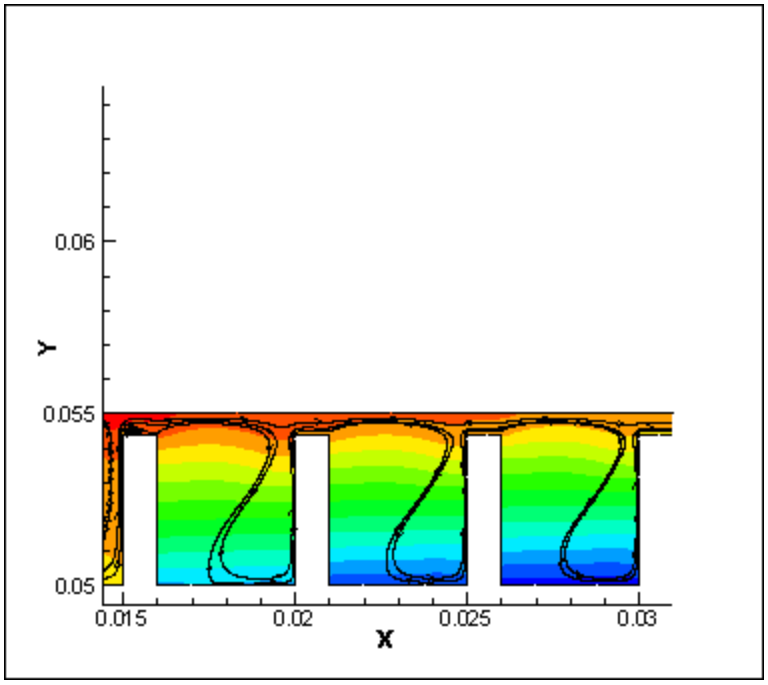

Figure 27. Fluid flow in a seal with teeth on rotor with incompressible flow for a shaft speed of 250 m/s.

6.1.1 Effect of clearance on flow parameters

To study the effect of clearance, the pitch and the tooth width of the seal are fixed at 5mm. and 1 mm. respectively, while varying the clearance from 0.10 mm. to 1.0 mm. The shaft speeds were varied from 0 to 350 m/s in multiples of 50.

Figure 28 summarizes the effect of clearance on the streamline curvature in the cavity of a seal with teeth on rotor.

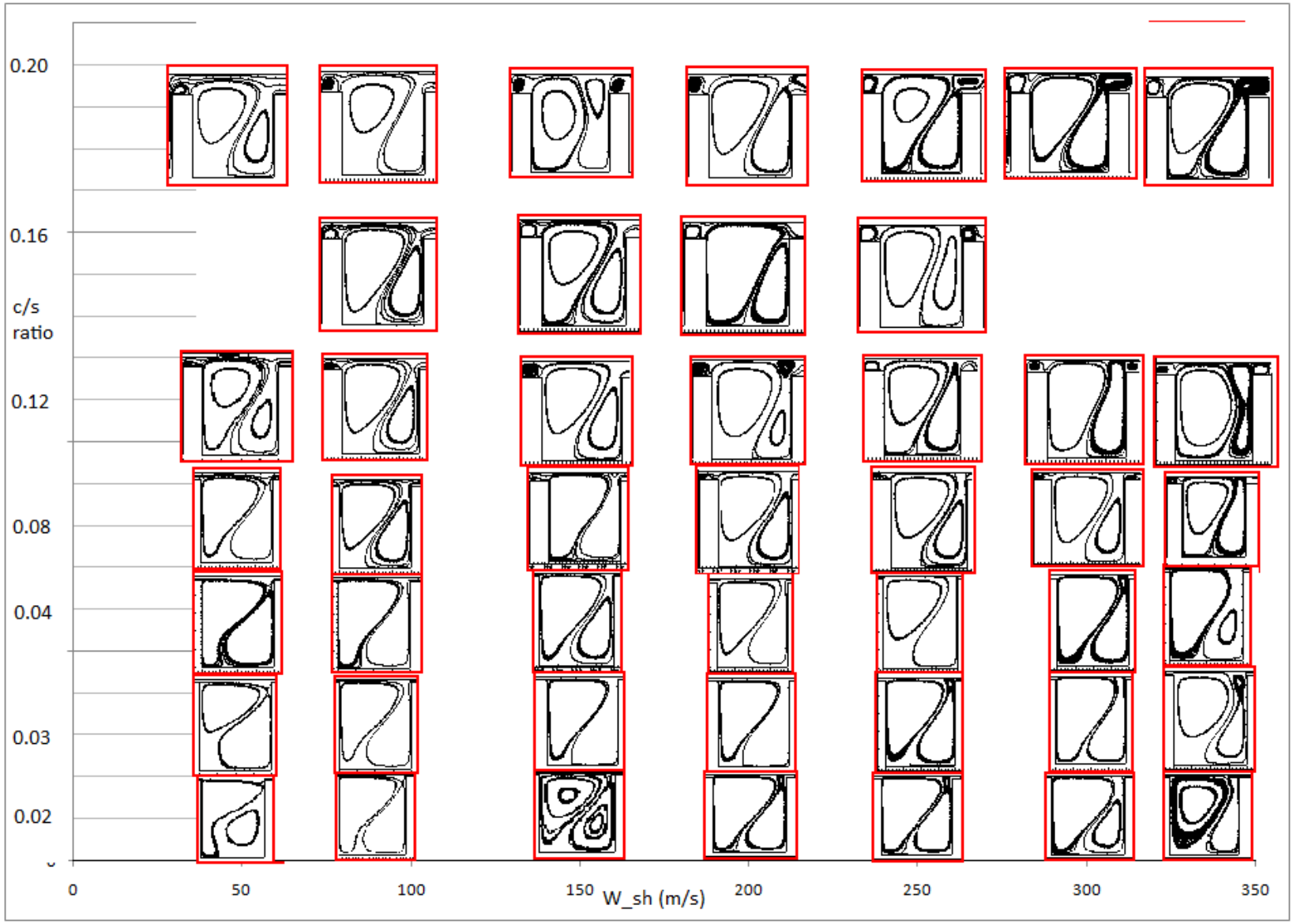

Figure 28. Different streamlines with varying clearance for tooth on rotor, Re =1000.

By increasing clearance from c/s of 0.02 to 0.20, it is observed that there is a transition from a large recirculation zone to a completely diverted flow recirculation. For c/s > 0.04, only diverted flow recirculating zones are observed at all Taylor numbers. Also, vortices begin to form under the teeth for c/s > 0.04. These vortices under the teeth reduce the effective clearance for the seal. For values of c/s > 0.04, the secondary recirculation zone also begins to protrude onto the through flow reducing the seal clearance in the cavity part of the seal.

At lower clearances (c/s ≤ 0.04), increasing shaft speeds causes the flow to transition from a large SRZ to a completely diverted SRZ. At higher clearances (c/s > 0.04), increasing Taylor number leads to the formation of vortices under tooth while forming a diverted SRZ.

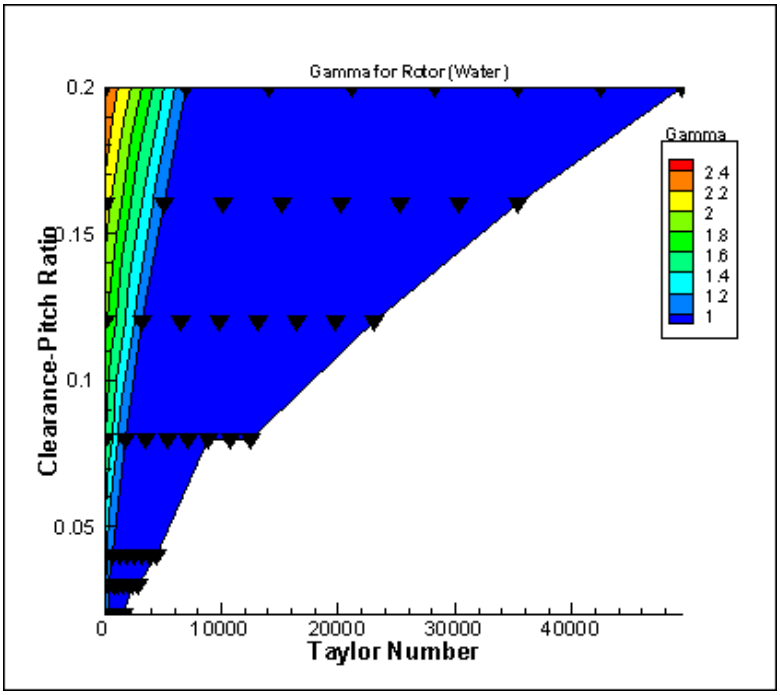

Figure 29. Effect of clearance on γ for a seal with teeth on rotor and water.

When there is a secondary vortex formation in the cavity, γ cannot be defined since there is no separating streamline downstream the tooth. Hence γ is taken as the least possible value of 1 in such cases. From **Figure 29**, it can be seen that the carry-over coefficients become one after a certain rotational speed. It is to be understood that the behavior of γ cannot be established since it cannot be defined at such flow scenarios. Such flow scenarios also imply the formation of SRZ's at such c/s ratios and Taylor numbers.

Figure 29 indicates that at higher Taylors number (even for shaft speeds greater than 50 m/s), a secondary recirculation zone is observed regardless of the clearance-pitch ratio of the seal. At a higher c/s value of 0.2, γ values increase from 1 to 2.4 suggesting decreasing seal cavity efficiency. γ value coupled with C_d values (greater than 1) at such higher clearances suggest the same. The seal fails to dissipate energy and the exiting stream under the tooth flows through the next tooth before dissipating its energy. This argument holds for lower Taylors numbers only since SRZ's are formed irrespective of the c/s ratio at higher Taylors number. **Table 6** summarizes the formation of SRZ's at various shaft speeds with varying clearance.

Table 6. Formation of SRZ's for seals with teeth on rotor with water.

Clearance (mm)	Shaft Speed (m/s)							
	0	50	100	150	200	250	300	350
0.1	No	*L*	*L*	*L*	*D*	*D*	*D*	*D*
0.15	No	*L*	*D*	*D*	*D*	*D*	*D*	*D*
0.2	No	*L*	*D*	*D*	*D*	*D*	*D*	*D*
0.4	No	*D*	*D*	*D*	*D*	*D*	*D*	*D*
0.6	No	*D*	*D*	*D*	*D*	*D*	*D*	*D*
0.8	No	*D*	*D*	*D*	*D*	*D*	*D*	*D*
1	No	*D*	*D*	*D*	*D*	*D*	*D*	*D*

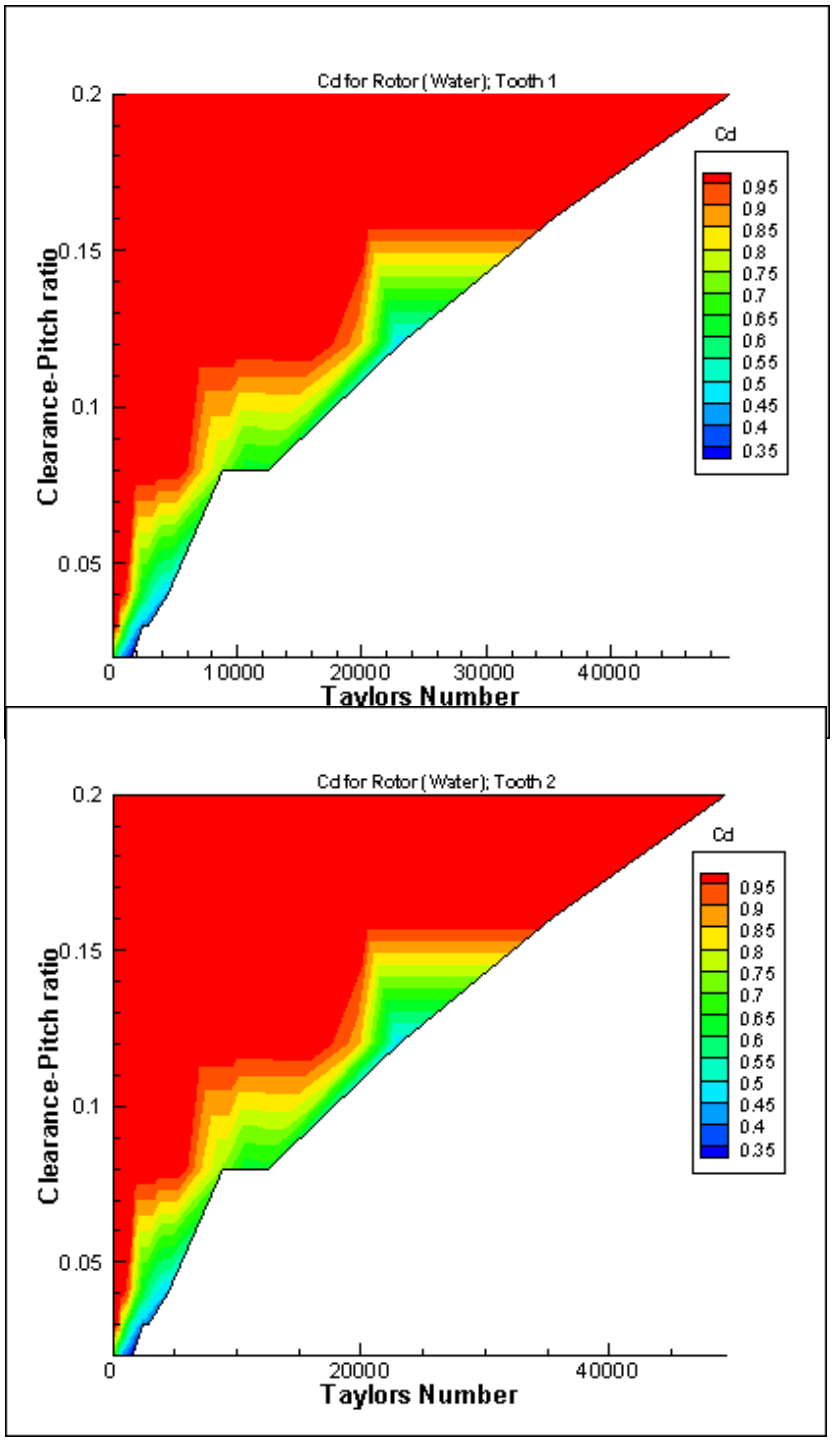

Figure 30. C_d contours at various clearances and **Ta** for rotor; compressible flow. s = 5mm, h = 5mm, w = 1mm.

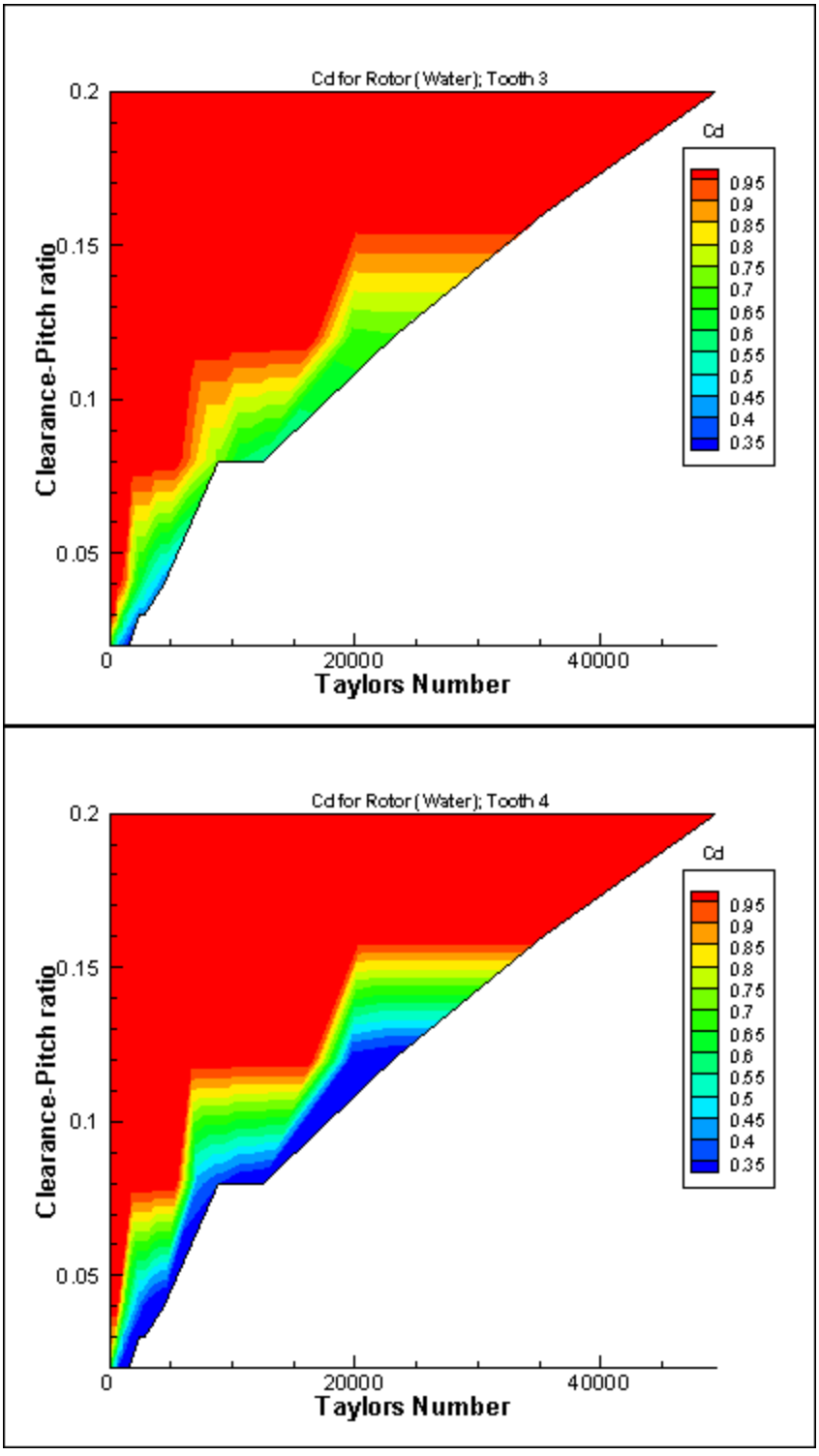

Figure 30. Continued.

The discharge coefficient is a measure of a seal's ability to reduce leakage. A value of 1 indicates an ineffective seal. Performance increases as C_d decreases. Unlike the tooth on stator case, the discharge coefficient C_d for the first tooth is similar to that of the subsequent teeth as shown in **Figure 30**. At zero shaft speed, the discharge coefficient increases from 0.7 to 0.95 as c/s increases showing that higher clearances are inefficient for a tooth on rotor seal. With increasing c/s ratio, the seal performs better only at higher Taylor numbers. At extremely high c/s of 0.20, the tooth on rotor seal is very inefficient at all shaft speeds. At lower c/s, C_d values suggest that increasing the Taylor number will result in an efficient seal as observed from a value of 0.35. But running at shaft speeds close to or less than 150 m/s (which is common today for many turbomachines) suggests an inefficient performance of the seal if the c/s ratio is greater than 0.04. Such shaft speeds render a seal efficient only if the seal has c/s $\leq$ 0.04 for tooth on rotor. To summarize, for a tooth on rotor, increasing shaft speeds above 200 m/s reduces C_d by 25% regardless of the clearance as long as c/s < 0.20 (or $\leq$ 0.16).

6.1.2 Effect of cavity depth on flow parameters

Figure 31 summarizes the streamline pattern for a seal with tooth on rotor at varying cavity depths. To understand the effect of cavity depth, the pitch and the tooth width were fixed at 5 mm. and 1 mm. respectively, while varying the depth from 10 mm. to 2.5 mm. This varies the pitch-height ratio from 2 to 0.5.

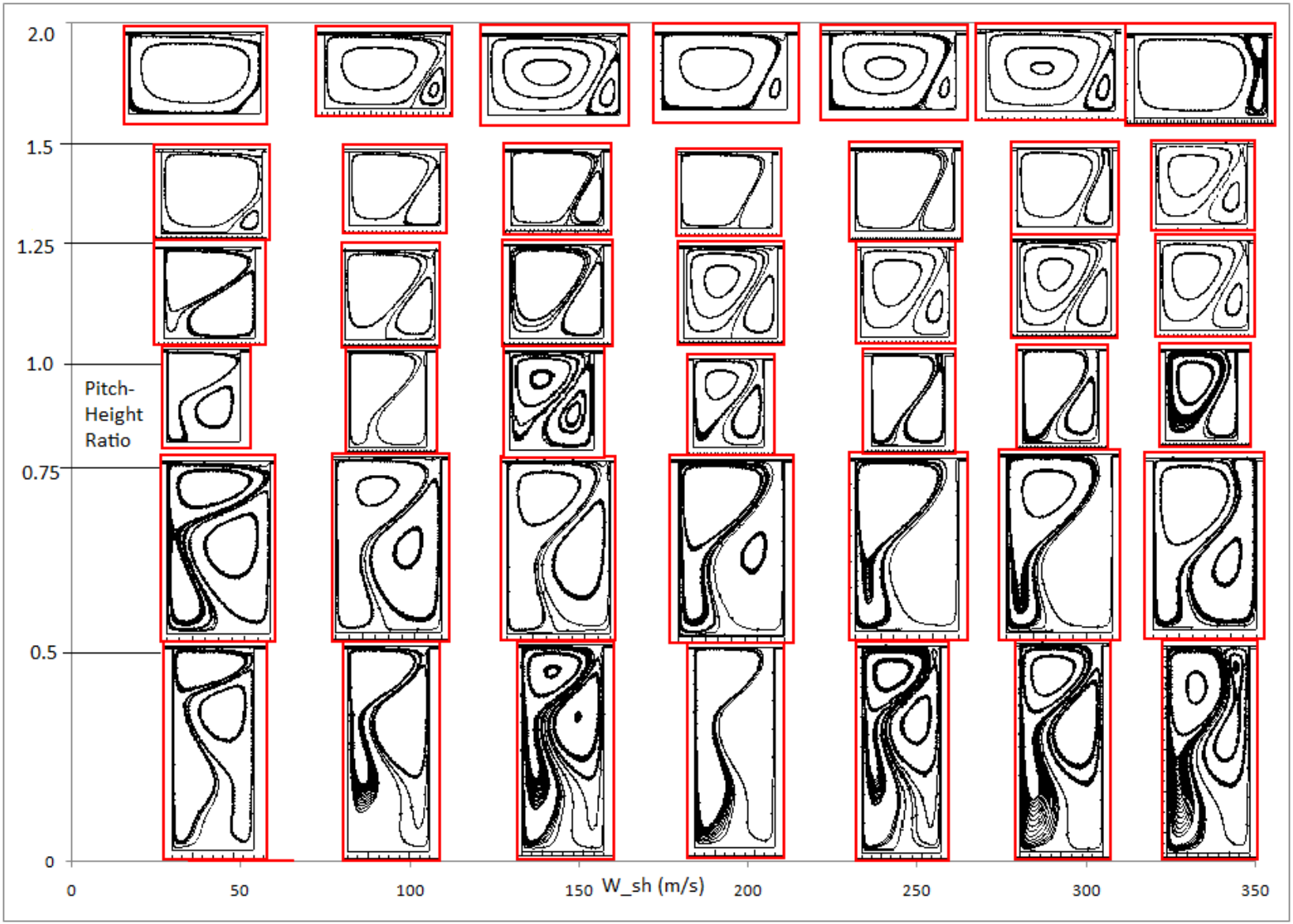

Figure 31. Streamlines with varying cavity depths for tooth on rotor.

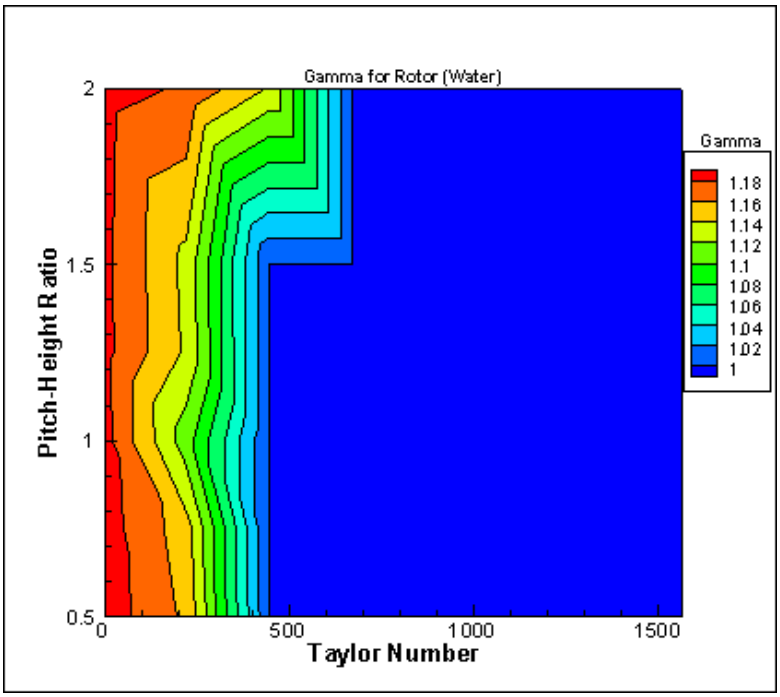

Figure 32. Effect of cavity depth on γ for a seal with teeth on rotor and water.

Figure 32 illustrates the effect of cavity depth on the flow field. Regardless of the cavity depth, as the Taylors number increases beyond a value close to 500, secondary vortices occur in the cavity diverting the flow into the cavity. This critical Taylors number, interestingly, is close to the value seen for a teeth on stator in incompressible flow. Although there was a transition zone in a teeth on stator, such transition occurs more quickly with increasing shaft speed to be noticeable in the case of a teeth on rotor seal. This is due the magnitude of the increase in pressure difference across a cavity (correlated against the body force of the fluid) with increasing shaft speeds which is discussed in further sections.

The effect of cavity depth does not seem to be very critical unless we are looking at medium ranges of shaft speeds such as 100-200 m/s. It is observed that deeper cavities

form secondary vortices at lower shaft speeds compared to shallower cavities. One such observation is illustrated in **Figure 33**. This is due to the larger rotating surface imparting higher levels of swirl which increases centrifugal body forces. In summary, γ is relatively independent upon cavity depth for a tooth on rotor seal.

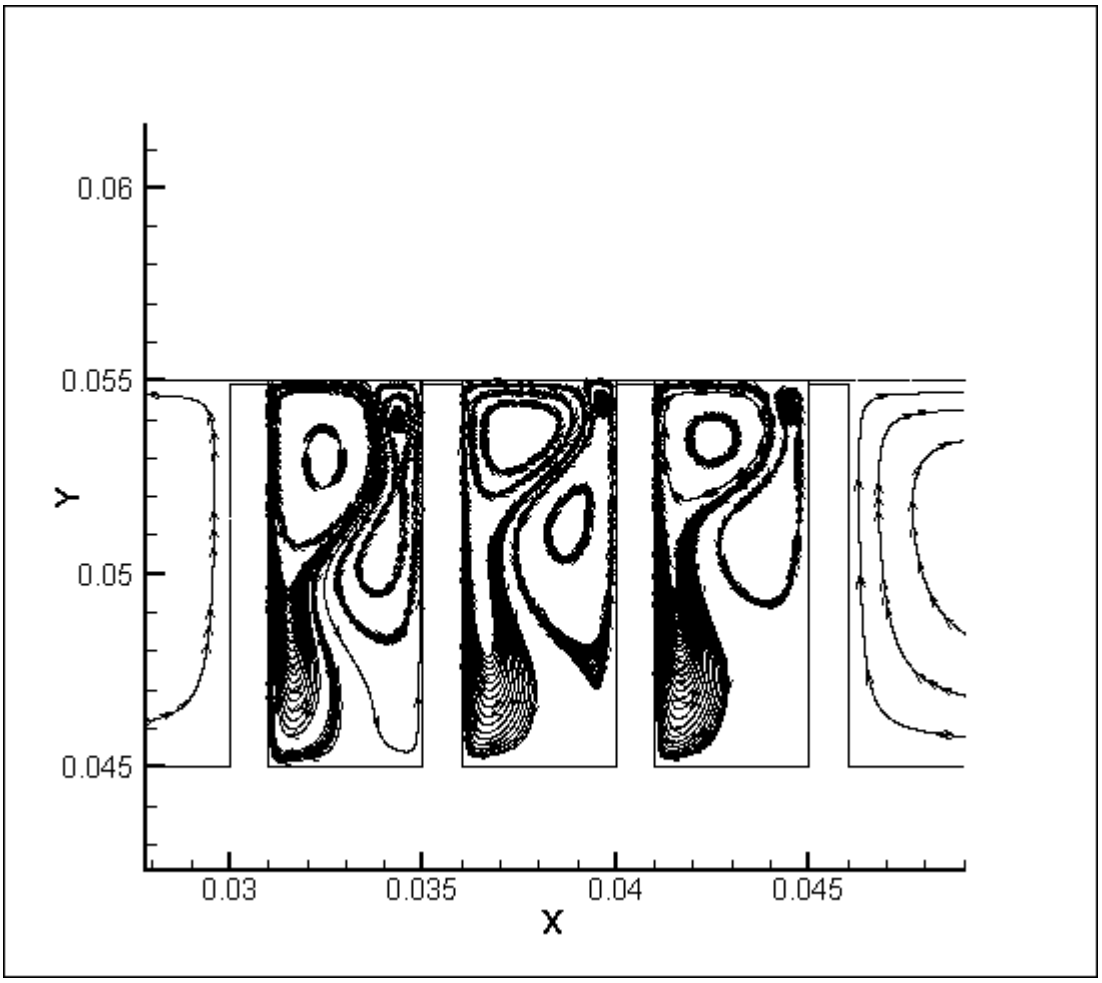

Figure 33. Formation of vortices in deeper cavities, with water, W_{sh} = 150m/s, s/h =0.5.

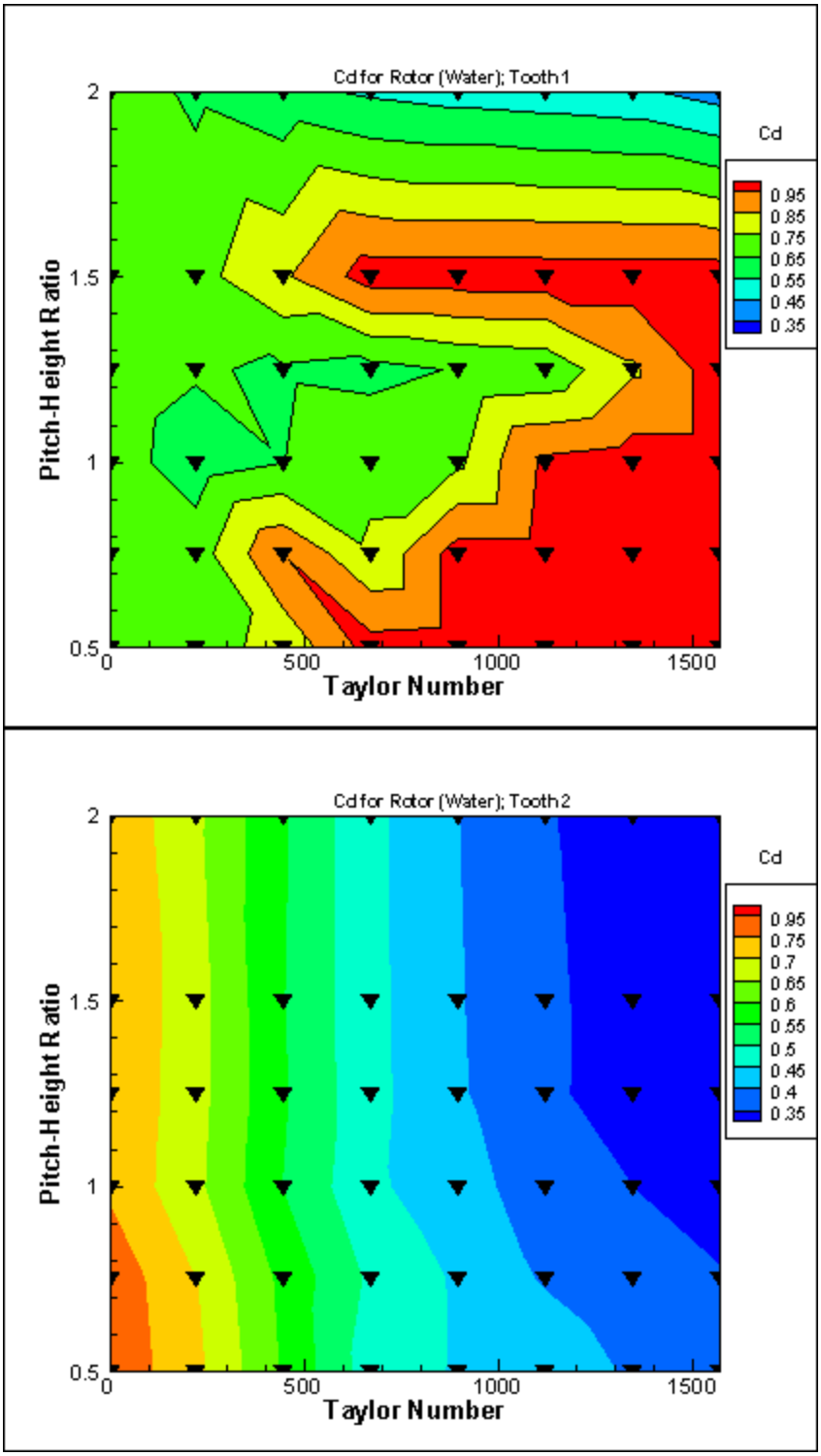

Figure 34. C_d for various cavity depths and **Ta** for rotor; incompressible flow, c = 0.1 mm, w =1 mm, s = 5mm.

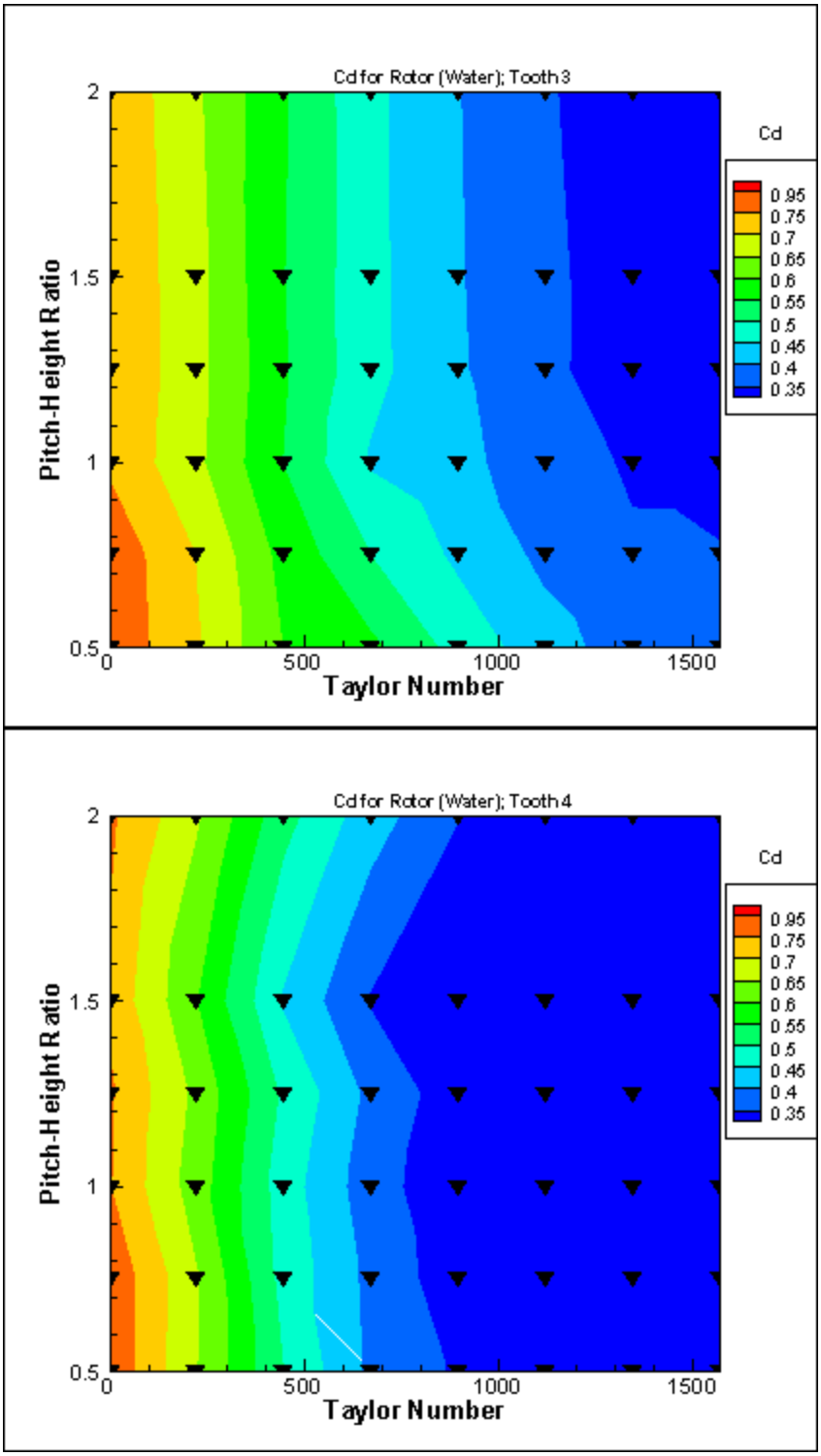

Figure 34. Continued.

Figure 34 illustrates how changing the cavity depth affects the discharge coefficient. The first tooth shows a complex relationship. In general, C_d is least (~0.65) for all cavity depths for Ta < 200. C_d remains low for h/s =1.0 and 1.25 for Ta < 900. For h/s values below 1 and a for a value of 1.5, C_d increases to above 0.95 (~1) as Ta exceeds 500. Only the very large cavity depth (h/s = 2.0) maintains a low value of C_d. In fact, for this case C_d decreases as the Taylor number increases.

The interior teeth are all the same with C_d decreasing to 0.85 for h/s = 0.5 to 0.8 for h/s ≥ 1 at Ta = 0. As the Taylor number increases, C_d decreases to below 0.4 with the lowest values present for the largest h/s and highest Taylor number. These data show that for a tooth on stator seal, a seal depth of 2 provides a seal with the least leakage.

Figure 35 shows the swirl at the inlet of the cavity that reduces the effective clearance and drastically changes the streamline curvature. This causes an erratic behavior in the discharge coefficients of the first cavity in each geometry of the seal. Also, subsequently, at higher clearances there are vortices under teeth and causes wide fluctuation in C_d values as described below.

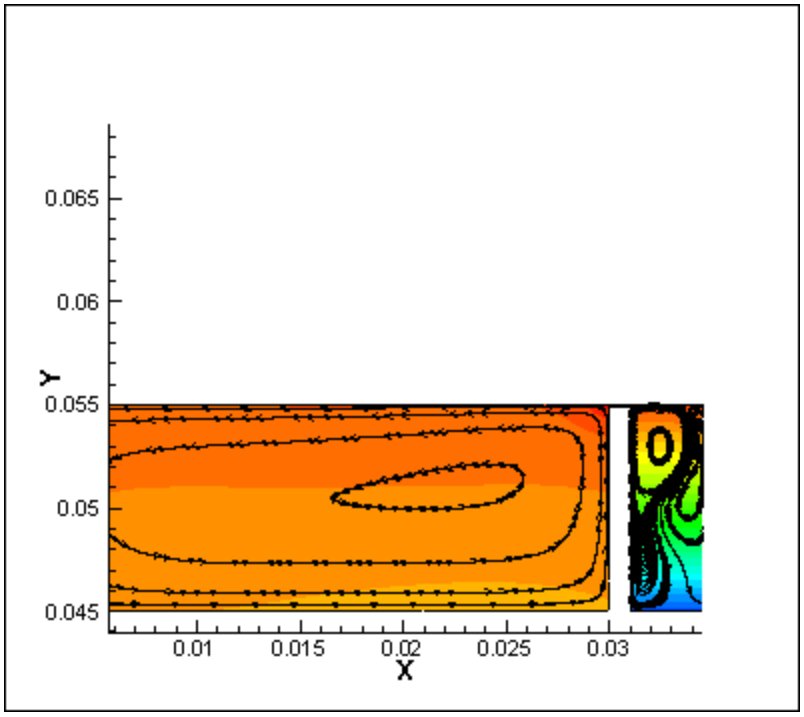

Figure 35. Initial swirl reduces the flow into the cavity.

6.1.3 Effect of rotational speed on flow parameters

The primary effect of shaft speed, as discussed earlier, is the formation of secondary vortices in the cavities. The formation of SRZ's is summarized in **Table 6**. Secondary vortices in the cavity are formed when the fluid close to the stator is being pushed into the cavity. The force necessary for the fluid to circulate into the cavity is driven from the fluid-rotor interaction. The fluid gains a certain swirl velocity which is proportional to the shaft speed (quantified and discussed in Section 7). This swirl momentum can be gained by a fluid if only the fluid has some viscous nature associated with it. This swirl momentum produces enough body force, $\frac{\rho u_\theta^2}{r}$, for the fluid to generate a pressure difference between the rotor and stator sections (dP/dr) of a cavity thereby

driving the fluid into circulating. The magnitude of the body force is proportional to the pressure difference within a cavity and is shown in **Figure 36**. The shear at the wall of the rotor, τ is responsible for the axial momentum gradient characterized by the axial velocity of the fluid (u_x). A clearance of 0.10 mm (c/s ratio of 0.02) would drive up the shear layer contribution to create more shear force on the working fluid. This shear force coupled with the body force along the radial direction drives the u_r-u_x vortex in the r-x plane.

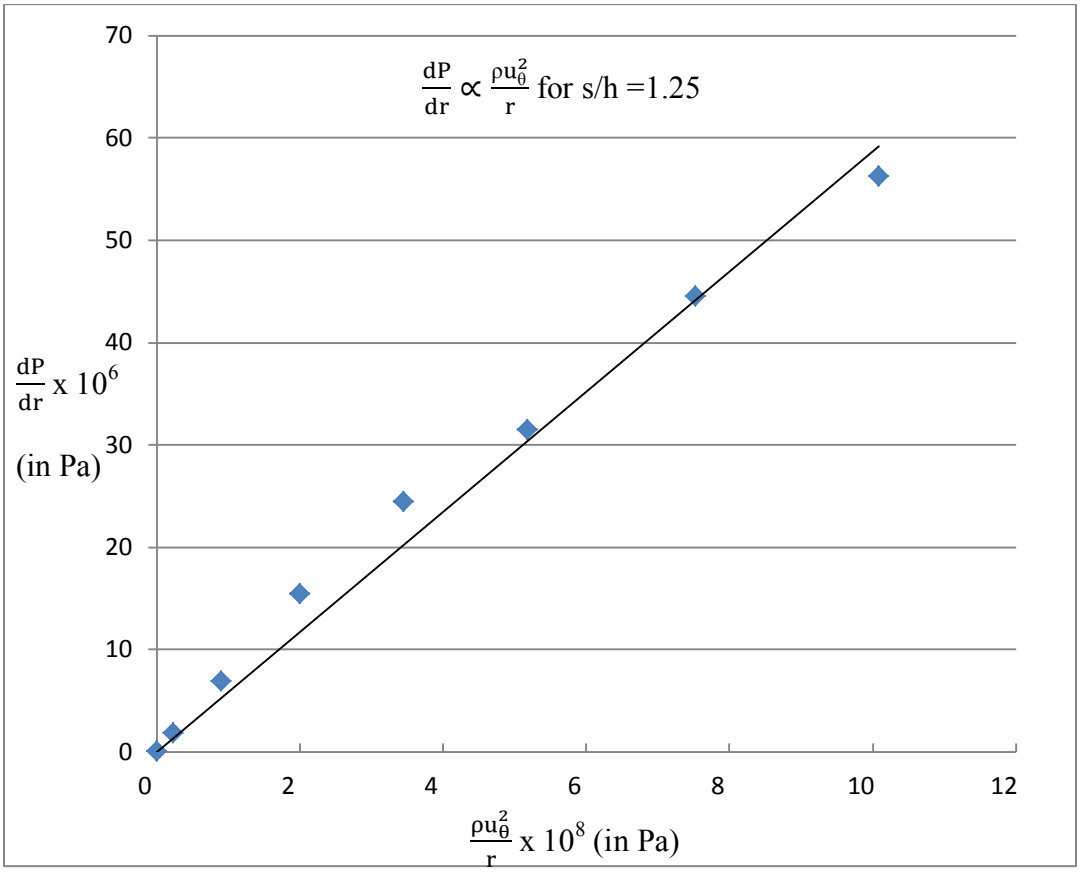

Figure 36. Body force creating pressure difference to cause recirculation in a cavity; teeth on rotor for water s/h =1.25, c = 0.1 mm, w = 1 mm, s = 5mm.

Figure 37 shows the level of pressure difference in a cavity with tooth on rotor running with water at a shaft speed of 350 m/s. The points to measure the pressure difference are shown for clarity. The pressure difference is dP = P_1-P_2 and radius of the shaft is used to calculate a pressure gradient that is evaluated against the body force, $\frac{\rho u_\theta^2}{r}$. For this seal the pressure difference from over the inlet tooth to over the exit tooth is 105 MPa while the radial pressure difference is 4 MPa indicating the body force effects are as great as the axial velocity effects.

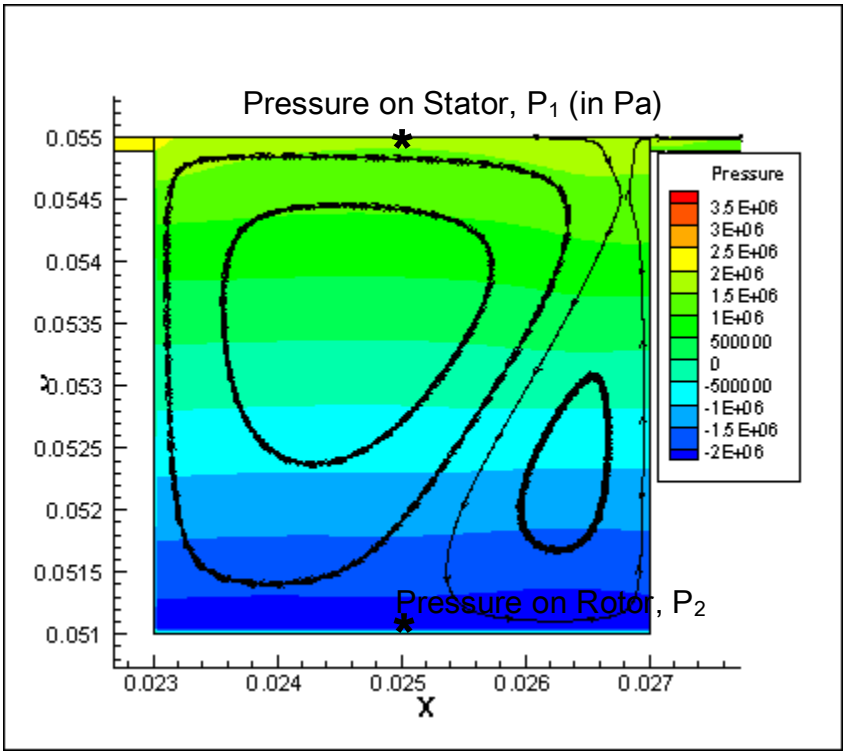

Figure 37. ΔP across stator and rotor in a cavity; s/h = 1.25 and W_{sh} = 350 m/s.

The influence of body force, $\frac{\rho u_\theta^2}{r}$ is observed in the different kinds of streamlines possible in a cavity leading to different flow structures. These flow fields are

characterized by the flow parameters, γ and C_d, which help understand the efficiency of the seals in dissipating energy of the fluid. **Figure 38** shows the streamlines in increasing order of the shaft speeds (50, 150 and 350 m/s), which results in greater body force for the fluid. The magnitude of body force is seen to increase by 8 times from case 1 to case 2 and by 5 times from case 2 to case 3 shown in the **Figure 38**. Hence, the fluid is subjected to higher radial pressure gradients within the cavity leading to detachment of the streamline that exits the preceding tooth and being drawn into forming a secondary vortex. For cases like the third, γ is not defined by Hodkinson's equation and are given a value of 1.

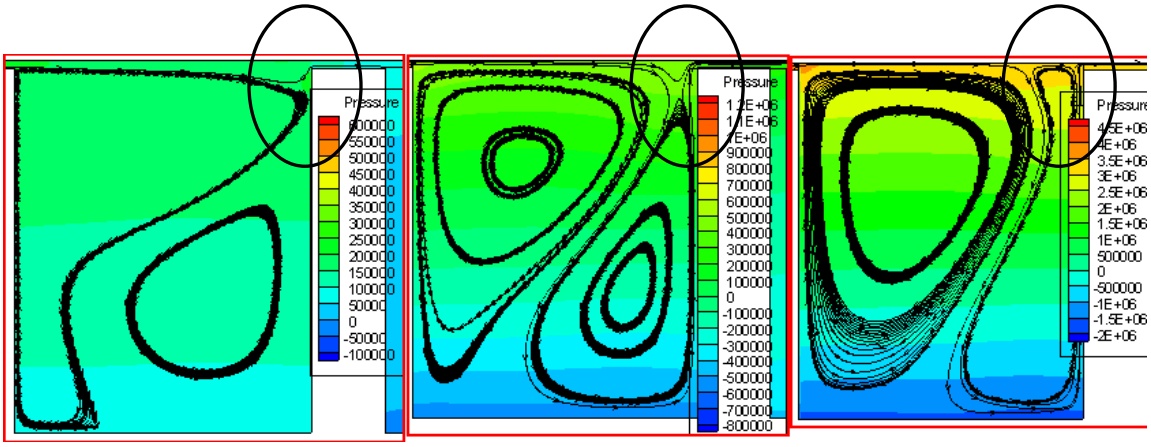

Figure 38. Influence of body force on streamlines in a cavity at various shaft speeds.

6.2 Compressible flow

This section deals with air as the working fluid that represents a compressible fluid in general. The effect of a compressible fluid on energy dissipation was discussed in a previous section under Section 5.2. **Table 7** and **Table 8** show the formation of large secondary recirculation zones at various clearances and cavity depths. The geometries of the seals considered for this study are the same as for the tooth on stator section.

Table 7. Formation of SRZ's with teeth on rotor for air with varying clearance.

Clearance (mm)	**Shaft Speed (m/s)**							
	0	50	100	150	200	250	300	350
0.1	No	No	No	No	No	No	No	**L**
0.15	No	No	No	No	No	No	No	**L**
0.2	No	No	No	No	No	No	**L**	**L**
0.4	No	No	No	No	**L**	**L**	**L**	**L**
0.6	No	No	No	**L**	**L**	**L**	**L**	**L**
0.8	No	No	No	**L**	**L**	**L**	**L**	**L**
1	No	No	No	**L**	**L**	**L**	**L**	**L**

Table 8. Formation of SRZ's with teeth on rotor for air with varying cavity depth.

Pitch/Height	**Shaft Speed (m/s)**							
	0	50	100	150	200	250	300	350
0.5	No	No	**L**	**L**	**L**	**L**	**L**	**L**
0.75	No	No	No	**L**	**L**	**L**	**L**	**L**
1	No	No	No	**L**	**L**	**L**	**L**	**L**
1.25	No	No	No	No	No	No	No	No
1.5	No	No	No	No	No	No	No	No
2	No	No	No	No	No	No	No	No

The Taylors numbers at which the simulations were performed are the same as in the case of a tooth on stator seal.

6.2.1 Effect of clearance and aspect ratio on flow parameters

As per Hodkinson's definition of carry-over coefficient, γ values have been estimated using Tecplot 360 for various simulations. As in the case of a seal with teeth on the stator, geometric parameters such as pitch, tooth width, and height are fixed to understand the effect of clearance on γ and Cd. The flow map with varying clearance-pitch ratio showing the formation of SRZ's is illustrated in **Figure 39**. With increasing clearance, the carry-over coefficient increases implying lower impingement of the streamline on the downstream part of the cavity. This can be understood from X-Y plots in **Figure 57** in Appendix F and are neatly summarized in a 3-D contour plot in **Figure 40**. The carry over coefficient increases from 1.0 to 2.8 as the clearance increases from Ta =0.

As the Taylor number increases, γ decreases indicating more energy dissipated in the seal cavity. A striking difference is seen in **Table 8** (compared with **Table 4**) where secondary recirculation zones are formed at higher clearances of 0.60 mm and above. At this stage, we have an incipient vortex as shown in **Figure 41** is present. This can be attributed to the imparting of high centrifugal force to the working fluid due to higher contact area with the rotating surface. The flow map with varying clearance-pitch ratio showing the formation of SRZ's is illustrated in **Figure 39**. **Figure 39** shows that a large SRZ is formed at higher shaft speeds of 350 m/s only for lower clearances ($c/s \leq 0.04$). For a c/s ratio of 0.08 and 0.12, SRZ formation is shifted to lower shaft speeds of 200 and 150 m/s respectively. For large c/s (≥ 0.16), SRZ's are formed quite easily at a shaft speed of 100 m/s. As seen for a seal with tooth on stator, the SRZ in the cavity presses down onto the through flow from the tooth at higher c/s of ≥ 0.16.

Figure 39. Streamlines with varying c/s ratio for tooth on rotor seal; compressible flow; c = 0.10 mm, w = 1 mm, h = 5 mm, s = 5 mm.

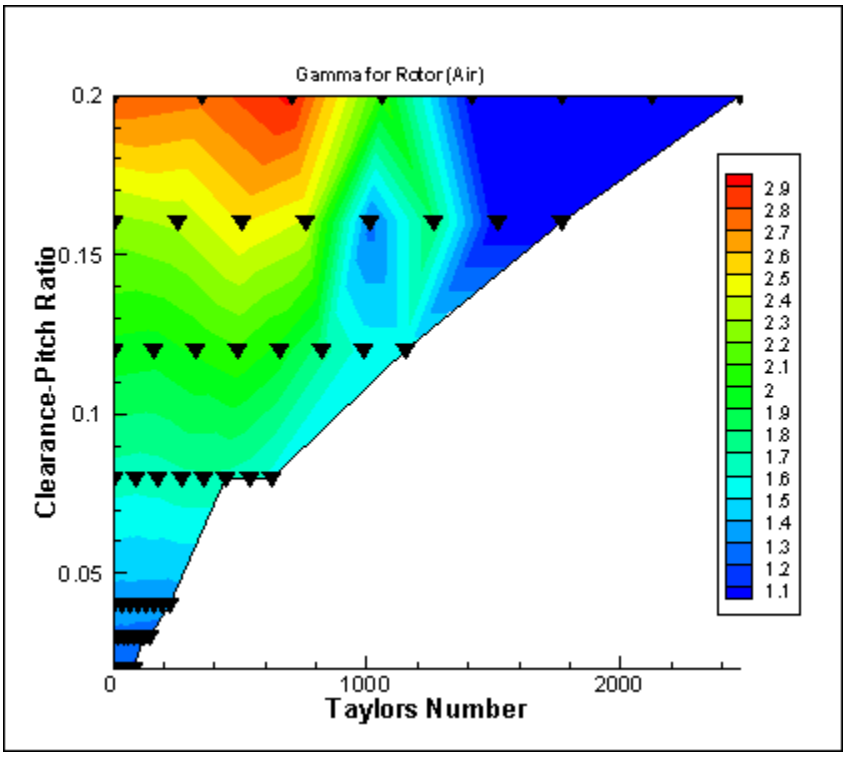

Figure 40. Contours of γ in rotor with various clearances and **Ta**; compressible flow.

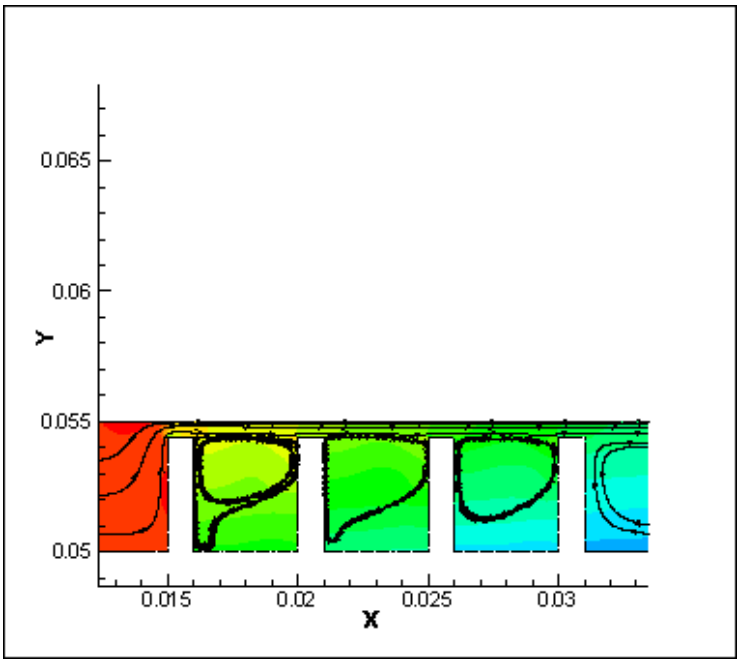

Figure 41. Incipience of SRZ for seal with teeth on shaft with air.

The effect of clearance on the discharge coefficients of a seal with teeth on rotor is summarized in **Figure 42**. It can be seen that C_d values do not change over a wide range. The lowest value is seen for the first tooth at 0.63 for higher Taylors number and a larger clearance (c/s > 0.12) while highest value of 0.77 is seen at lower Taylors number for the same c/s range. This means that the first tooth of the seal is slightly better at higher Taylors number for higher clearance and such similar results were seen with the teeth on stator for a compressible working fluid. This figure strengthens the earlier observation where c/s ratios greater than 0.08 lead to inefficient designs in seal as illustrated here. However, for the subsequent teeth in the seal the discharge coefficient is near 1 for the same regions where C_d is low for the first tooth. This indicates these subsequent teeth are not sealing the flow. Therefore, for the overall seal to work effectively, the seal clearance must be reduced so the subsequent teeth contribute to sealing the flow. Since C_d represents the overall seal effectiveness, the seal must be designed based upon the overall effectiveness. For these flows, this conclusion is also supported by the contour plots of γ (**Figure 40**) which show low values (close to 1) of the carry-over at higher Taylors numbers and lower c/s ratios.

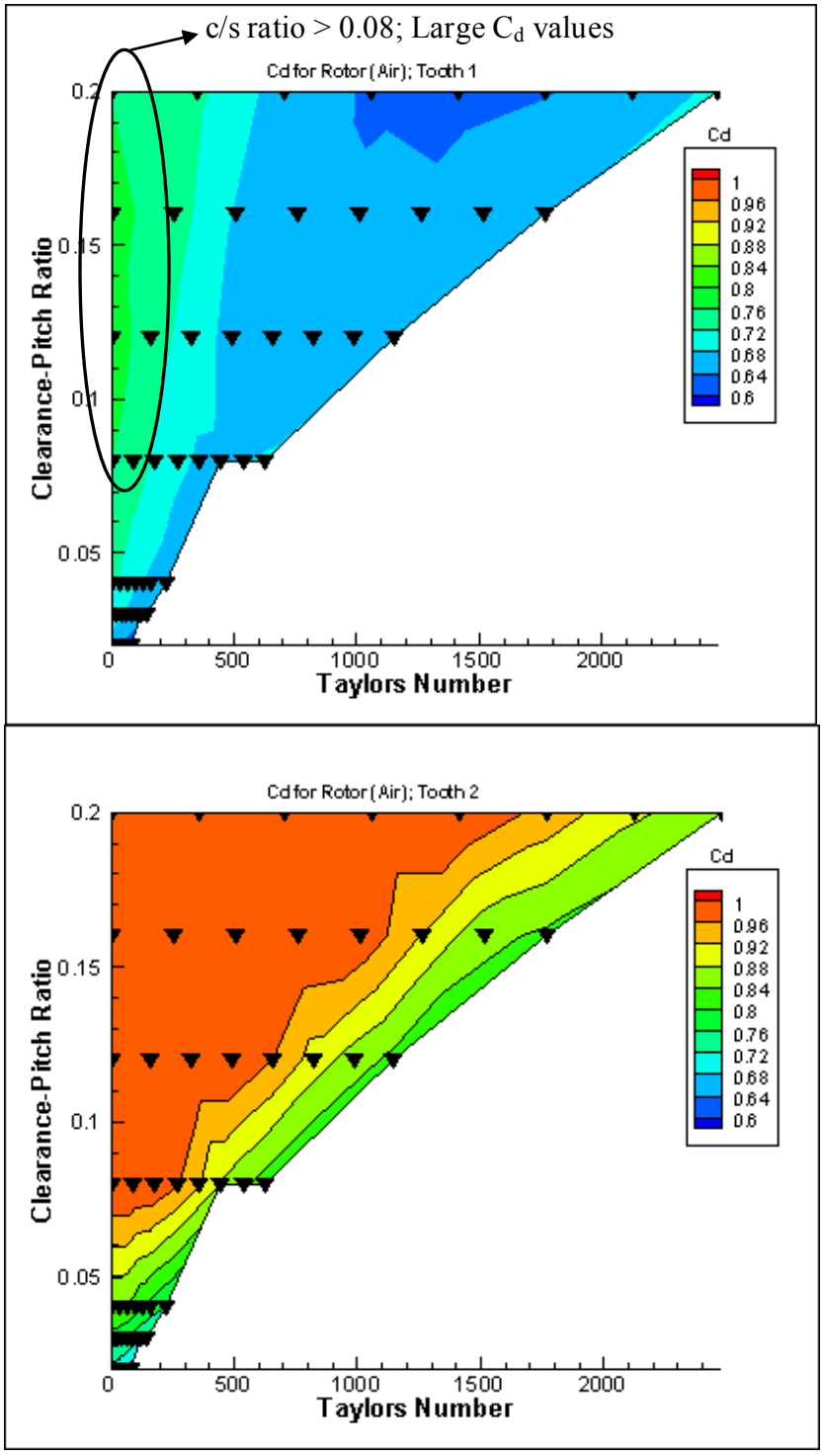

Figure 42. Contours of C_d in rotor with various clearances and **Ta**; compressible flow. s = 5 mm, w = 1 mm, h = 5mm.

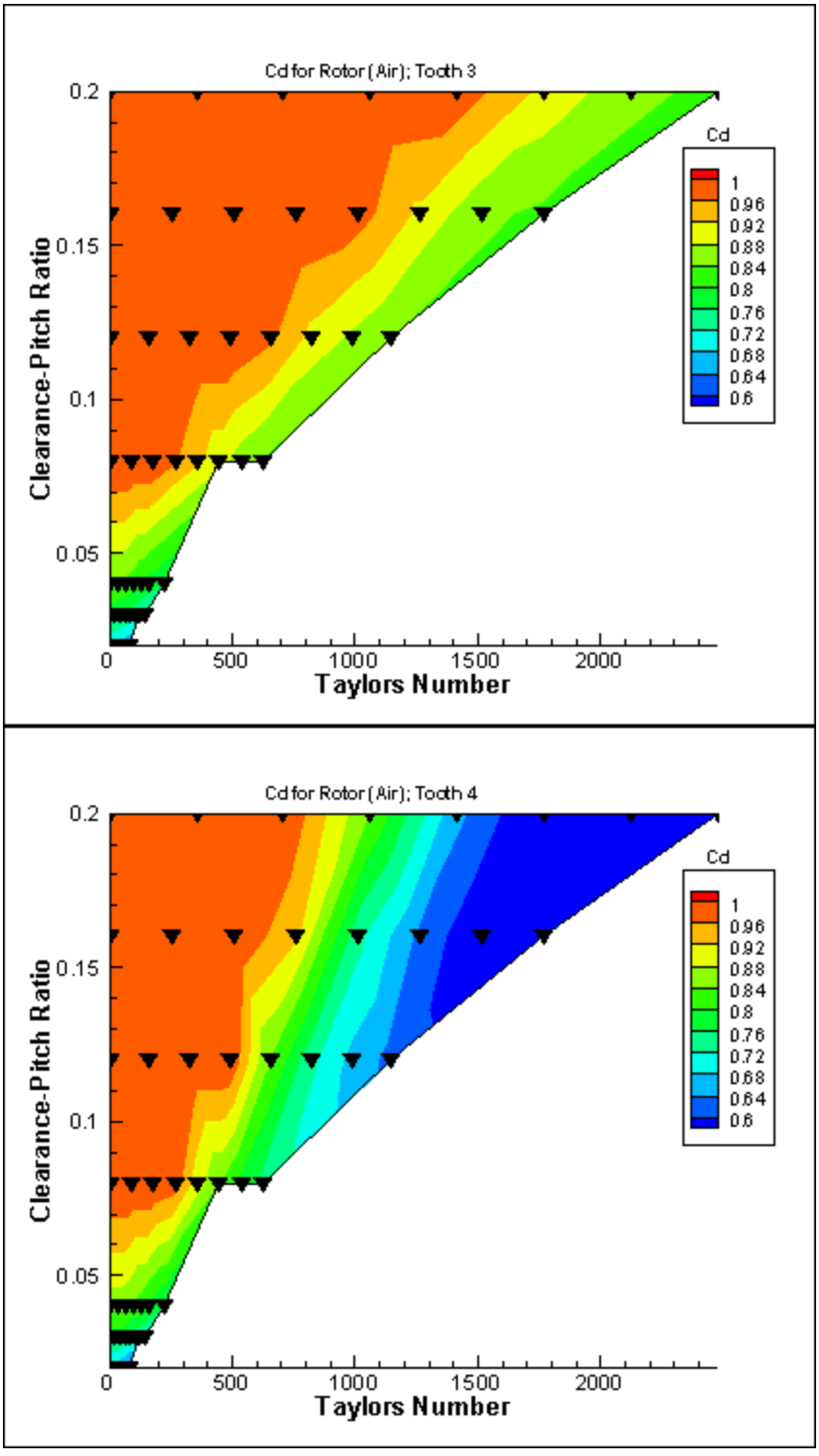

Figure 42. Continued.

Figure 43 shows the axial velocity distributions for teeth on stator and on rotor are very similar at a shaft speed of 350 m/s at a clearance of 0.10 mm. While there is no incipience of a secondary vortex within the cavity, the fluid is being dragged and rotated in the case of a seal with teeth on rotor at similar conditions leading to vortex formation.

This is a case of compressible effects and rotor effects working together changing the flow field drastically compared to a seal with teeth on stator.

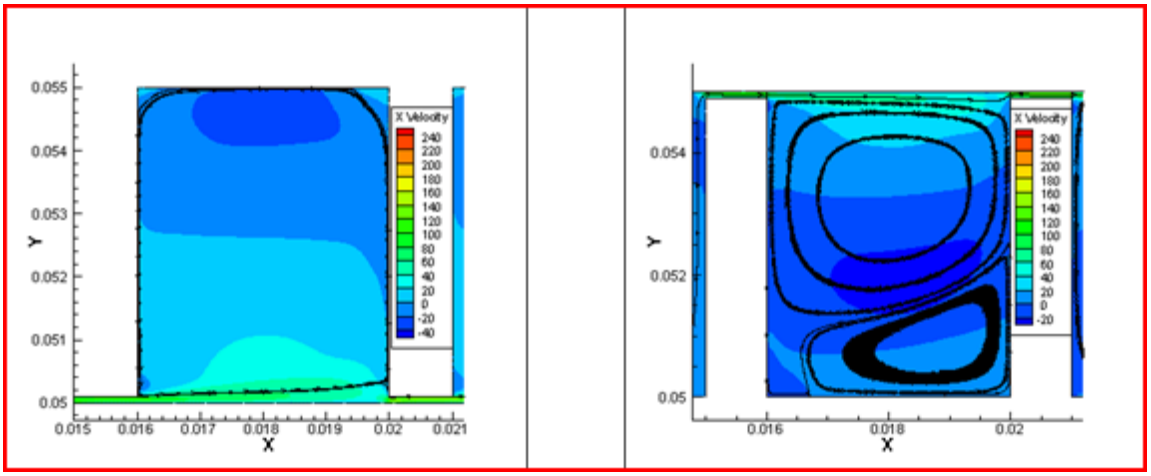

Figure 43. u_x is similar at same shaft speed for teeth on stator and rotor, SRZ's present.

The effect of cavity depth can be assumed to be negligible on the discharge coefficients in a seal and can be clearly observed to be so from **Figure 44** and also on carry-over coefficients from **Figure 45**. Interestingly, the trends and even values in γ and C_d do not change as compared to the values for a seal with teeth on stator using air as working fluid. This can be observed by comparing them against **Figure 23** and **Figure 25**. Also, the behavior of downstream tooth is similar to the first tooth as seen from **Figure 44**. The C_d values change by only 2-3 % among the four teeth with varying cavity depths.

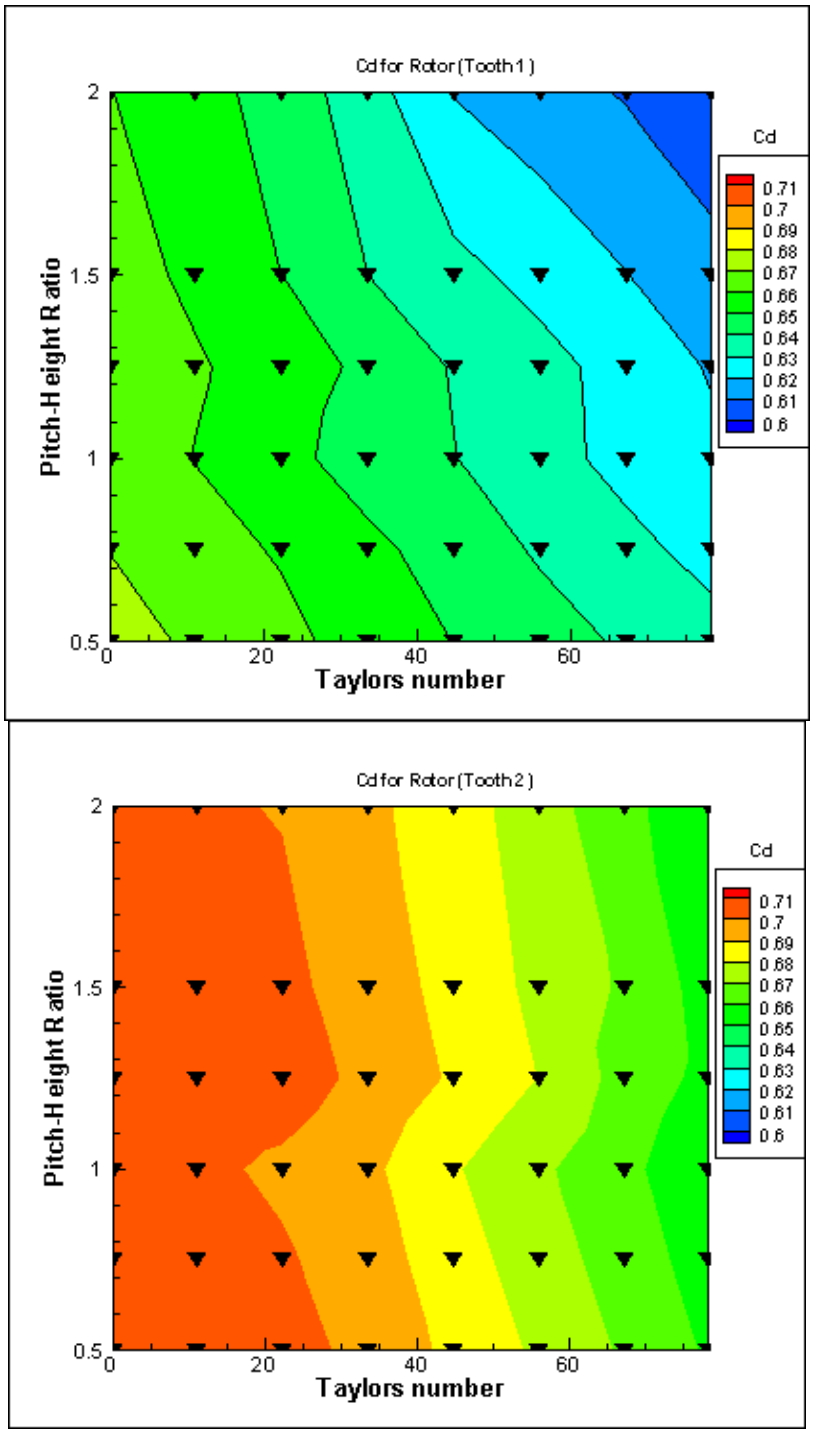

Figure 44. Contour plot for C_d in rotor with various depths and **Ta**; compressible flow. c = 0.1 mm, w = 1 mm, s = 5 mm.

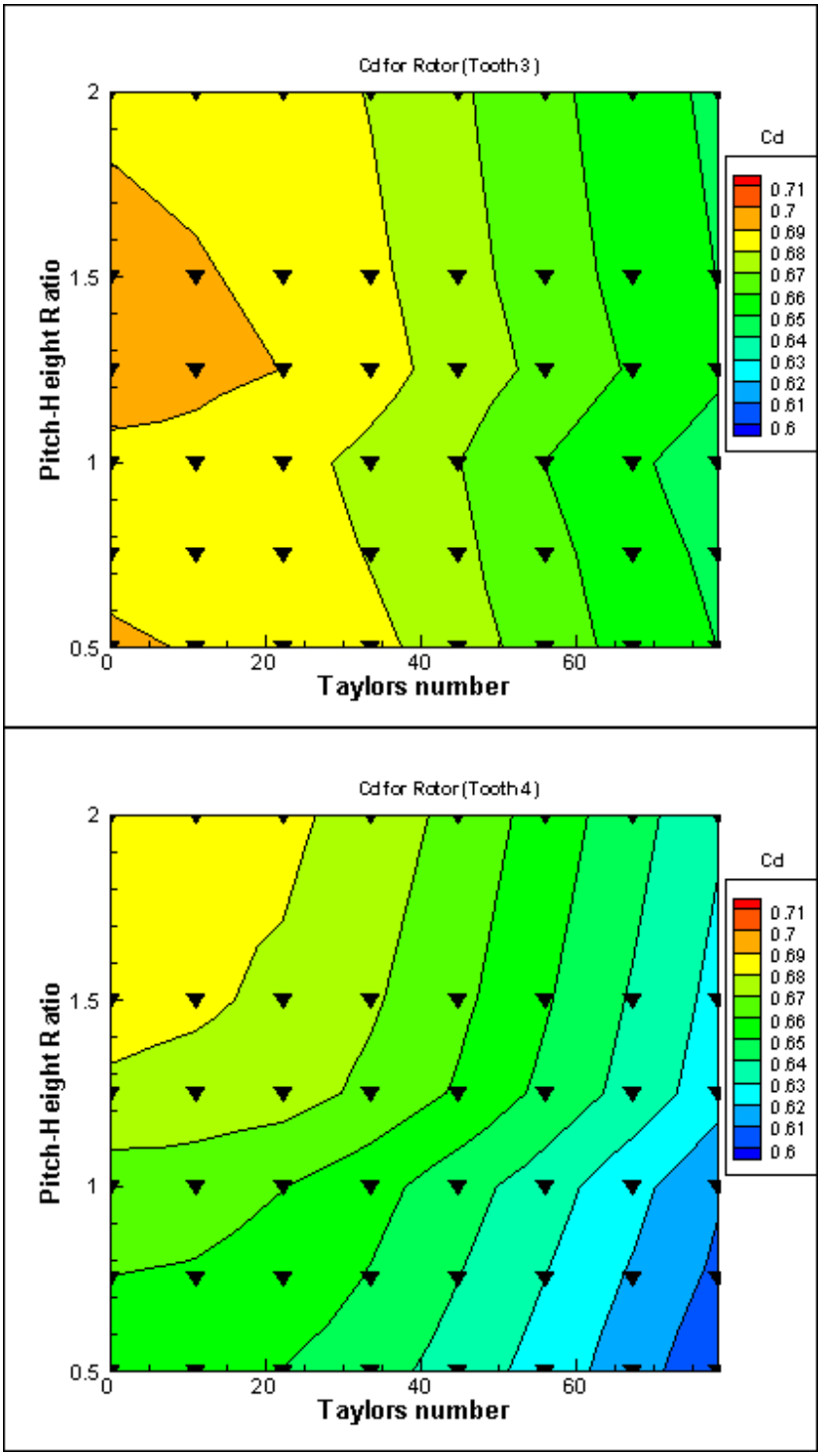

Figure 44. Continued.

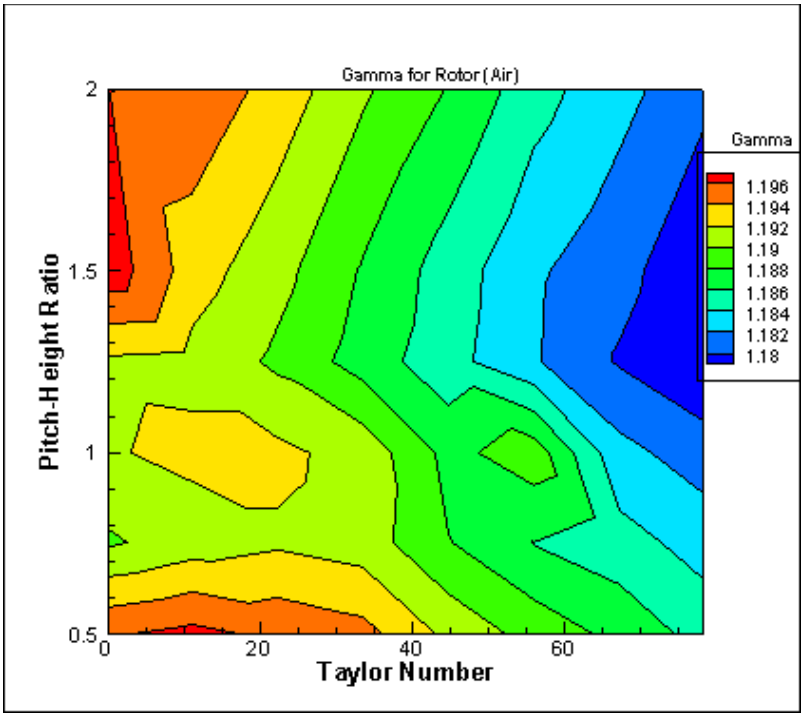

Figure 45. Contour plot for γ in rotor with various depths and **Ta**; compressible flow. c = 0.10 mm, s = 5mm, w = 1 mm.

Figure 43 shows the difference between cases with teeth on rotor and those on stator for a compressible fluid. While the rest of the flow parameters are identical. Interestingly, the compressible fluid tends to form secondary vortices for deeper cavities, but not for shallow cavities.

While for shallower cavities, there is no difference in the discharge coefficients with increasing shaft speed, it is observed that γ decreases with increasing shaft speed at lower clearances while the cavity depth is equal to its pitch. This observation is similar to our previous analysis with teeth on stator and the physics essentially remains the same as discussed in section 5.2.2

7. SWIRL VELOCITY DISTRIBUTION

The present section has focused on calculating the average values of swirl velocity within each cavity of a seal to assess the difference in nature between compressible and incompressible fluid flow. The average swirl velocity, u_θ is calculated using the following equation:

$$\overline{u_\theta} = \frac{\sqrt{\iint_{cavity} u_\theta{}^2(x, r)\,dA}}{\iint_{cavity} dA} \tag{8}$$

Different observations have been made for teeth on rotor and stator. The average swirl velocities have been compared to the tangential velocities of the shaft and interestingly, their relation seems to be linear. These relations have been obtained for changing cavity depths and can be seen in **Figure 46** for a seal with teeth on stator and in **Figure 47** for a seal with teeth on rotor.

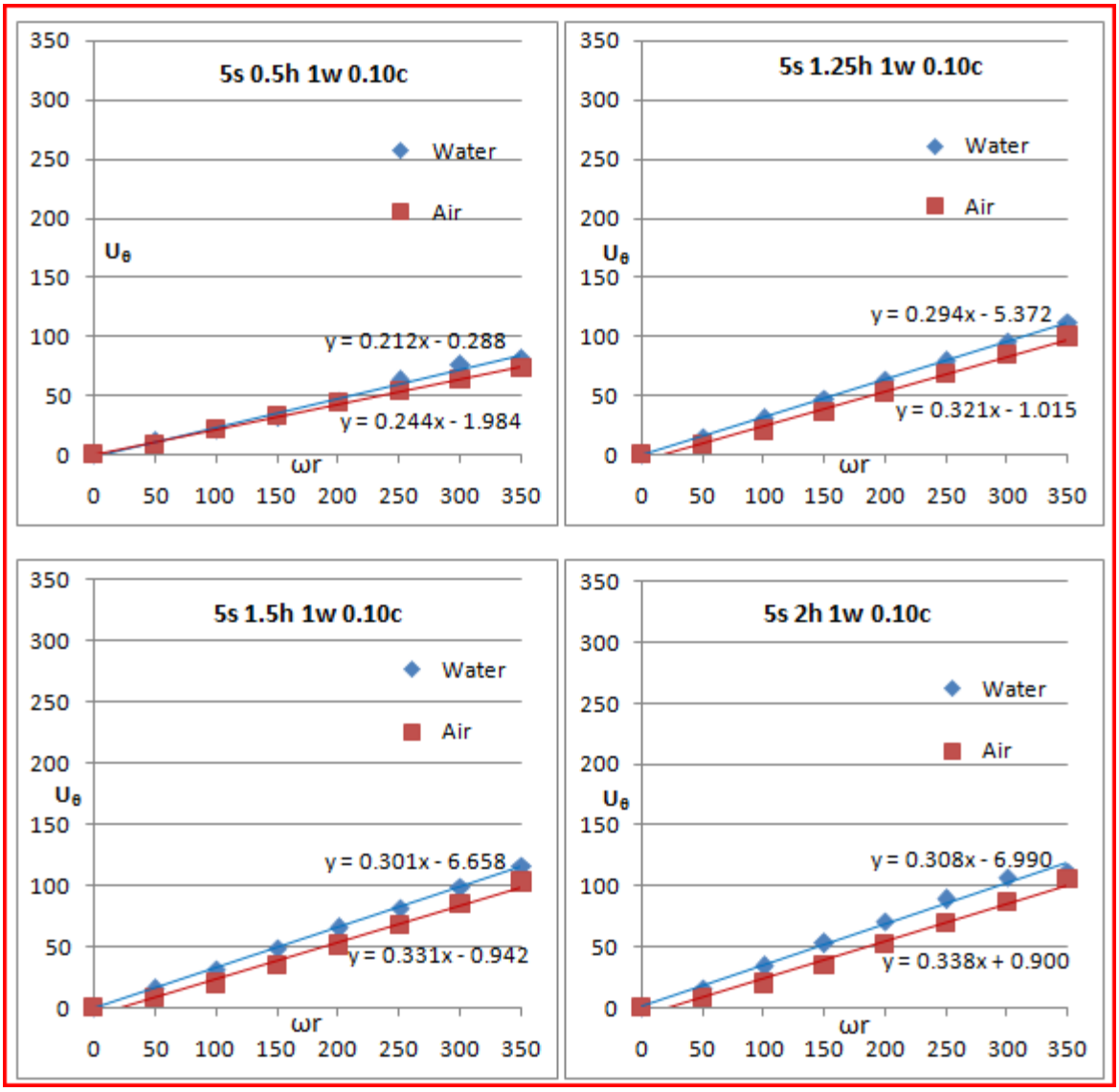

Figure 46. Average swirl velocity in the cavity with teeth on stator.

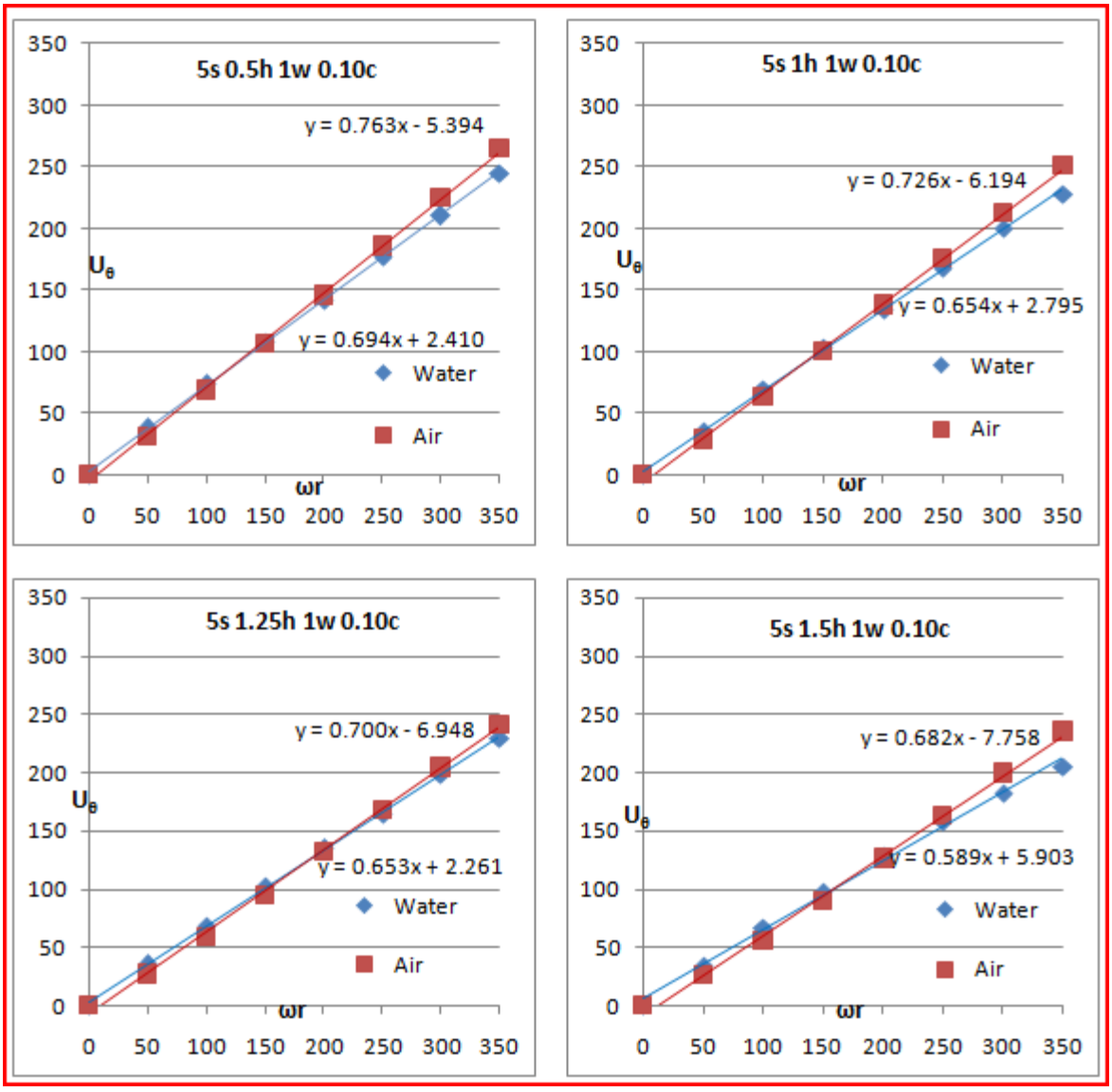

Figure 47. Average swirl velocity in the cavity with teeth on rotor.

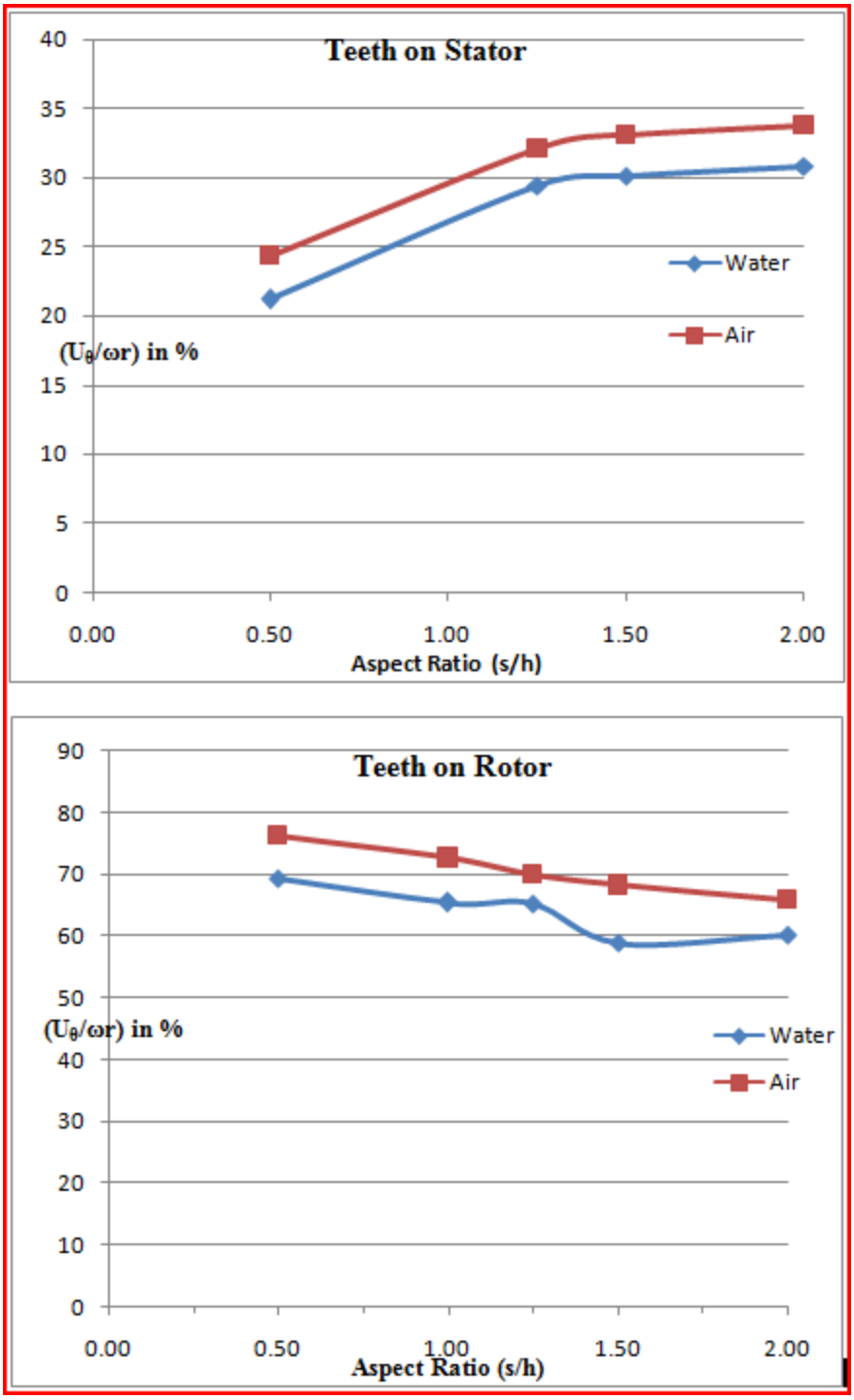

Figure 48. Average induced swirl velocity ratio for a stator and rotor.

The ratio of the swirl induced in the cavity to the tangential speed of the rotor decreases with increasing aspect ratio for a tooth on rotor. The tooth on stator cases illustrate the opposite trend with this ratio increasing with increasing aspect ratio. **Figure 48** shows that the swirl induced in the case of teeth on rotor are ~70% of the shaft speed while it is at close to ~30% for a seal with teeth on stator. The average values of the swirl velocity is slightly higher for air as compared to that of water. The compressible effects of air seem to help increase the average swirl in the cavity. This effect coupled with less viscosity of air leads to lower dissipation of swirl momentum. Hence the average swirl velocity is higher for air. Also, the averaged swirl velocity increases with increasing cavity depth due to increase in the rotating surface area. The observed rule of thumb for the amount of swirl present in the cavity is to calculate the difference in the cavity surface speed and that of the opposing smooth wall. The average tangential speed in the cavity will be 30% for tooth on stator and 70% for tooth on rotor.

An interesting result is the asymptotic increase in this ratio in the case of teeth on stator, and an asymptotic decrease in the ratio for teeth on rotor with increasing aspect ratio (increasing shallowness of the cavity).So, if it comes to placing a larger number of teeth between a given space for decreasing leakage across the seal, one can place deeper cavities with teeth on rotor and could consider lesser number of teeth for teeth on stator. While the former approach would make it more effective and also lead to stricter operational constraints, the latter one would reduce cost and operational effort.

7. SUMMARY

The dependence of flow parameters, γ and C_d on the seal clearance and cavity depth has been studied. The carry-over coefficients for all the cavities are similar in most of the cases showing that the cavities dissipate energy in a similar manner. The discharge coefficients are dependent on the geometric parameters such as clearance and cavity depth. The behavior of first tooth has been established to be different from other teeth. The work has also looked at exceptionally high shaft speeds of 350 m/s while establishing the dependence of the flow parameters on the shaft speed. The difference in flow fields for compressible and incompressible working fluid has been presented in terms of these flow parameters for both tooth on stator seal and tooth on rotor seal.

For a fixed Reynolds number, the effect of changing Taylors number is seen in the formation of large recirculation zones and completely diverted flow recirculation zones. The formation of SRZ's is prominent for incompressible flow for both tooth on stator and tooth on rotor seals. For compressible flow regimes, SRZ's are formed only in a seal with tooth on rotor. Increasing shaft speeds also causes formation of vortices under the teeth for a seal with incompressible working fluid beyond a critical c/s ratio of 0.08. A critical Taylors number in the range of 500-600 is observed at which SRZ's begin to form for both tooth on stator and tooth on rotor seals.

For a seal with tooth on stator with incompressible fluid, higher clearances and lower Taylors numbers are not advisable. Lower clearances with high Taylors numbers also make a seal inefficient. The effect of cavity depth on the flow parameters is minimal in this case. For compressible flow regimes in tooth on stator seal, lower clearances and

higher Taylors numbers perform better. A clearance-pitch ratio of greater than 0.08 is not advisable for compressible working fluid in a tooth on stator seal. If it is inevitable to use seals with $c/s \geq 0.08$, increasing the operational shaft speed of the turbomachine will help with better seal performance.

For a tooth on rotor seal with incompressible fluid, increasing the shaft speed beyond 200 m/s makes the seal perform efficiently regardless of the c/s ratio. A very high c/s ratio of 0.20 is very inefficient at all Taylors numbers. A seal with pitch-depth ratio of 0.5 shows greater efficiency compared to seals with lower cavity depths. For compressible fluid flow regimes, the formation of SRZ's observed at various shaft speeds depending on the clearance of the seal. The relation between the formation of SRZ's and clearance is established in a flow map.

The average values of swirl velocity have been calculated for both water and air in a cavity for tooth on stator and tooth on rotor seals. The ratio of the swirl induced in the cavity to the shaft speed has been discussed. The average swirl velocity in the cavity will be 30% for tooth on stator and 70% for tooth on rotor.

Future studies can include the effect of changing shaft diameter which might influence the flow field due to the difference in shaft curvature. Effect of real gases can be studied by using appropriate state equations for gases. It might be important to establish the effect of changing viscosity of gases on the leakage estimation.

REFERENCES

[1] Sneck, 1974, "Labyrinth Seal Literature Survey," J. Lub. Tech., **96**, pp. 579-581.

[2] Martin, H., 1908, "Labyrinth Packings," Engineering, **10**, pp. 35-36.

[3] Egli, A., 1935, "The Leakage of Steam through Labyrinth Seals," Trans. ASME, **57**, pp. 115-122.

[4] Hodkinson, B., 1939, "Estimation of the Leakage through a Labyrinth Gland," Proceedings of the Institution of Mechanical Engineers, **141**, pp. 283-288.

[5] Heffner, F. E., 1960, "A General Method for Correlating Labyrinth-Seal Leak-Rate Data," ASME Journal of Basic Engineering, **82**, pp. 265-275.

[6] Vermes, G., 1961, "A Fluid Mechanics Approach to the Labyrinth-Seal Leakage Problem," ASME Journal of Basic Engineering, , **83**, pp. 161-169.

[7] Morrison, G. L., and Al-Ghasem, A., 2007, "Experimental and Computational Analysis of a Gas Compressor Windback Seal," GT2007-27986, Proceedings of ASME Turbo Expo 2007, Montreal, Canada, May 14-17.

[8] Saikishan, S., and Morrison, G.L., 2009, "Labyrinth Seal Lekage Equation," M.S., Texas A&M University, College Station.

[9] Jeri, J., 1948, "Flow through Straight-through Labyrinth Seals," Proceedings of the Seventh International Congress of Applied Mechanics, **2**, pp. 70-82.

[10] Benvenuti, E., 1980, "Analytical and Experimental Development of Labyrinth Seals for Process Centrifugal Compressors," Proceedings of the 25th Annual International Gas Turbine Conference and Exhibition, New Orleans, LA., March 9-13, 1980.

[11] Waschka, W., Wittig, S., Kim, S., Scherer, T.,, 1993, "Heat Transfer and Leakage in High-Speed Rotating Stepped Labyrinth Seals," AGARD, Heat Transfer and Cooling in Gas Turbines, February.

[12] Waschka, W., Wittig, S., 1990, "Influence of High Rotational Speeds on the Heat Transfer and Discharge Coefficients in Labyrinth Seals," ASME 90-GT-330, Brussels, June 11-14.

[13] Yamada, Y., 1962, "Resistance of a Flow through an Annulus with an Inner Rotating Cylinder," Bulletin of JSME, **5**, pp. 302-310.

[14] Rao, K. V., and Narayanamurthi, R.G., 1973, "An Expreimental Study of the Performance Characteristics of Labyrinth Seals," India Engineering Journal - Mechanical Engineering, **53**, pp. 277-281.

[15] Demko, J. A., 1986, "The Prediction and Measurement of Incompressible Flow in a Labyrinth Seal," Ph.D. dissertation, Texas A&M University, College Station.

[16] Johnson, M. C., 1989, "Development of a 3-D Laser Doppler Anemometry System with Measurements in Annular and Labyrinth Seals," Ph.D. dissertation, Texas A&M University, College Station.

[17] Guide, Fluent User Services., Fluent Inc., Lebanon, New Hampshire.

[18] Kaye, E., 1958, "Modes of Adiabatic and Diabatic Fluid Flow in an Annulus with an Inner Rotating Cylinder," ASME Transactions, **123**, pp. 753-765.

APPENDIX A

The standard *k*- ε model is a semi-empirical model based on model transport equations for the turbulence kinetic energy (*k*) and its dissipation rate (ε).In the derivation of the *k*- ε model, it was assumed that the flow is fully turbulent, and the effects of molecular viscosity are negligible.

The turbulence kinetic energy, *k*, and its rate of dissipation, ε, are obtained from the following transport equations:

$$\frac{\partial}{\partial t}(\rho k)+\frac{\partial}{\partial x_i}(\rho k u_i)=\frac{\partial}{\partial x_j}\left[\left(\mu+\frac{\mu_t}{\sigma_k}\right)\frac{\partial k}{\partial x_j}\right]+G_k+G_b-\rho\varepsilon-Y_M+S_k \tag{9}$$

$$\frac{\partial}{\partial t}(\rho \varepsilon)+\frac{\partial}{\partial x_i}(\rho \varepsilon u_i)=\frac{\partial}{\partial x_j}\left[\left(\mu+\frac{\mu_t}{\sigma_\varepsilon}\right)\frac{\partial \varepsilon}{\partial x_j}\right]+C_{1\varepsilon}\frac{\varepsilon}{k}(G_k+C_{3\varepsilon}G_b) \tag{10}$$

$$-C_{2\varepsilon}\rho\frac{\varepsilon^2}{k}+S_\varepsilon$$

Where $Y_M$represents the contribution of the fluctuating dilatation in compressible turbulence to the overall dissipation rate and for the present incompressible it can be easily set to zero.

$G_k$represents the generation of turbulence kinetic energy due to the mean velocity gradients and is given by :

$$G_k=-\rho\overline{u_i'u_j'}\frac{\partial u_j}{\partial x_i} \tag{11}$$

$G_b$is the generation of turbulence kinetic energy due to buoyancy

$$G_b = \beta g_i \frac{\mu_t}{\mathrm{Pr}_t} \frac{\partial T}{\partial x_i} \tag{12}$$

where$\mathrm{Pr}_t$is the turbulent Prandtl number for energy and $g_i$is the component of the gravitational vector in the ith direction. For the standard k- εmodels, the default value of $\mathrm{Pr}_t$is 0.85. The coefficient of thermal expansion, β, is defined as:

$$\beta = -\frac{1}{\rho}\left(\frac{\partial \rho}{\partial T}\right)_p \tag{13}$$

The turbulent (or eddy) viscosity, μ_t, is computed by combining k and εas follows:

$$\mu_t = \rho C_\mu \frac{k^2}{\varepsilon} \tag{14}$$

The buoyancy effects on $\varepsilon$are neglected simply by setting $G_b$to zero in the transport equation for ε. The degree to which $\varepsilon$is affected by the buoyancy is determined by the constant $C_{3\varepsilon}$and is given by:

$$C_{3\varepsilon} = \tanh\left|\frac{v}{u}\right| \tag{15}$$

APPENDIX B

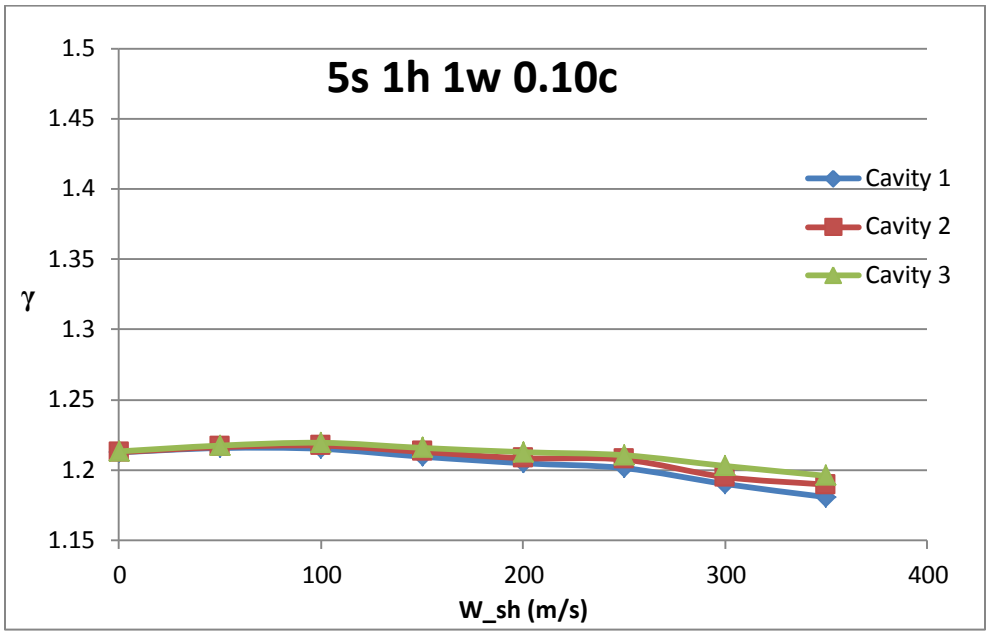
5s 1h 1w 0.10c
1.5
1.45
1.4
1.35
1.3
1.25
1.2
1.15
γ
0
100
200
300
400
W_sh (m/s)
Cavity 1
Cavity 2
Cavity 3

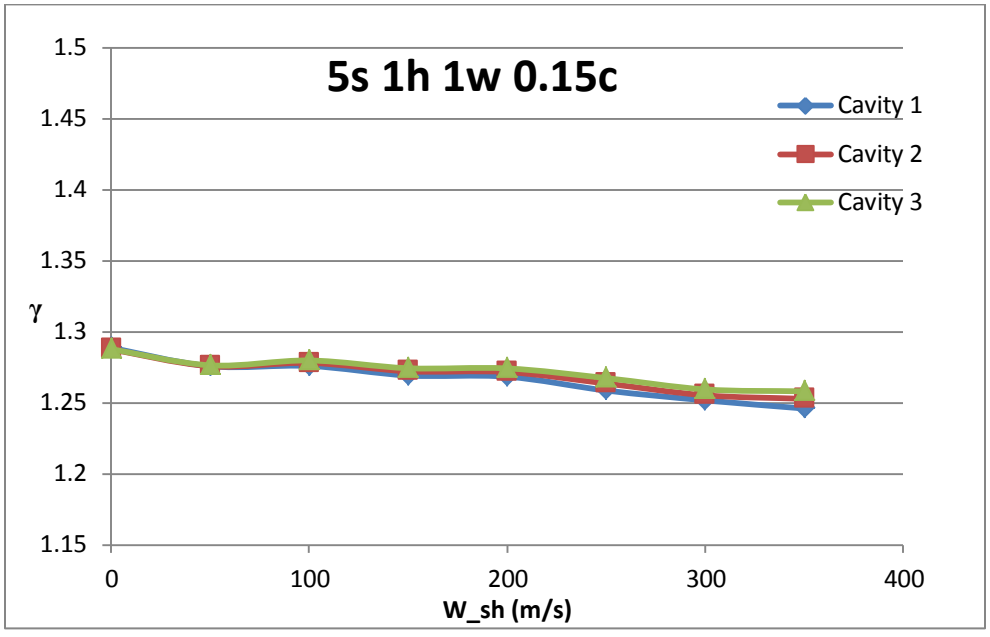
5s 1h 1w 0.15c
1.5
1.45
1.4
1.35
1.3
1.25
1.2
1.15
γ
0
100
200
300
400
W_sh (m/s)
Cavity 1
Cavity 2
Cavity 3

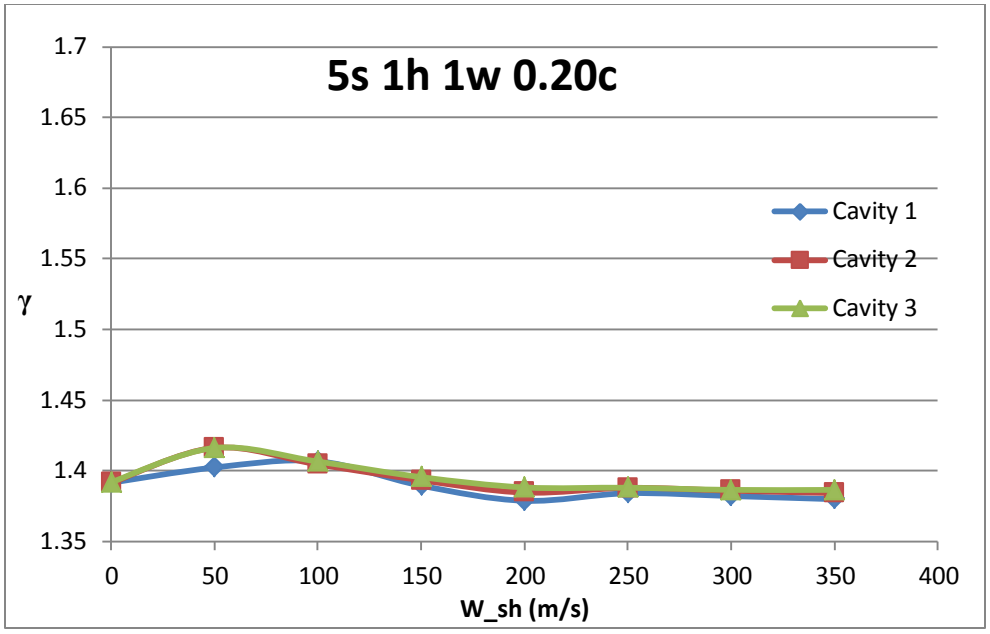
5s 1h 1w 0.20c
1.7
1.65
1.6
1.55
1.5
1.45
1.4
1.35
γ
0
50
100
150
200
250
300
350
400
W_sh (m/s)
Cavity 1
Cavity 2
Cavity 3

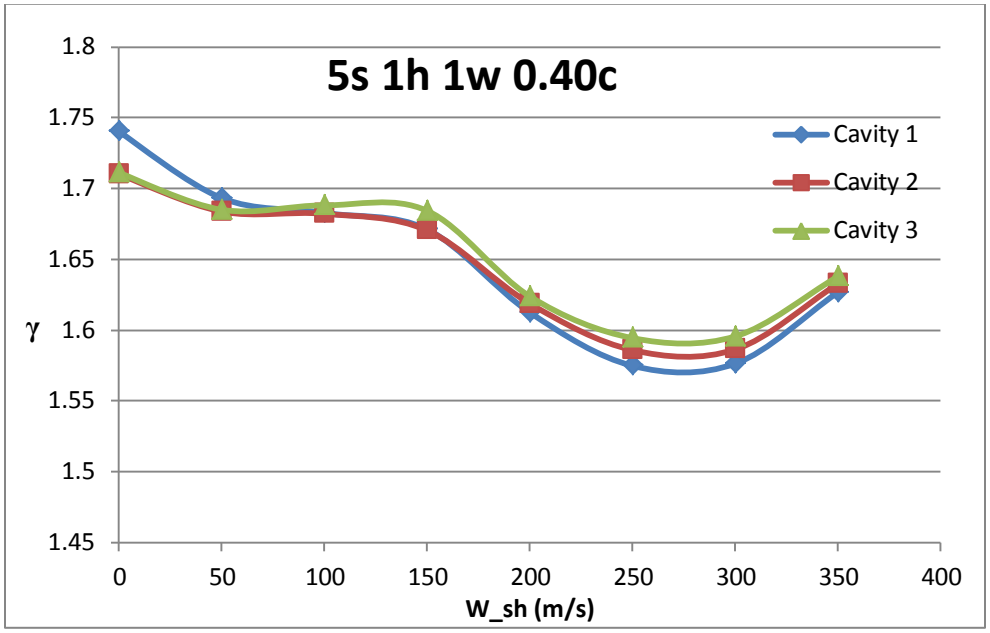
5s 1h 1w 0.40c
1.8
1.75
1.7
1.65
1.6
1.55
1.5
1.45
γ
0
50
100
150
200
250
300
350
400
W_sh (m/s)
Cavity 1
Cavity 2
Cavity 3

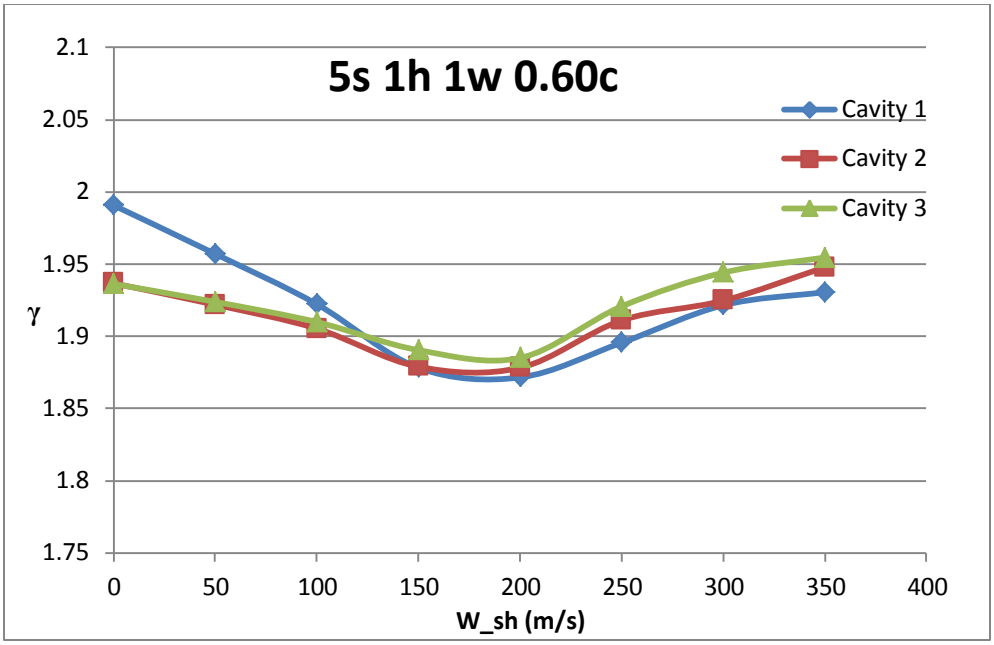
5s 1h 1w 0.60c
Cavity 1
Cavity 2
Cavity 3
γ
W_sh (m/s)
2.1
2.05
2
1.95
1.9
1.85
1.8
1.75
0
50
100
150
200
250
300
350
400

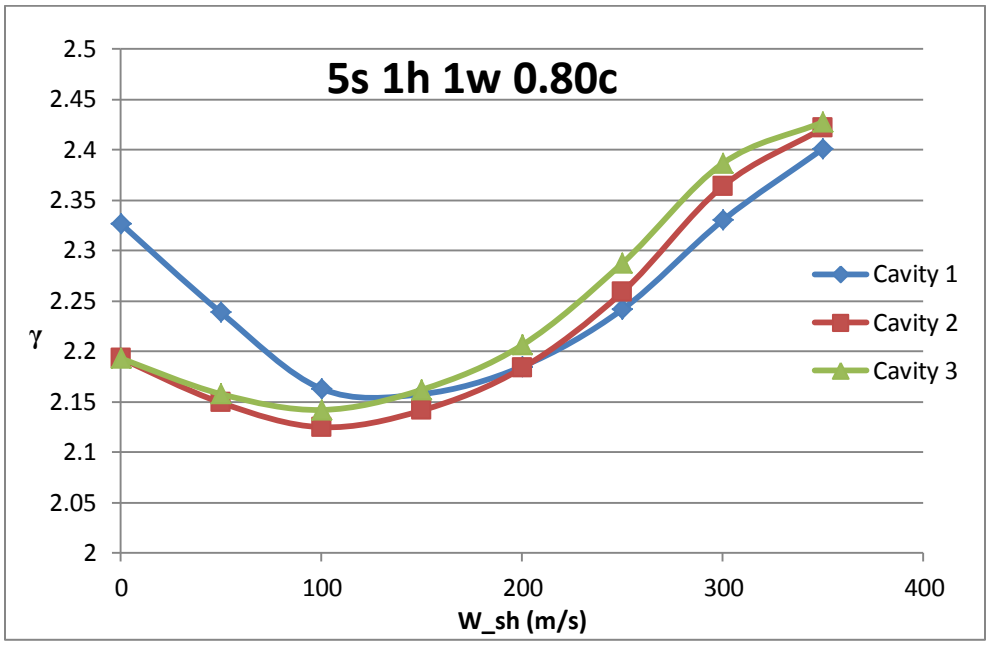
5s 1h 1w 0.80c
Cavity 1
Cavity 2
Cavity 3
γ
W_sh (m/s)
2.5
2.45
2.4
2.35
2.3
2.25
2.2
2.15
2.1
2.05
2
0
100
200
300
400

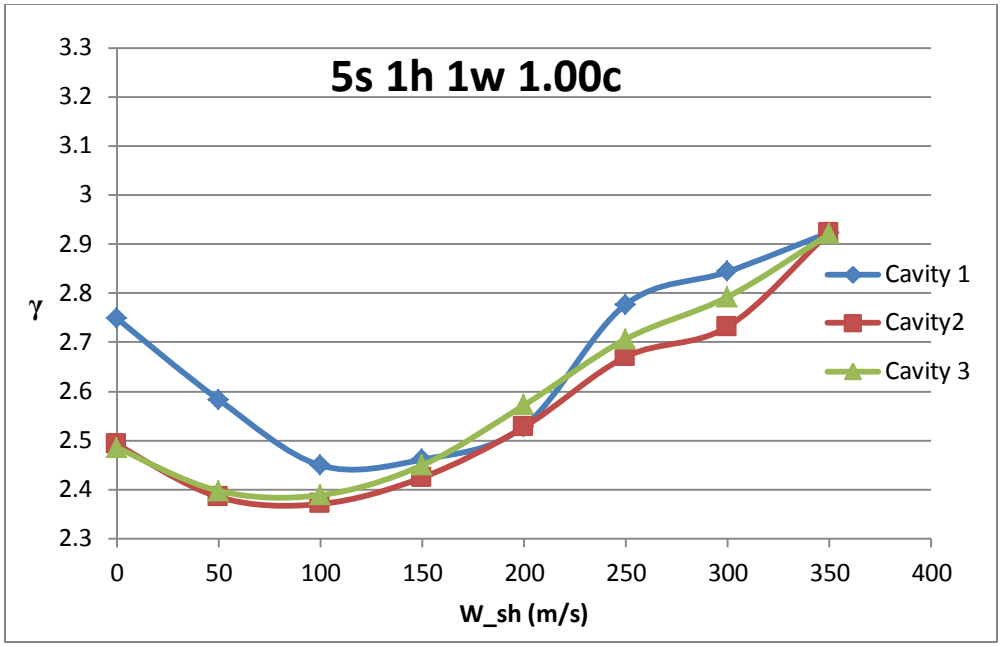

Figure 49. Effect of clearance on γ with tooth on stator for a seal with air.

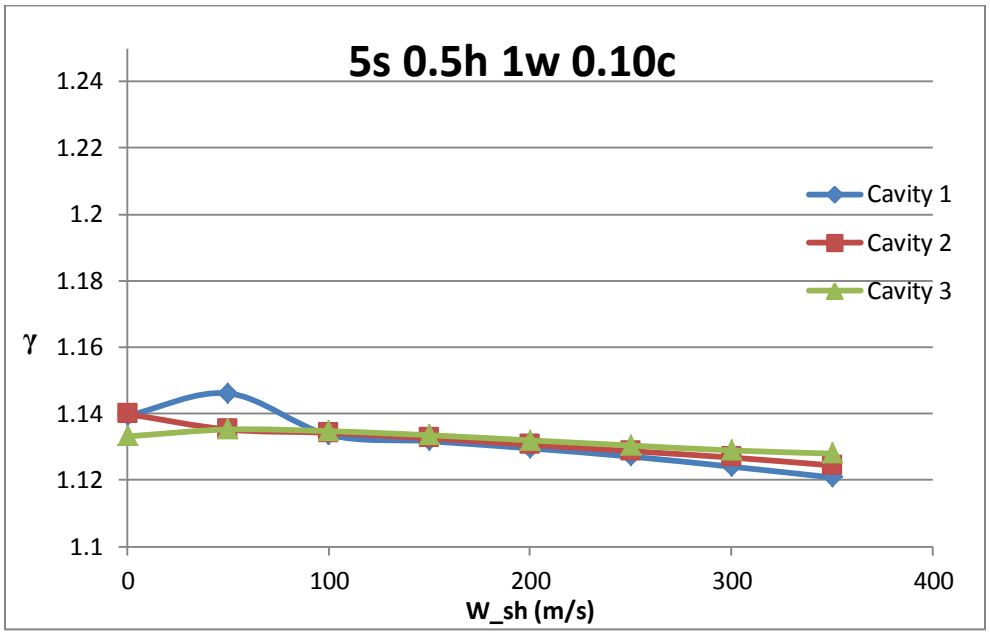

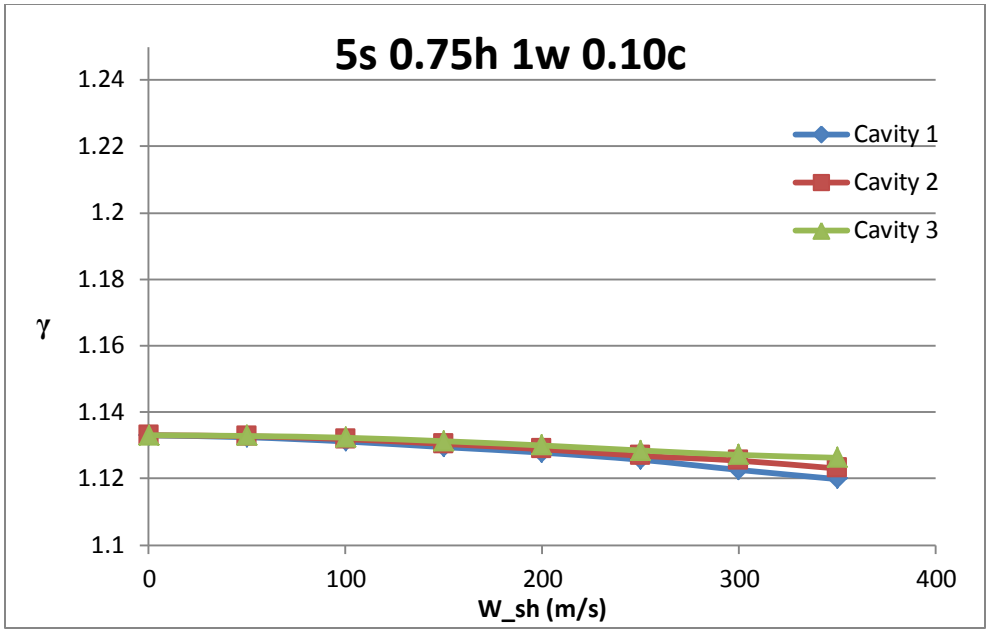
5s 0.75h 1w 0.10c
1.24
1.22
1.2
1.18
γ
1.16
1.14
1.12
1.1
0
100
200
300
400
W_sh (m/s)
Cavity 1
Cavity 2
Cavity 3

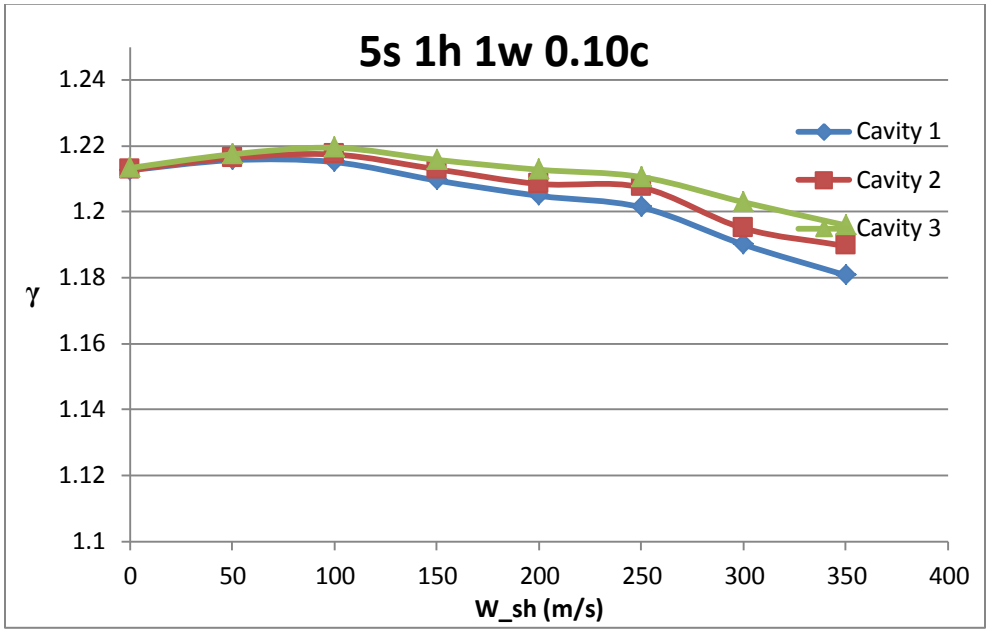
5s 1h 1w 0.10c
1.24
1.22
1.2
1.18
γ
1.16
1.14
1.12
1.1
0
50
100
150
200
250
300
350
400
W_sh (m/s)
Cavity 1
Cavity 2
Cavity 3

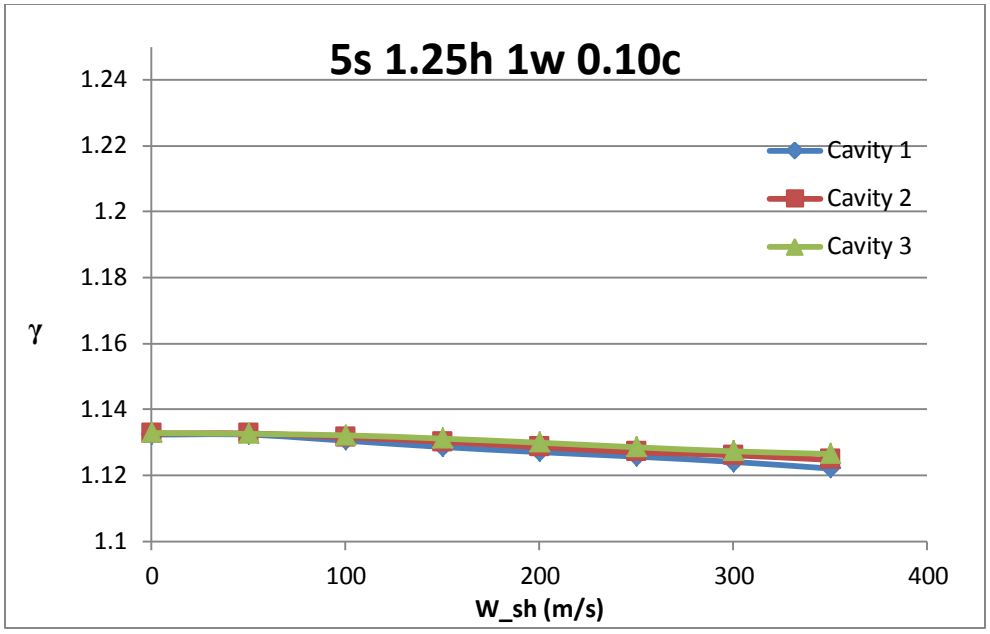
5s 1.25h 1w 0.10c
1.24
1.22
1.2
1.18
1.16
1.14
1.12
1.1
γ
0
100
200
300
400
W_sh (m/s)
Cavity 1
Cavity 2
Cavity 3

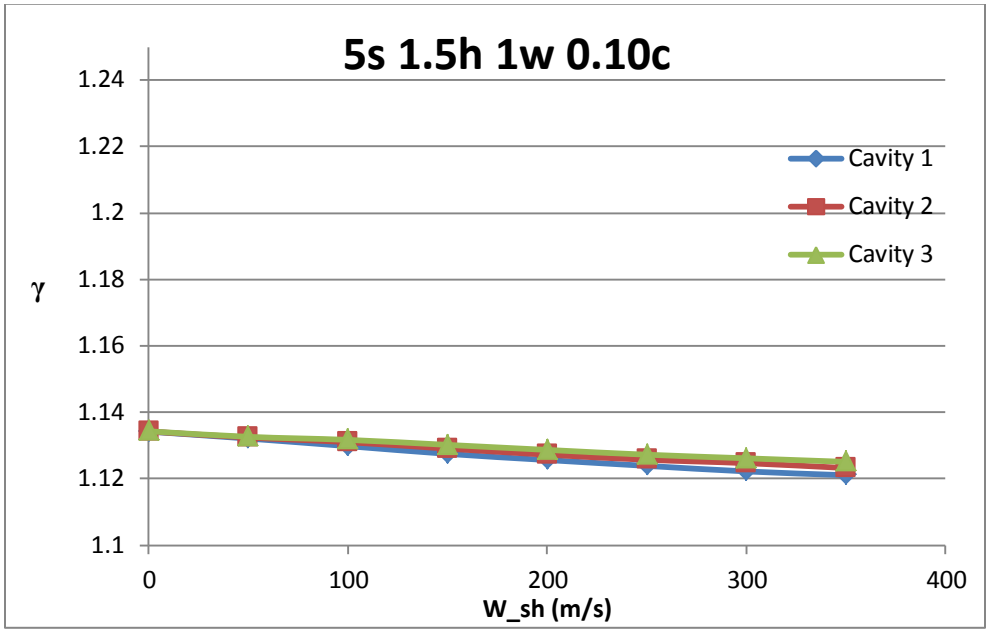
5s 1.5h 1w 0.10c
1.24
1.22
1.2
1.18
1.16
1.14
1.12
1.1
γ
0
100
200
300
400
W_sh (m/s)
Cavity 1
Cavity 2
Cavity 3

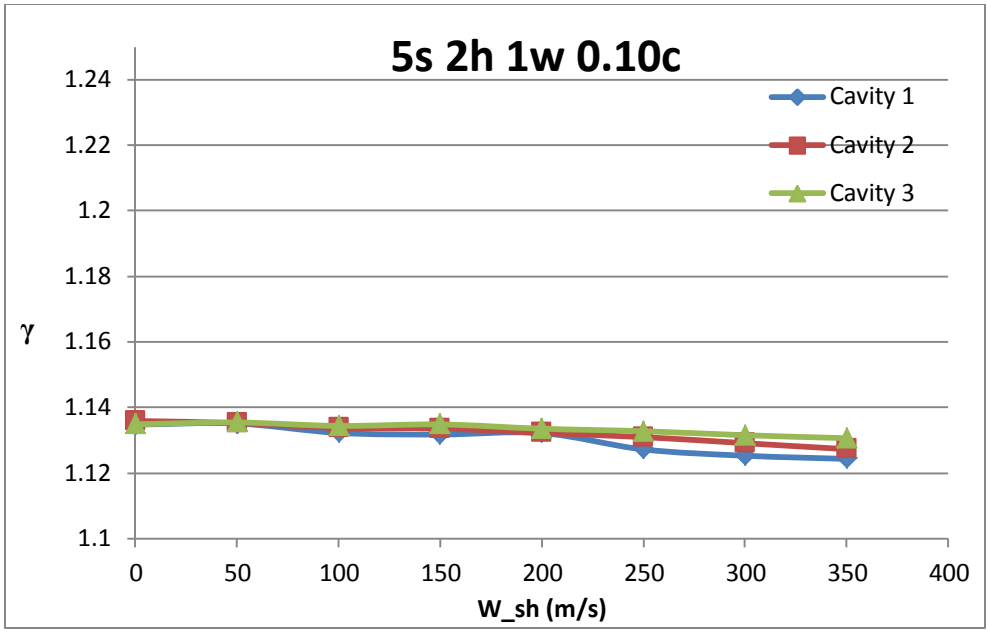

Figure 50. Effect of pitch-height ratio on γ with tooth on stator for a seal with air.

APPENDIX C

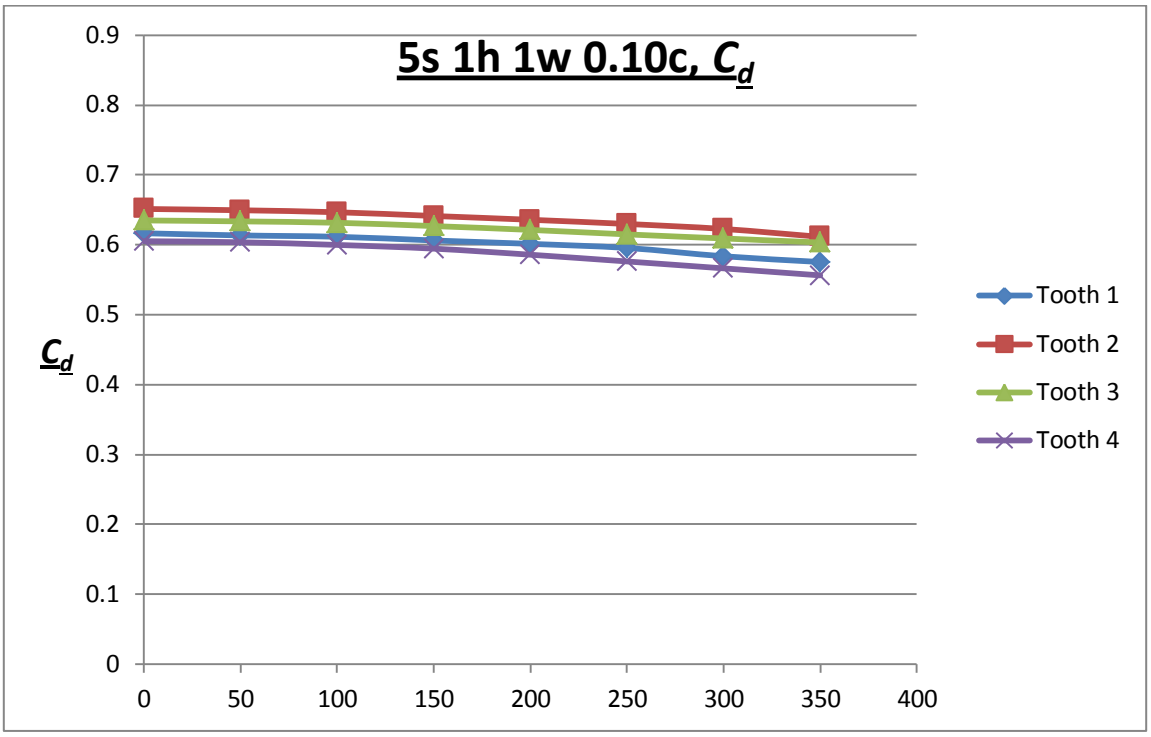
5s 1h 1w 0.10c, C_d
C_d
0.9
0.8
0.7
0.6
0.5
0.4
0.3
0.2
0.1
0
0
50
100
150
200
250
300
350
400
Tooth 1
Tooth 2
Tooth 3
Tooth 4

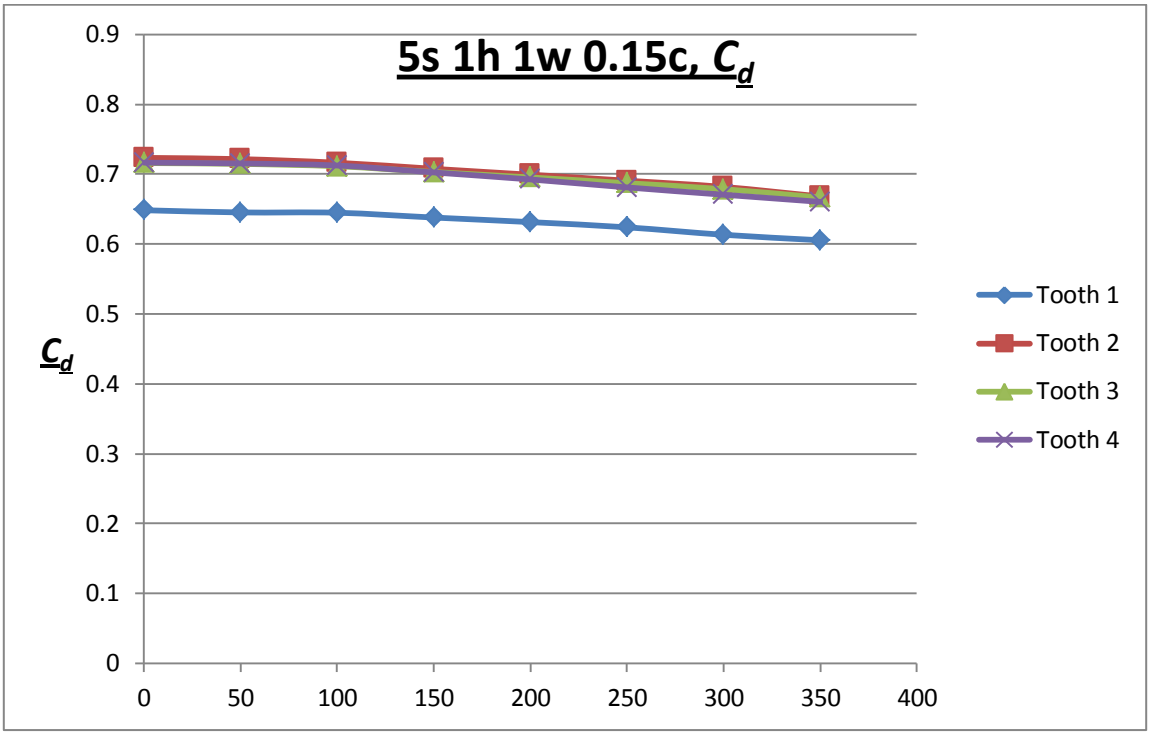
5s 1h 1w 0.15c, C_d
C_d
0.9
0.8
0.7
0.6
0.5
0.4
0.3
0.2
0.1
0
0
50
100
150
200
250
300
350
400
Tooth 1
Tooth 2
Tooth 3
Tooth 4

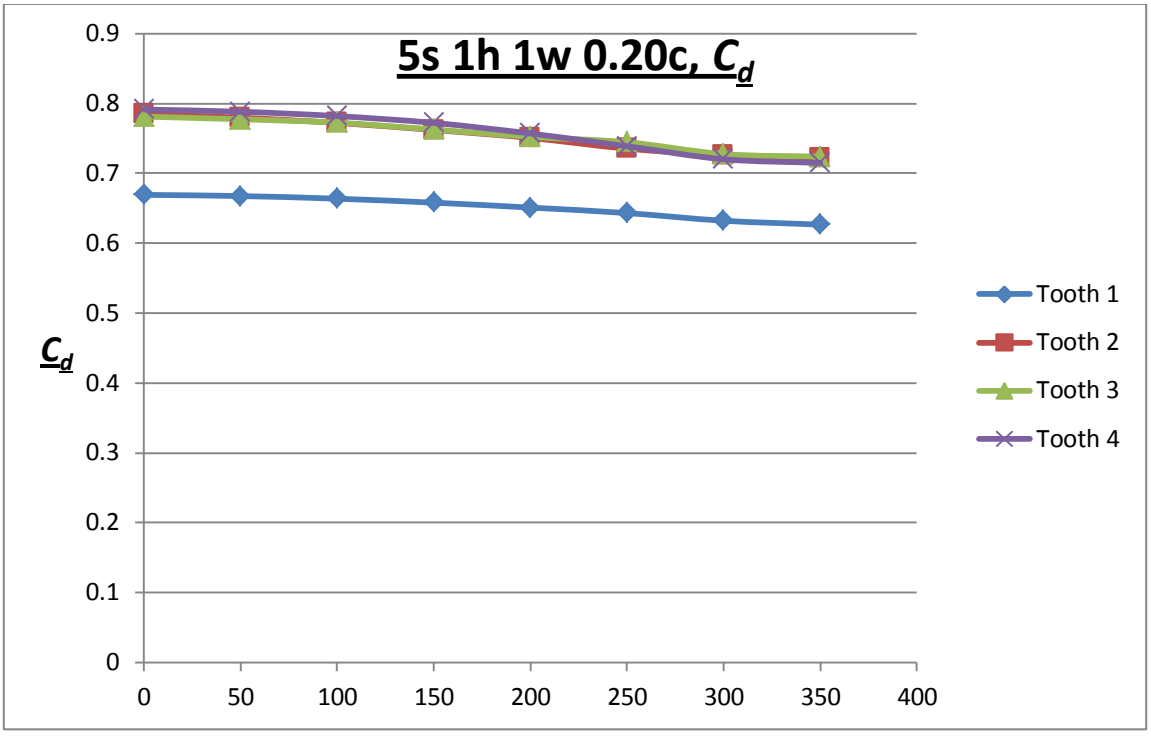
5s 1h 1w 0.20c, C_d
C_d
0.9
0.8
0.7
0.6
0.5
0.4
0.3
0.2
0.1
0
0
50
100
150
200
250
300
350
400
Tooth 1
Tooth 2
Tooth 3
Tooth 4

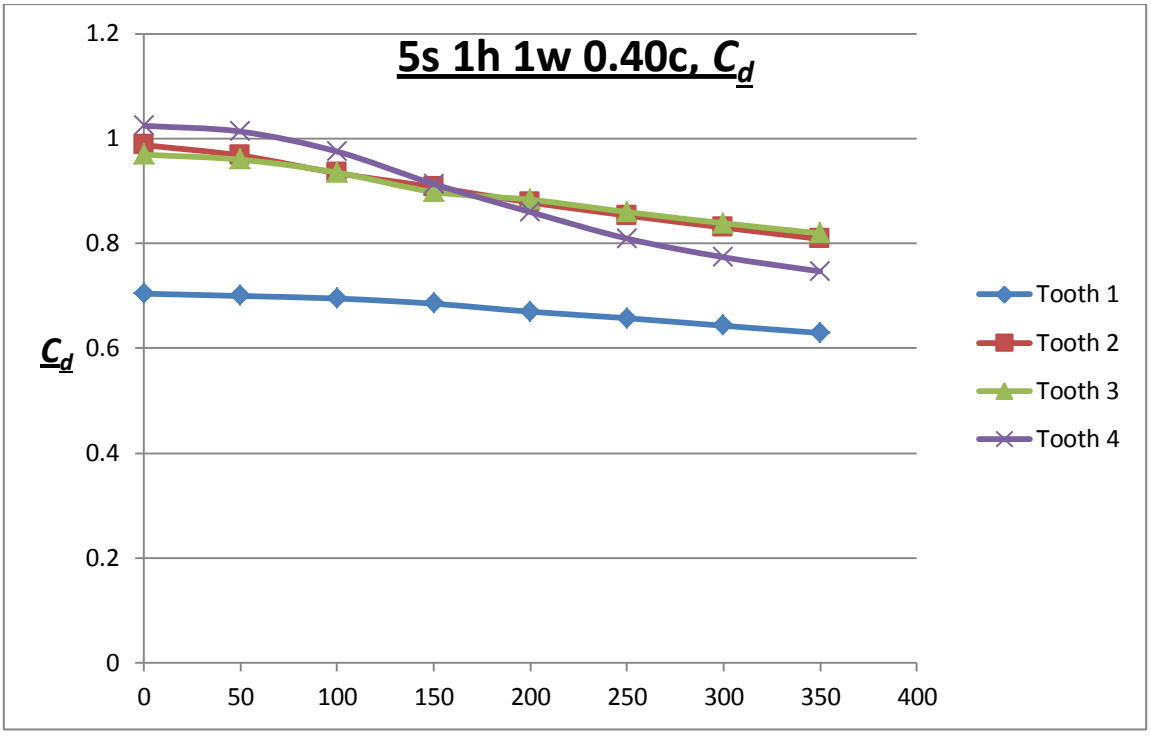
5s 1h 1w 0.40c, C_d
C_d
1.2
1
0.8
0.6
0.4
0.2
0
0
50
100
150
200
250
300
350
400
Tooth 1
Tooth 2
Tooth 3
Tooth 4

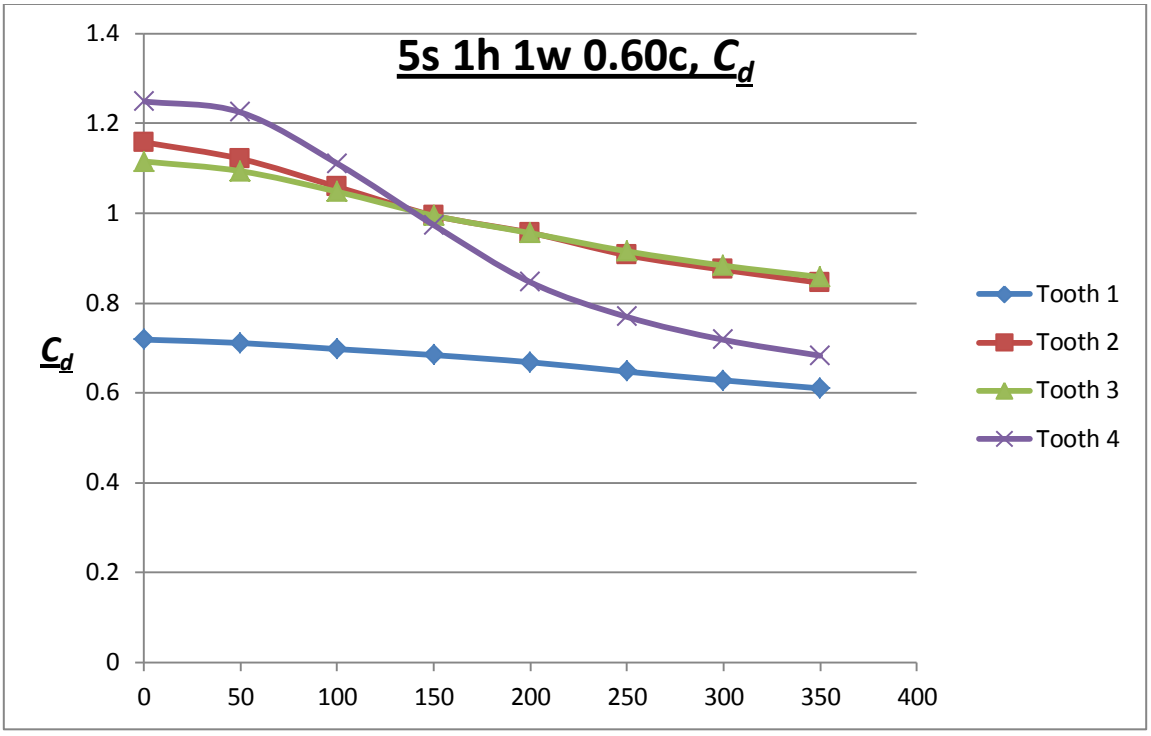
5s 1h 1w 0.60c, C_d
C_d
1.4
1.2
1
0.8
0.6
0.4
0.2
0
0
50
100
150
200
250
300
350
400
Tooth 1
Tooth 2
Tooth 3
Tooth 4

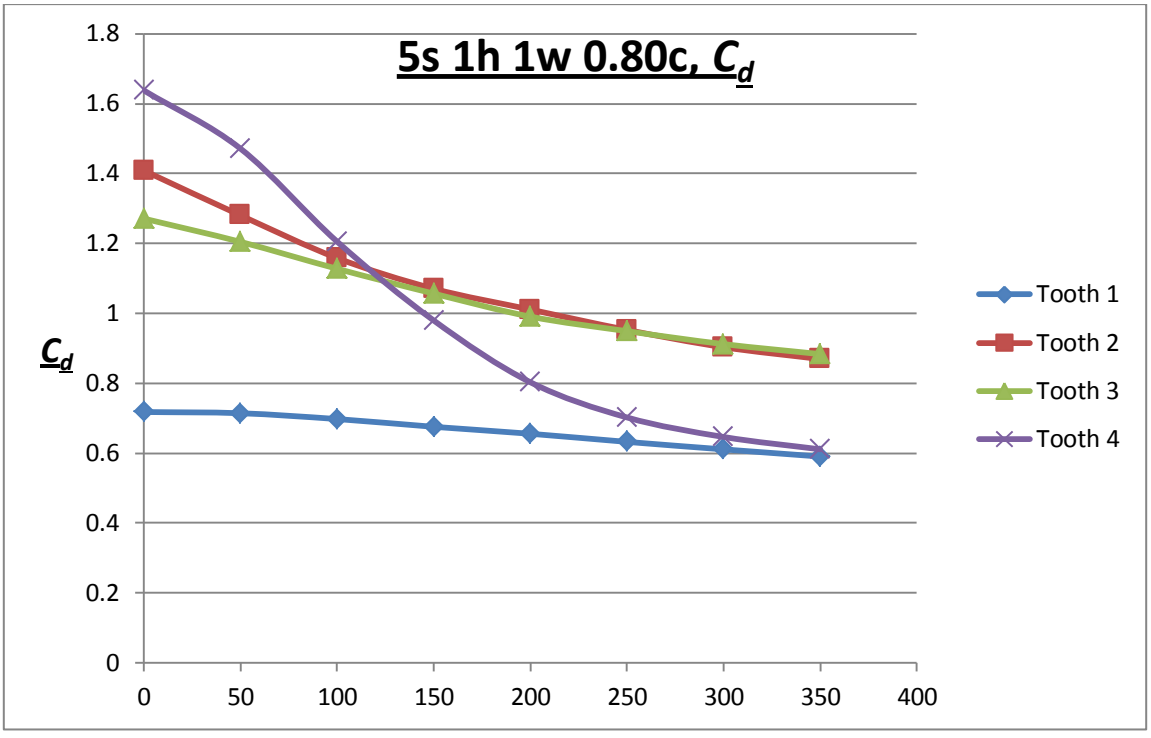
5s 1h 1w 0.80c, C_d
C_d
1.8
1.6
1.4
1.2
1
0.8
0.6
0.4
0.2
0
0
50
100
150
200
250
300
350
400
Tooth 1
Tooth 2
Tooth 3
Tooth 4

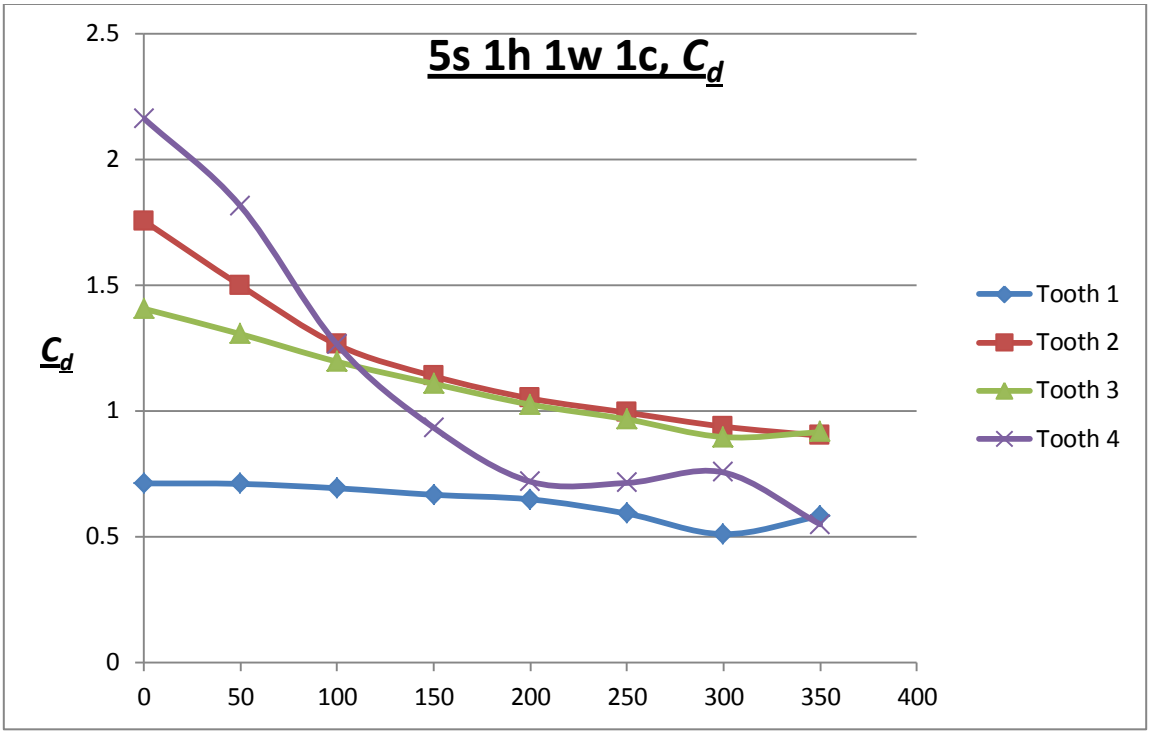

Figure 51. Effect of clearance on C_d with tooth on stator for a seal with air.

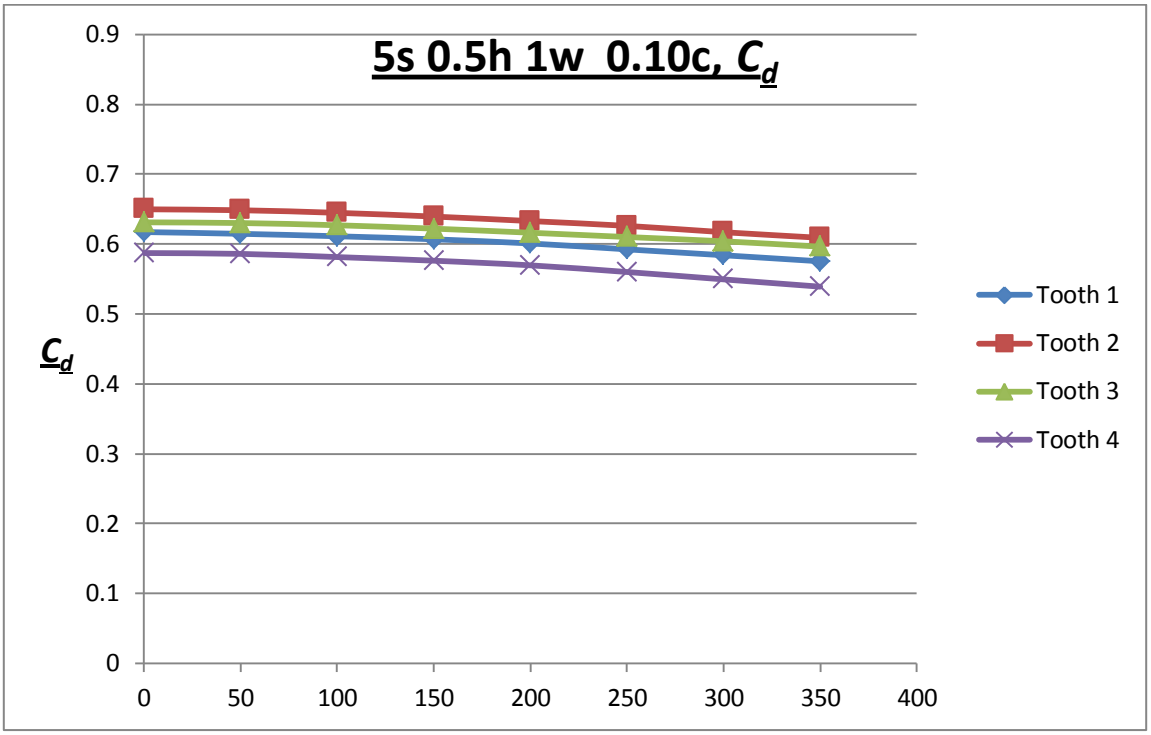

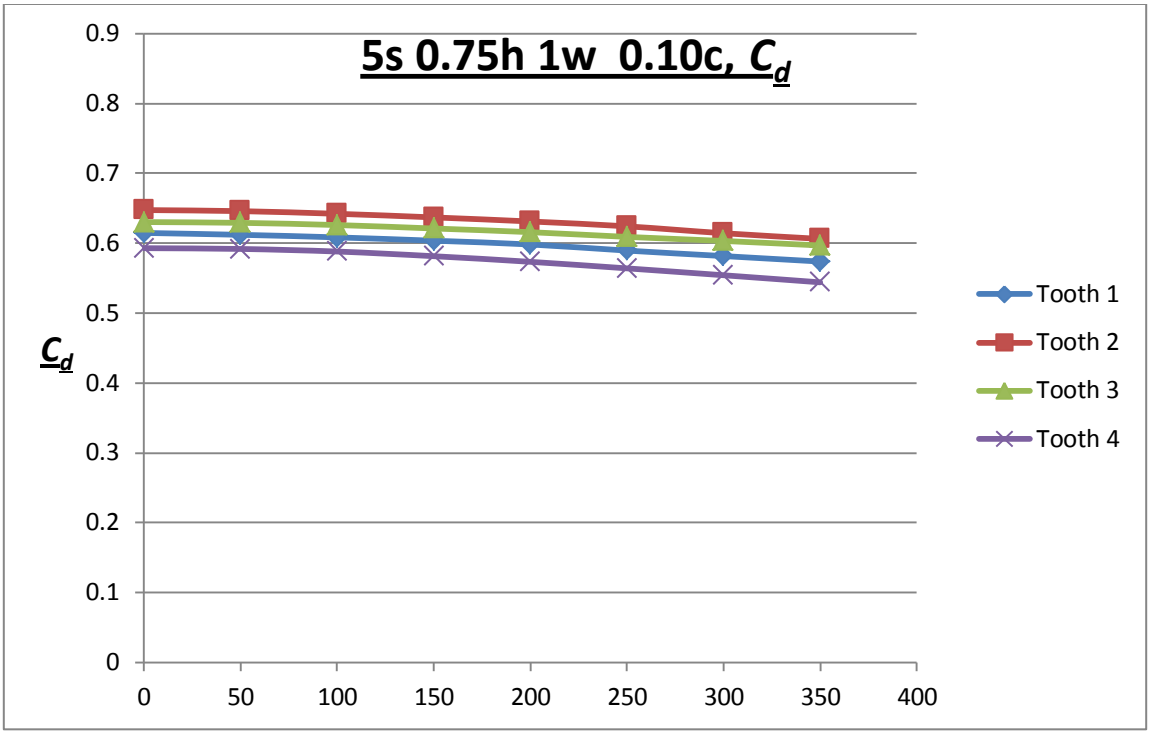
5s 0.75h 1w 0.10c, C_d
C_d
0.9
0.8
0.7
0.6
0.5
0.4
0.3
0.2
0.1
0
0
50
100
150
200
250
300
350
400
Tooth 1
Tooth 2
Tooth 3
Tooth 4

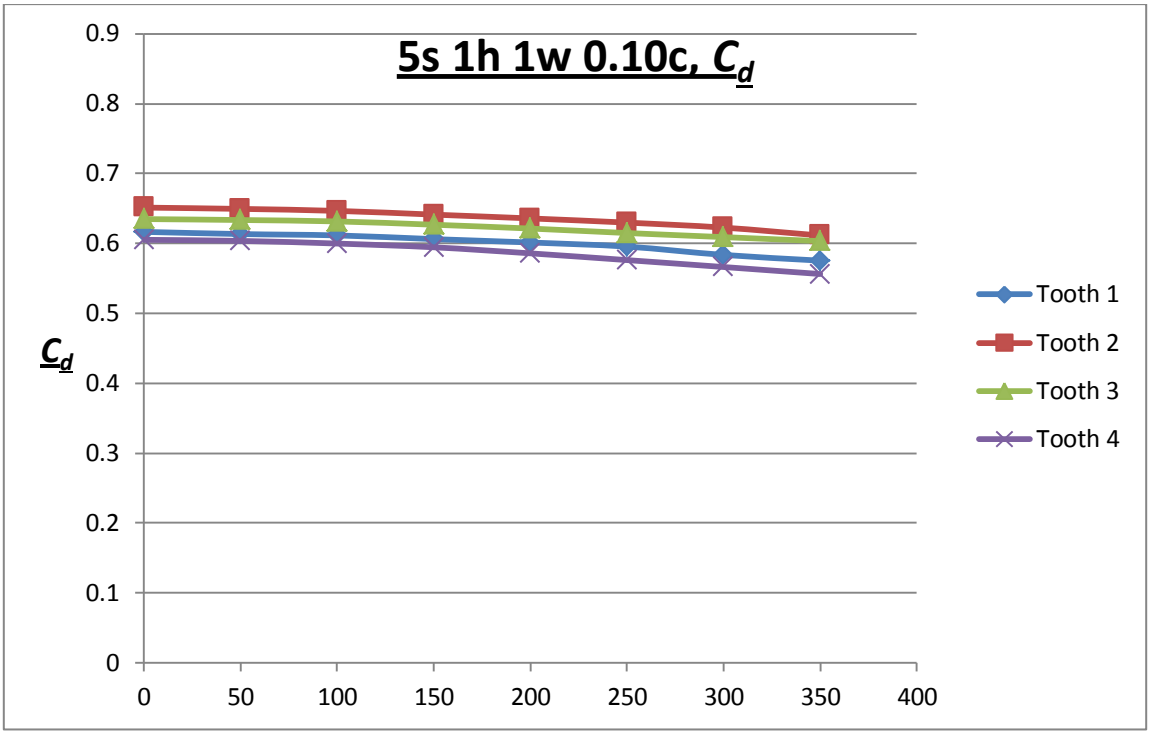
5s 1h 1w 0.10c, C_d
C_d
0.9
0.8
0.7
0.6
0.5
0.4
0.3
0.2
0.1
0
0
50
100
150
200
250
300
350
400
Tooth 1
Tooth 2
Tooth 3
Tooth 4

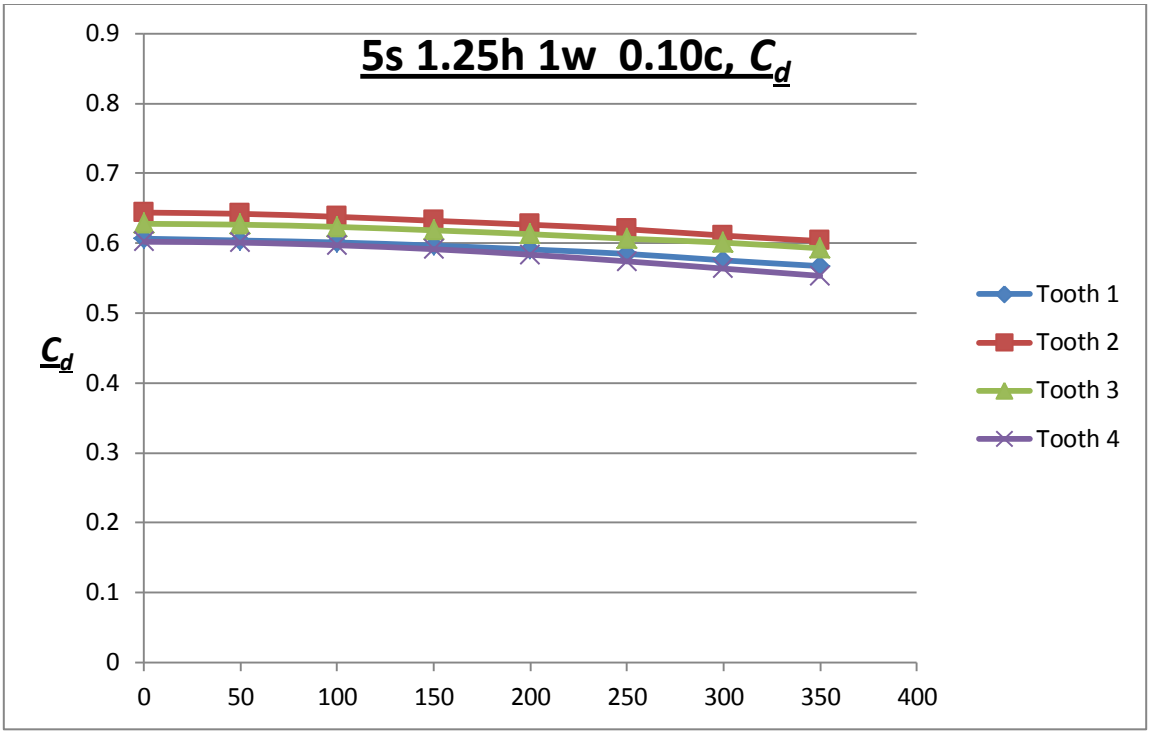
5s 1.25h 1w 0.10c, C_d
C_d
0.9
0.8
0.7
0.6
0.5
0.4
0.3
0.2
0.1
0
0
50
100
150
200
250
300
350
400
Tooth 1
Tooth 2
Tooth 3
Tooth 4

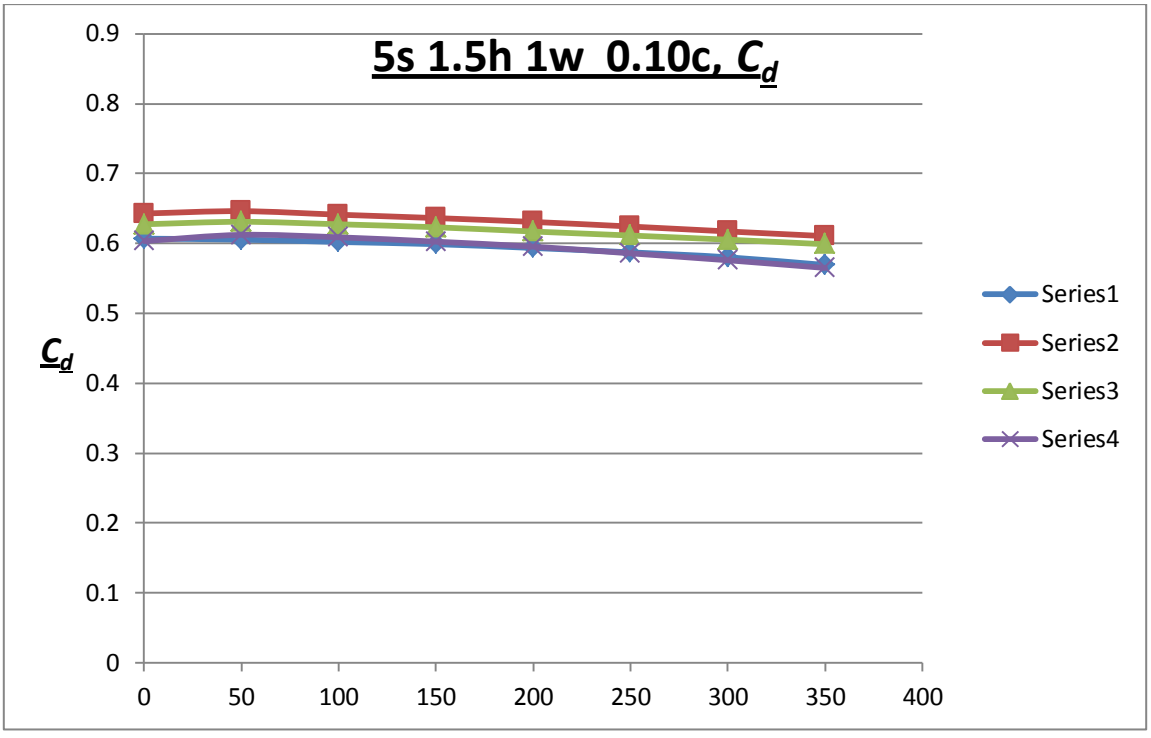
5s 1.5h 1w 0.10c, C_d
C_d
0.9
0.8
0.7
0.6
0.5
0.4
0.3
0.2
0.1
0
0
50
100
150
200
250
300
350
400
Series1
Series2
Series3
Series4

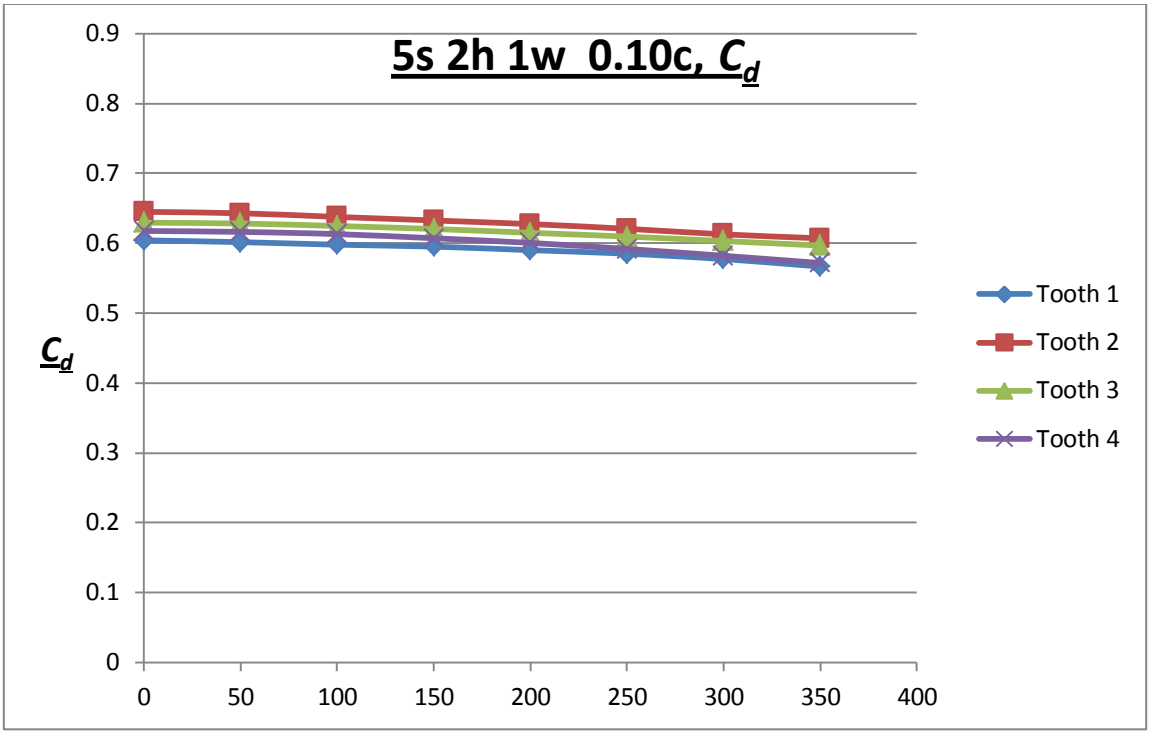

Figure 52. Effect of pitch-height ratio on C_d with tooth on stator for a seal with air.

APPENDIX D

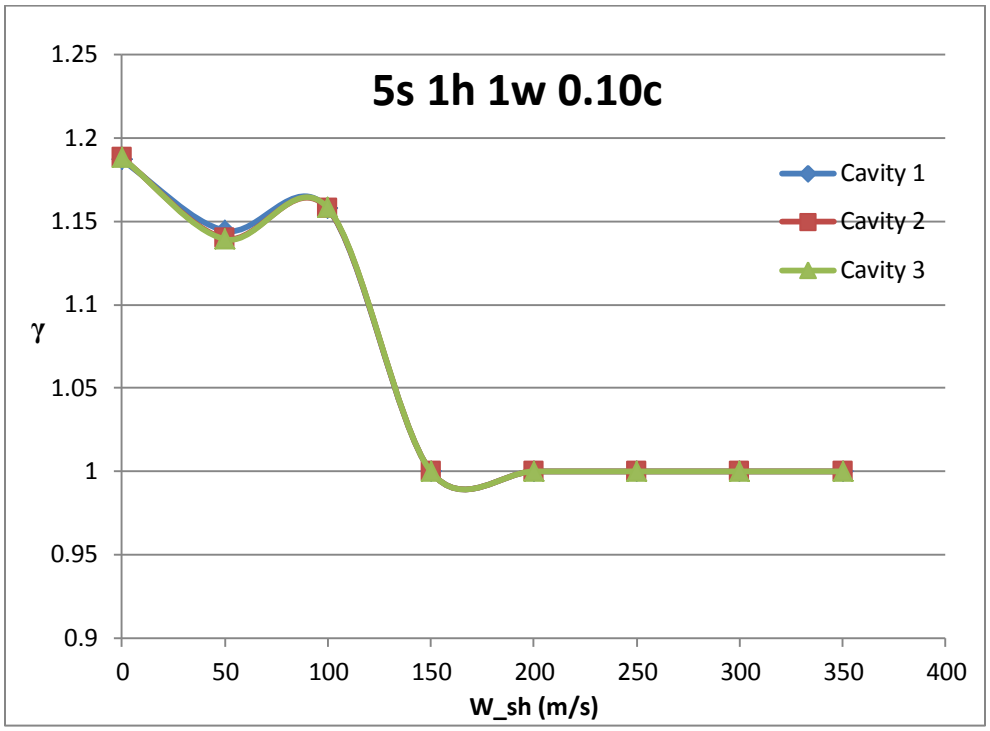
5s 1h 1w 0.10c
Cavity 1
Cavity 2
Cavity 3
γ
1.25
1.2
1.15
1.1
1.05
1
0.95
0.9
0
50
100
150
200
250
300
350
400
W_sh (m/s)

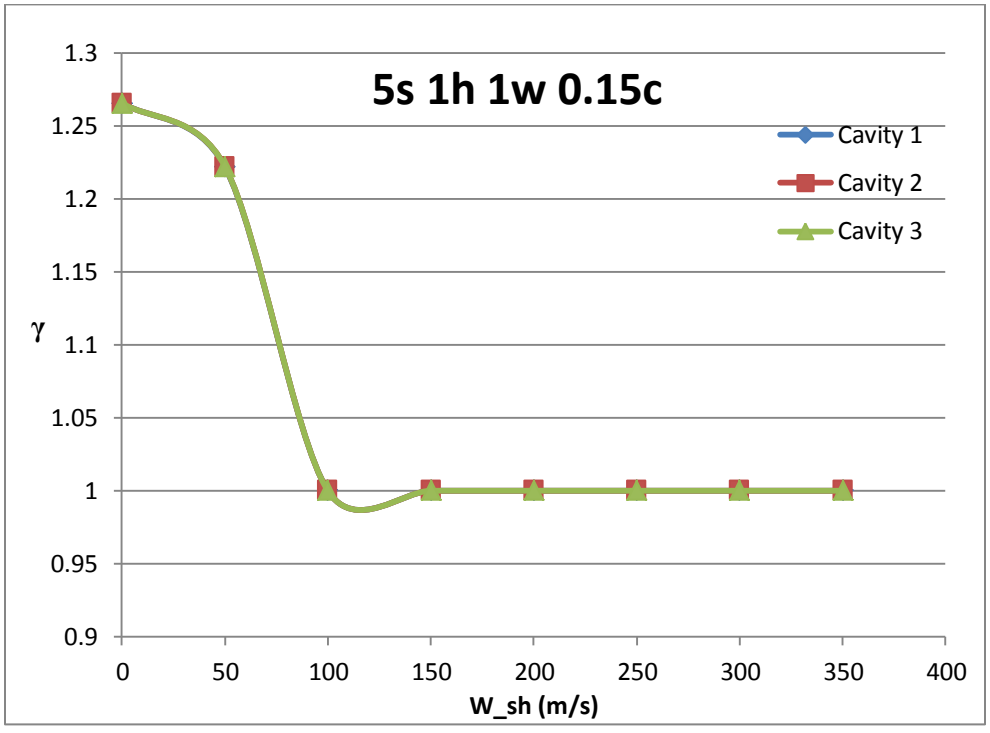
5s 1h 1w 0.15c
Cavity 1
Cavity 2
Cavity 3
γ
1.3
1.25
1.2
1.15
1.1
1.05
1
0.95
0.9
0
50
100
150
200
250
300
350
400
W_sh (m/s)

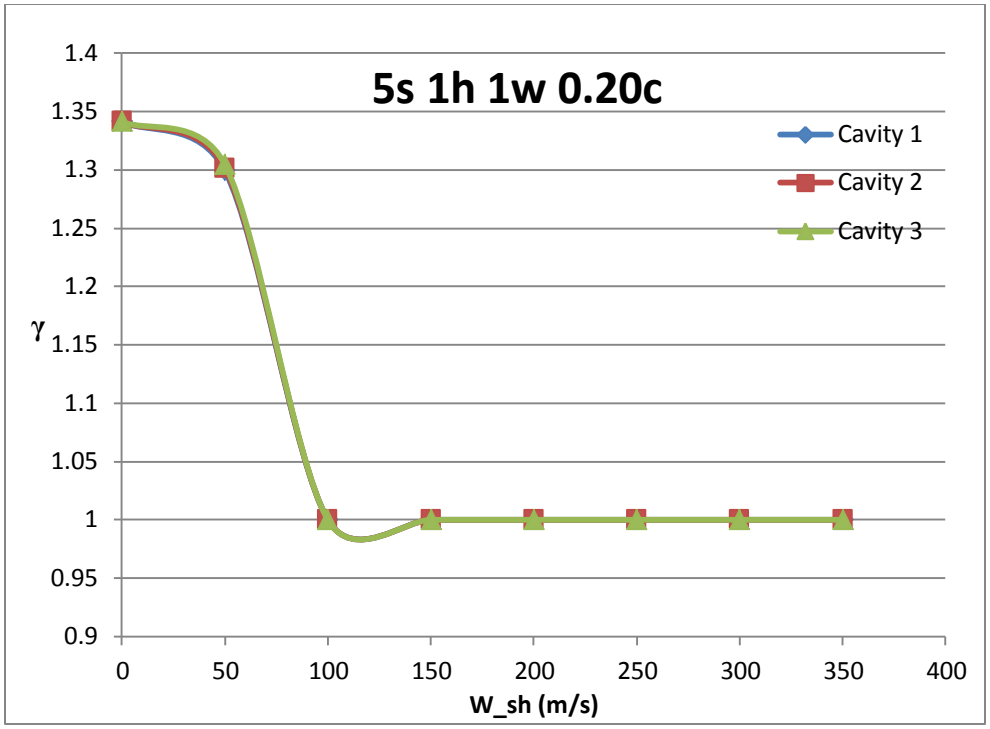
5s 1h 1w 0.20c
Cavity 1
Cavity 2
Cavity 3
γ
1.4
1.35
1.3
1.25
1.2
1.15
1.1
1.05
1
0.95
0.9
0
50
100
150
200
250
300
350
400
W_sh (m/s)

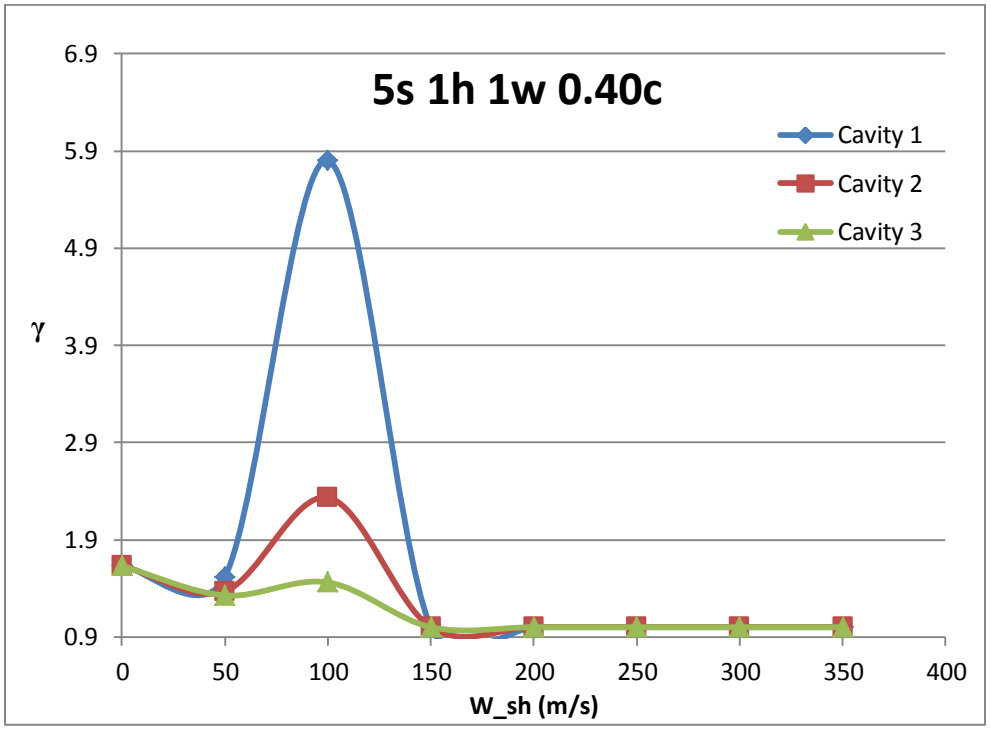
5s 1h 1w 0.40c
Cavity 1
Cavity 2
Cavity 3
γ
6.9
5.9
4.9
3.9
2.9
1.9
0.9
0
50
100
150
200
250
300
350
400
W_sh (m/s)

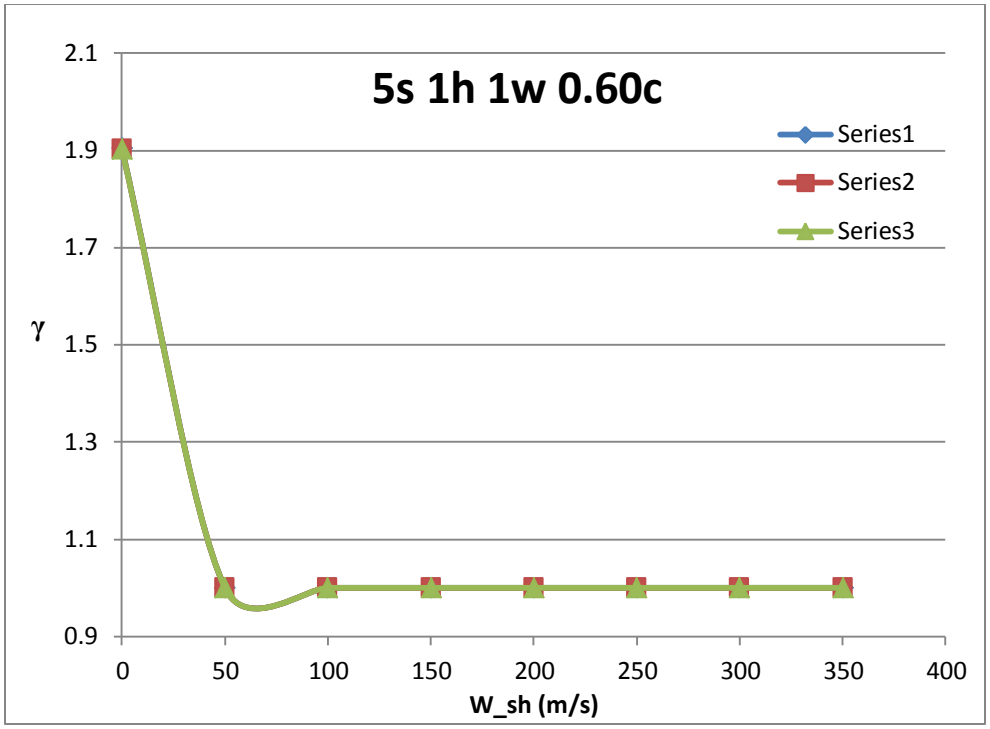
5s 1h 1w 0.60c
Series1
Series2
Series3
γ
2.1
1.9
1.7
1.5
1.3
1.1
0.9
0
50
100
150
200
250
300
350
400
W_sh (m/s)

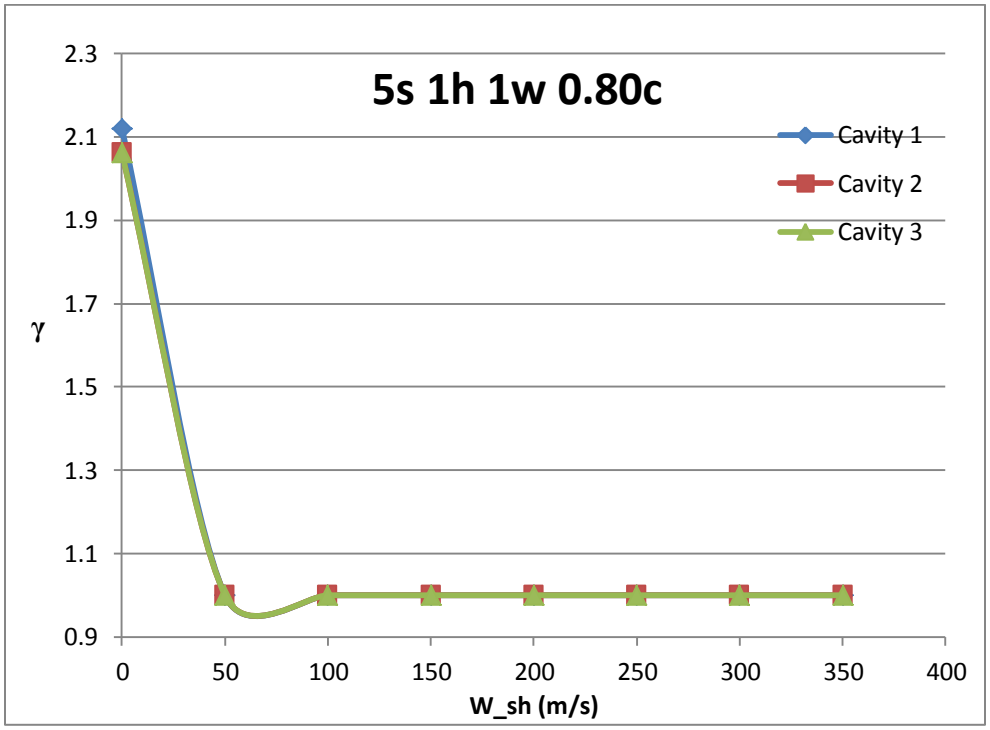
5s 1h 1w 0.80c
Cavity 1
Cavity 2
Cavity 3
γ
2.3
2.1
1.9
1.7
1.5
1.3
1.1
0.9
0
50
100
150
200
250
300
350
400
W_sh (m/s)

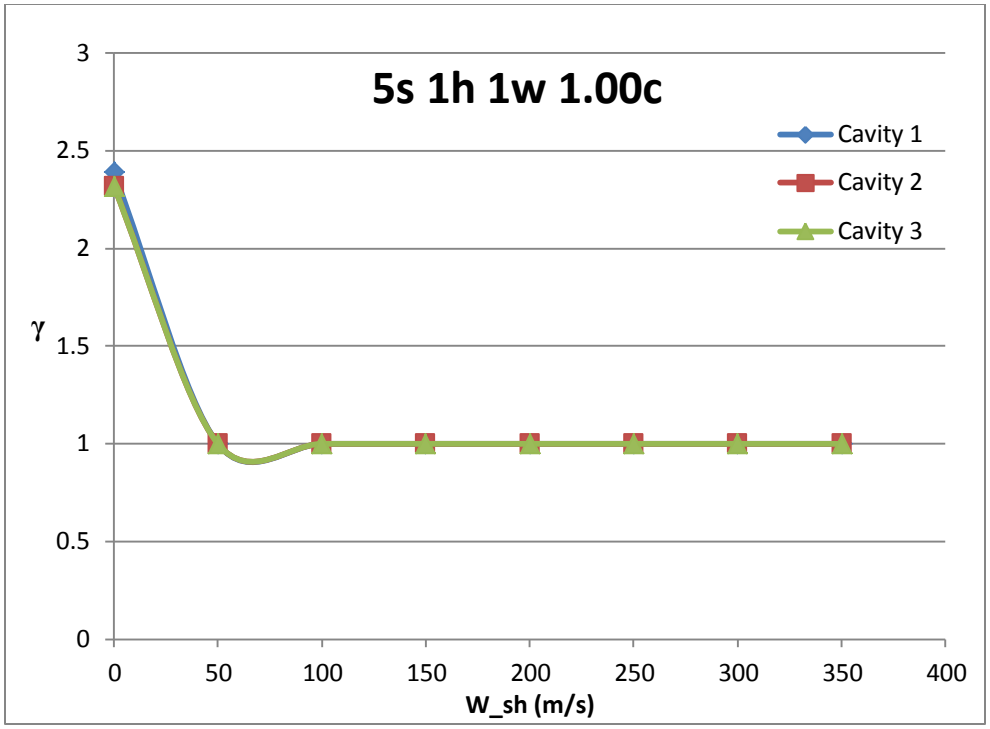

Figure 53. Effect of clearance on γ on seal with tooth on stator with water.

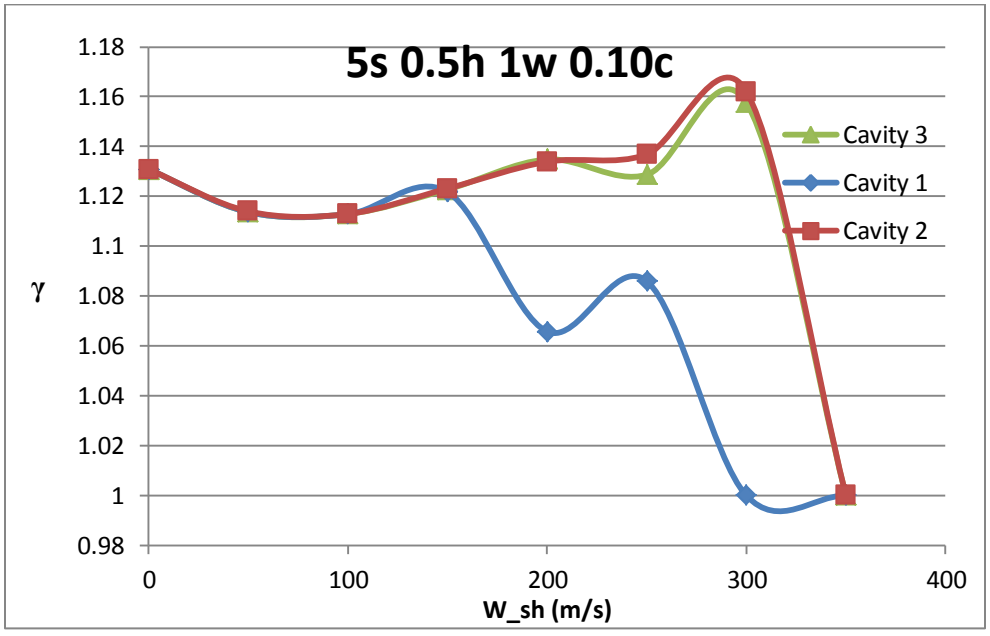

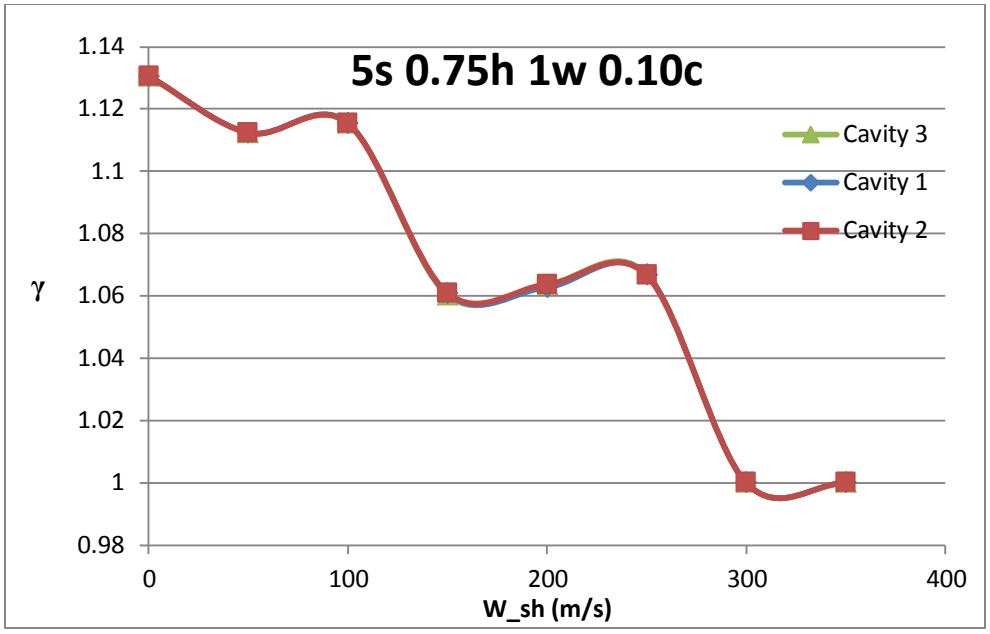
5s 0.75h 1w 0.10c
1.14
1.12
1.1
1.08
1.06
1.04
1.02
1
0.98
γ
0
100
200
300
400
W_sh (m/s)
Cavity 3
Cavity 1
Cavity 2

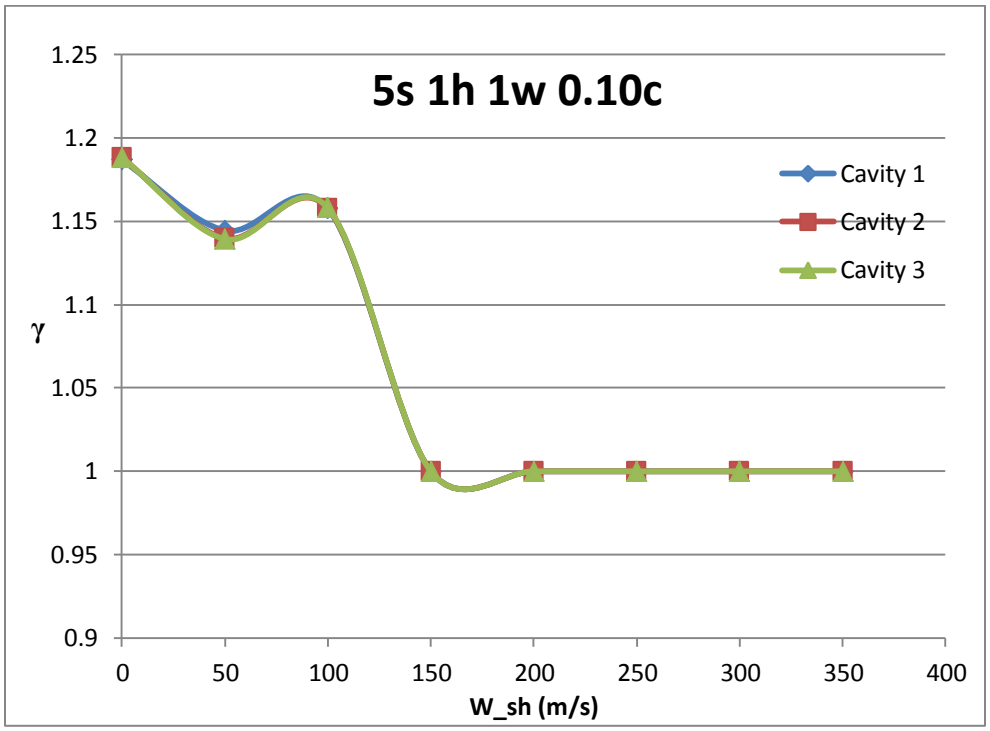
5s 1h 1w 0.10c
1.25
1.2
1.15
1.1
1.05
1
0.95
0.9
γ
0
50
100
150
200
250
300
350
400
W_sh (m/s)
Cavity 1
Cavity 2
Cavity 3

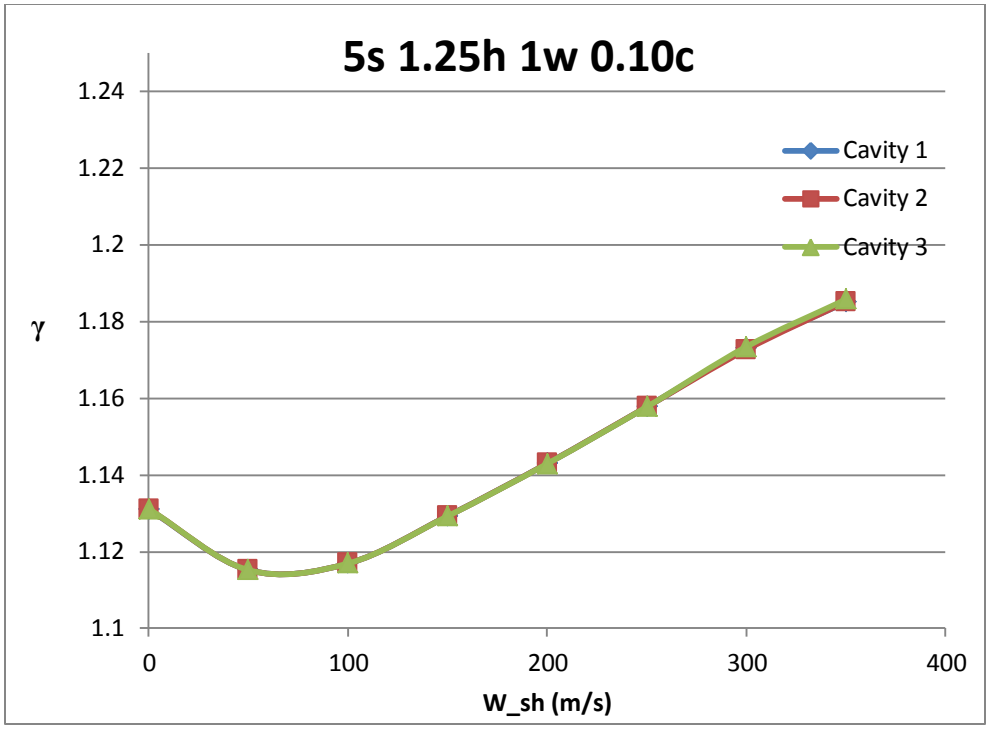
5s 1.25h 1w 0.10c
1.24
1.22
1.2
1.18
1.16
1.14
1.12
1.1
γ
0
100
200
300
400
W_sh (m/s)
Cavity 1
Cavity 2
Cavity 3

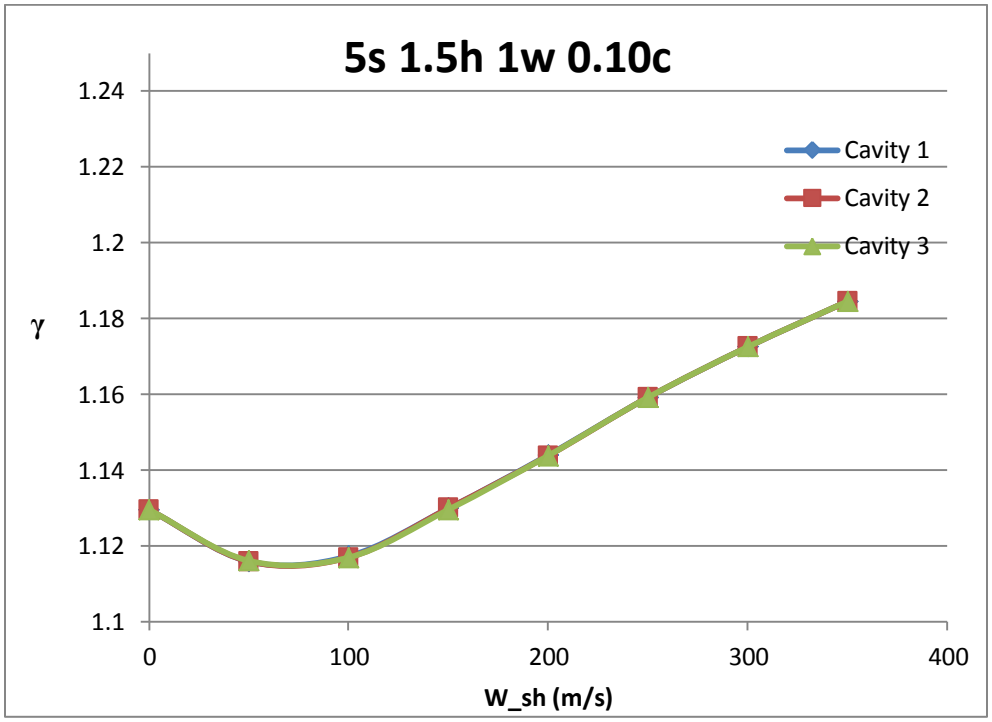
5s 1.5h 1w 0.10c
1.24
1.22
1.2
1.18
1.16
1.14
1.12
1.1
γ
0
100
200
300
400
W_sh (m/s)
Cavity 1
Cavity 2
Cavity 3

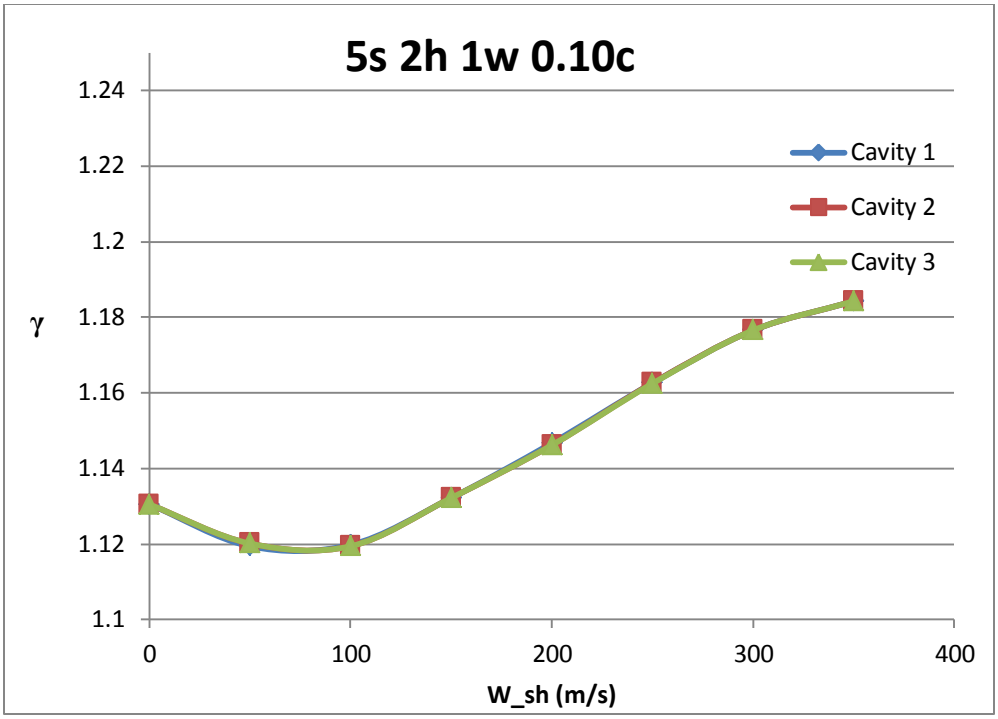

Figure 54. Effect of pitch-height ratio on γ on seal with tooth on stator with water.

APPENDIX E

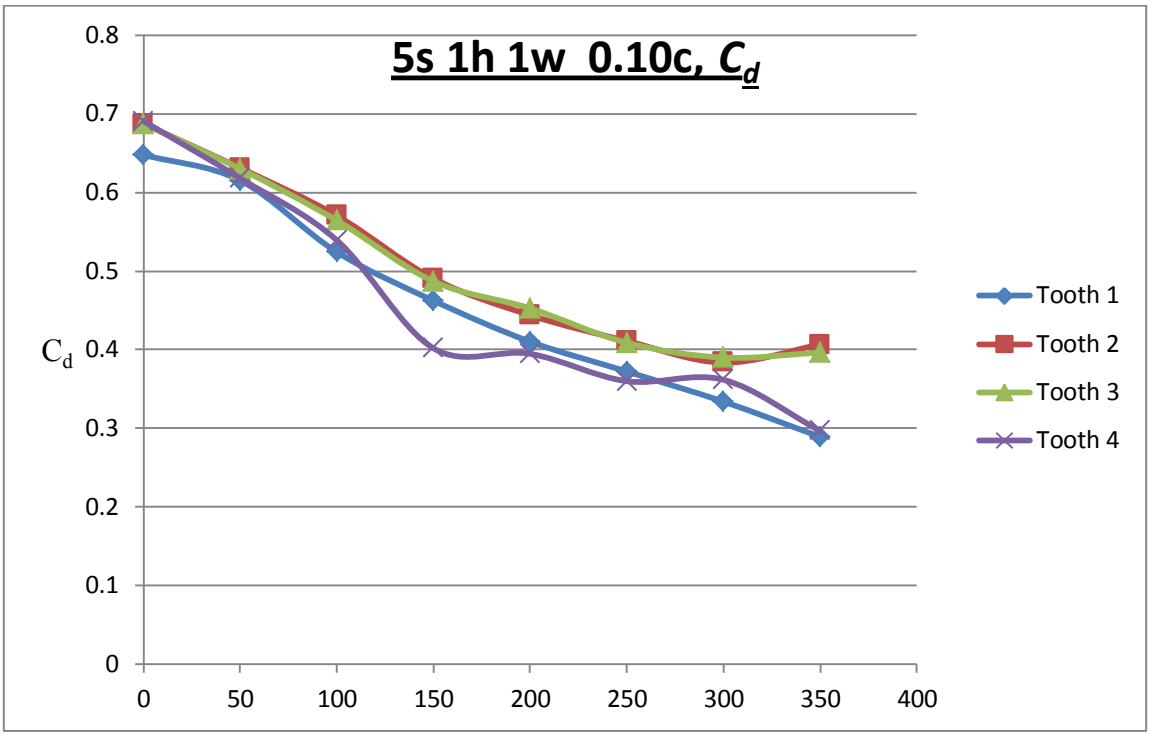
5s 1h 1w 0.10c, C_d
C_d
0.8
0.7
0.6
0.5
0.4
0.3
0.2
0.1
0
0
50
100
150
200
250
300
350
400
Tooth 1
Tooth 2
Tooth 3
Tooth 4

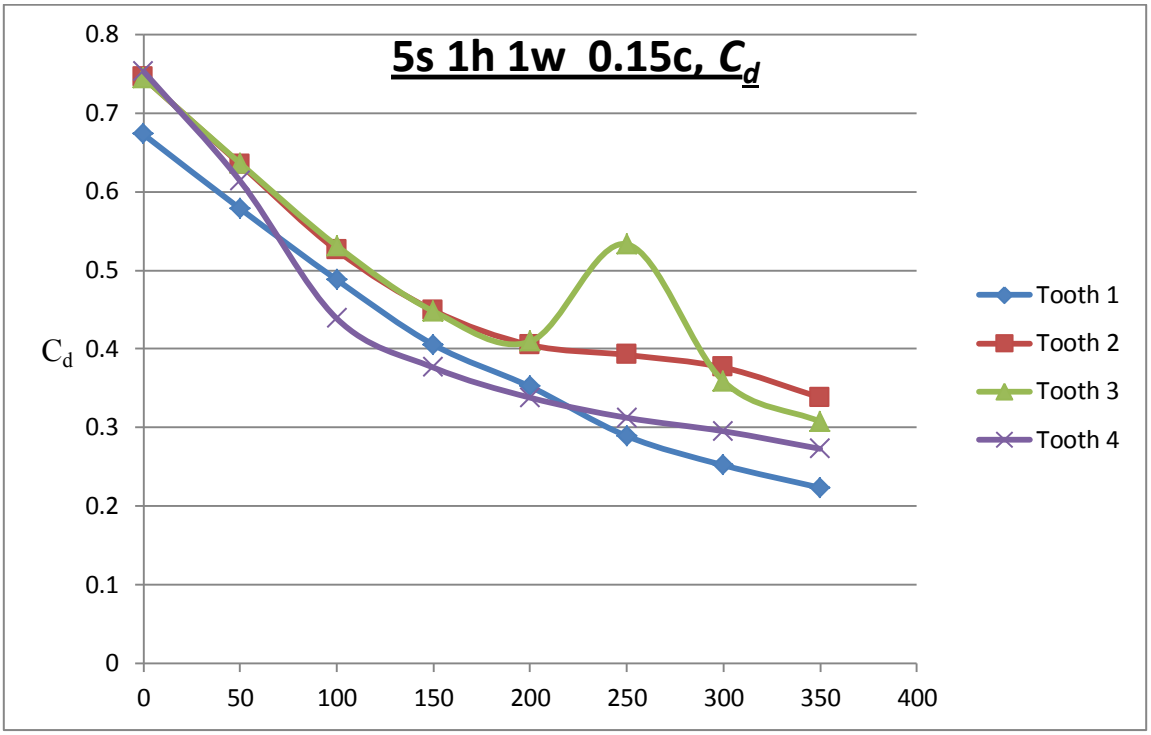
5s 1h 1w 0.15c, C_d
C_d
0.8
0.7
0.6
0.5
0.4
0.3
0.2
0.1
0
0
50
100
150
200
250
300
350
400
Tooth 1
Tooth 2
Tooth 3
Tooth 4

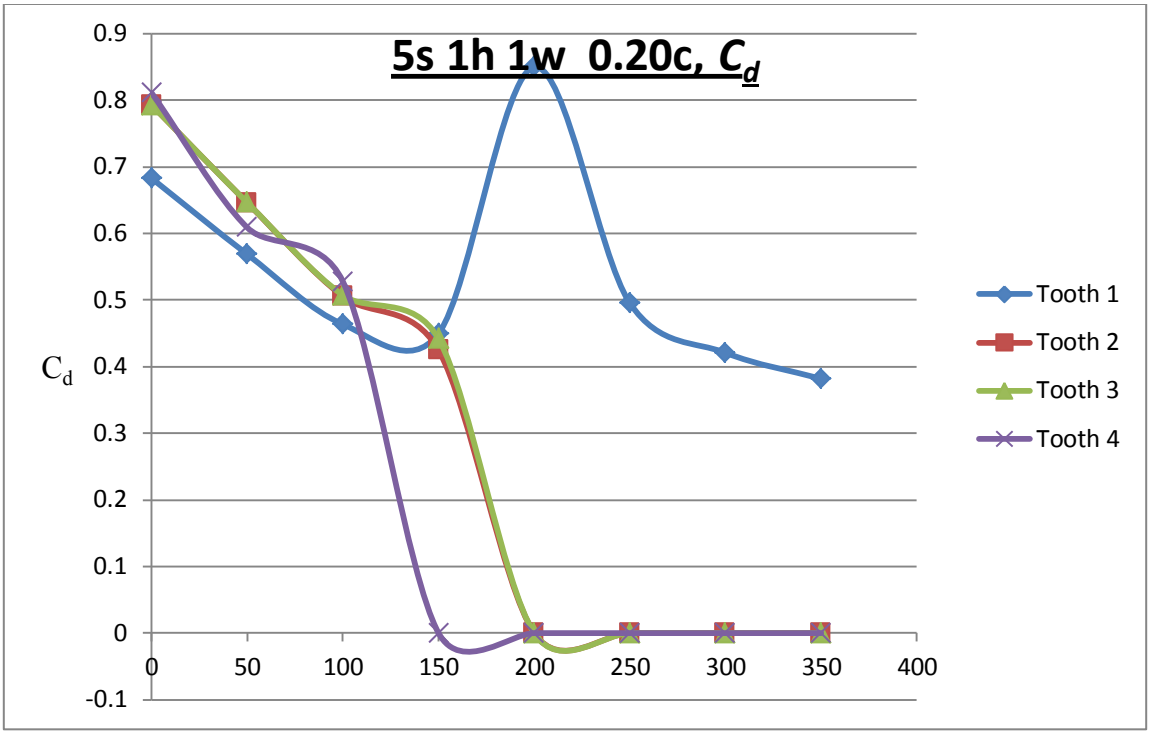
5s 1h 1w 0.20c, C_d
C_d
0.9
0.8
0.7
0.6
0.5
0.4
0.3
0.2
0.1
0
-0.1
0
50
100
150
200
250
300
350
400
Tooth 1
Tooth 2
Tooth 3
Tooth 4

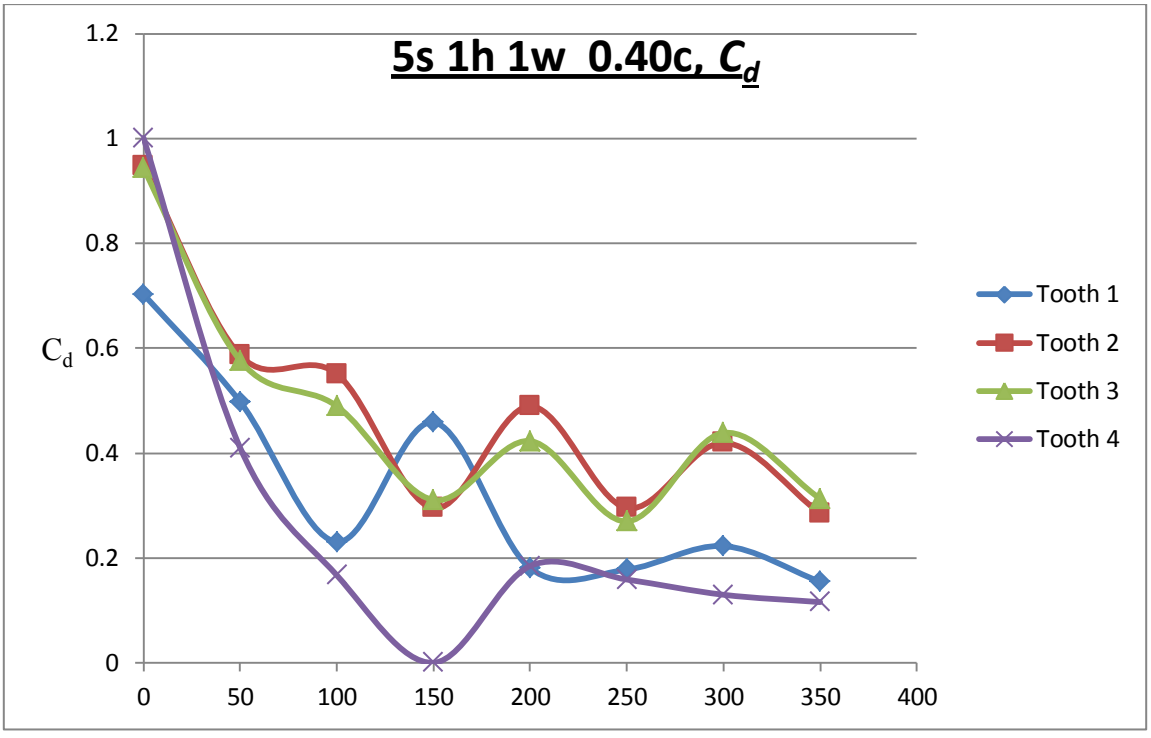
5s 1h 1w 0.40c, C_d
C_d
1.2
1
0.8
0.6
0.4
0.2
0
0
50
100
150
200
250
300
350
400
Tooth 1
Tooth 2
Tooth 3
Tooth 4

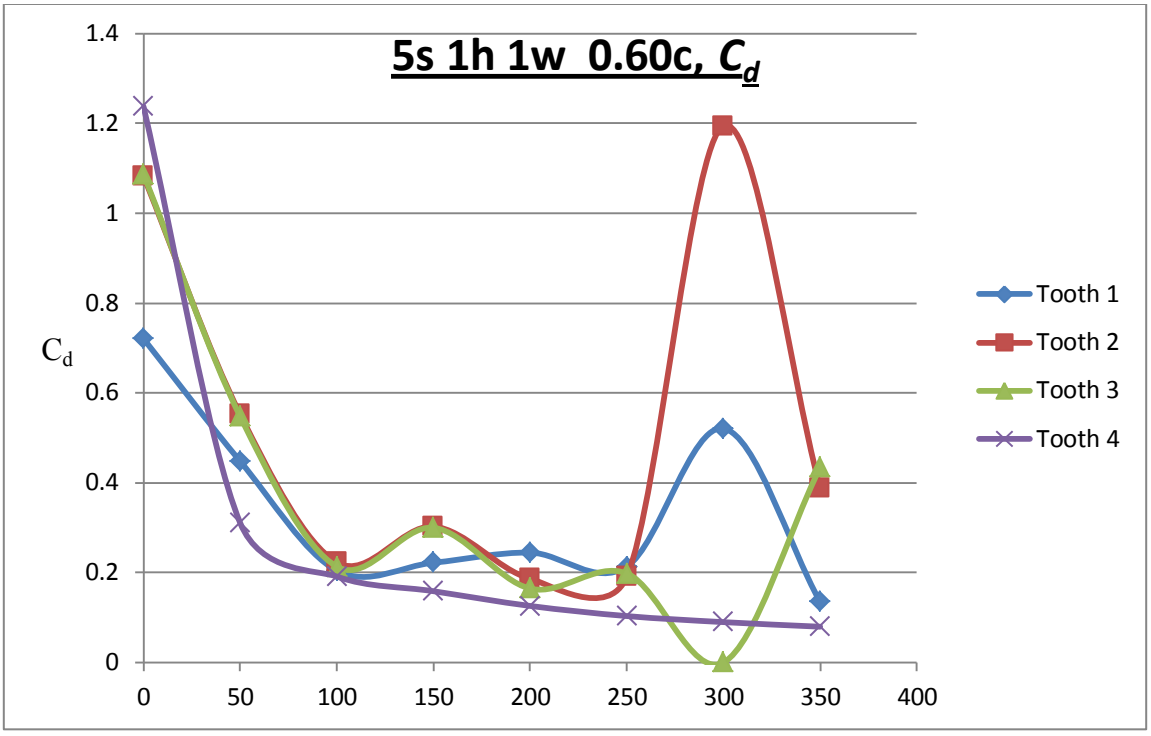
5s 1h 1w 0.60c, C_d
C_d
1.4
1.2
1
0.8
0.6
0.4
0.2
0
0
50
100
150
200
250
300
350
400
Tooth 1
Tooth 2
Tooth 3
Tooth 4

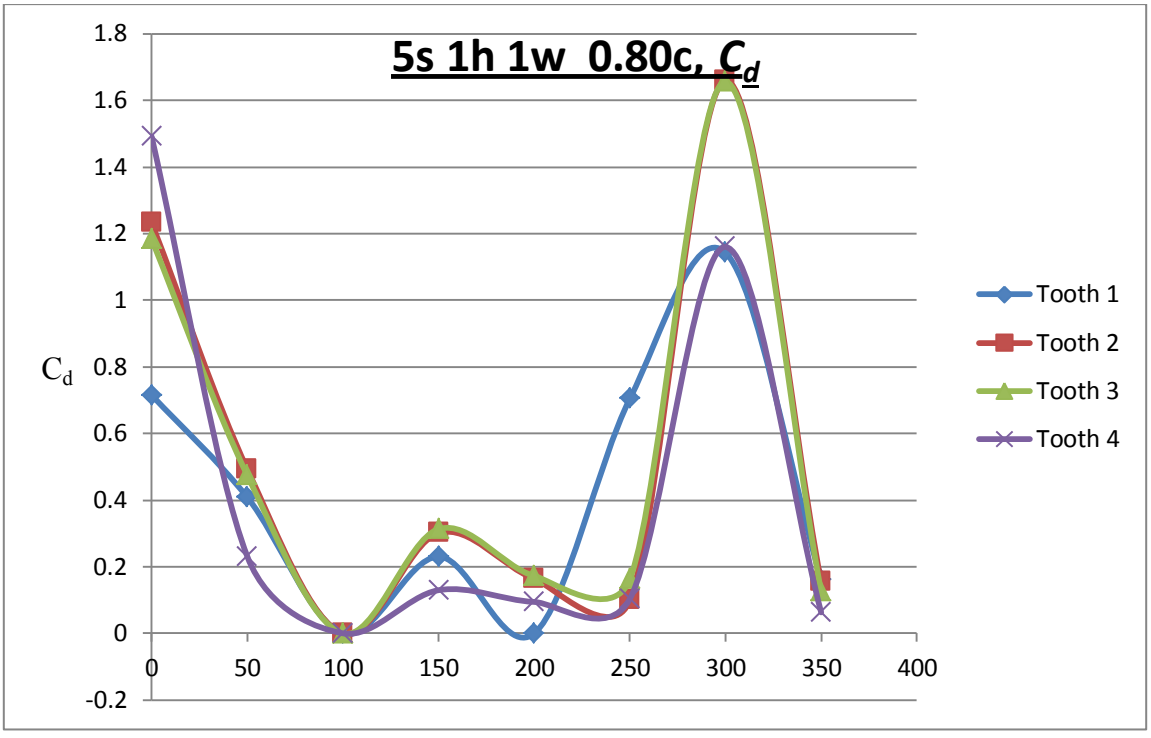
5s 1h 1w 0.80c, C_d
C_d
1.8
1.6
1.4
1.2
1
0.8
0.6
0.4
0.2
0
-0.2
0
50
100
150
200
250
300
350
400
Tooth 1
Tooth 2
Tooth 3
Tooth 4

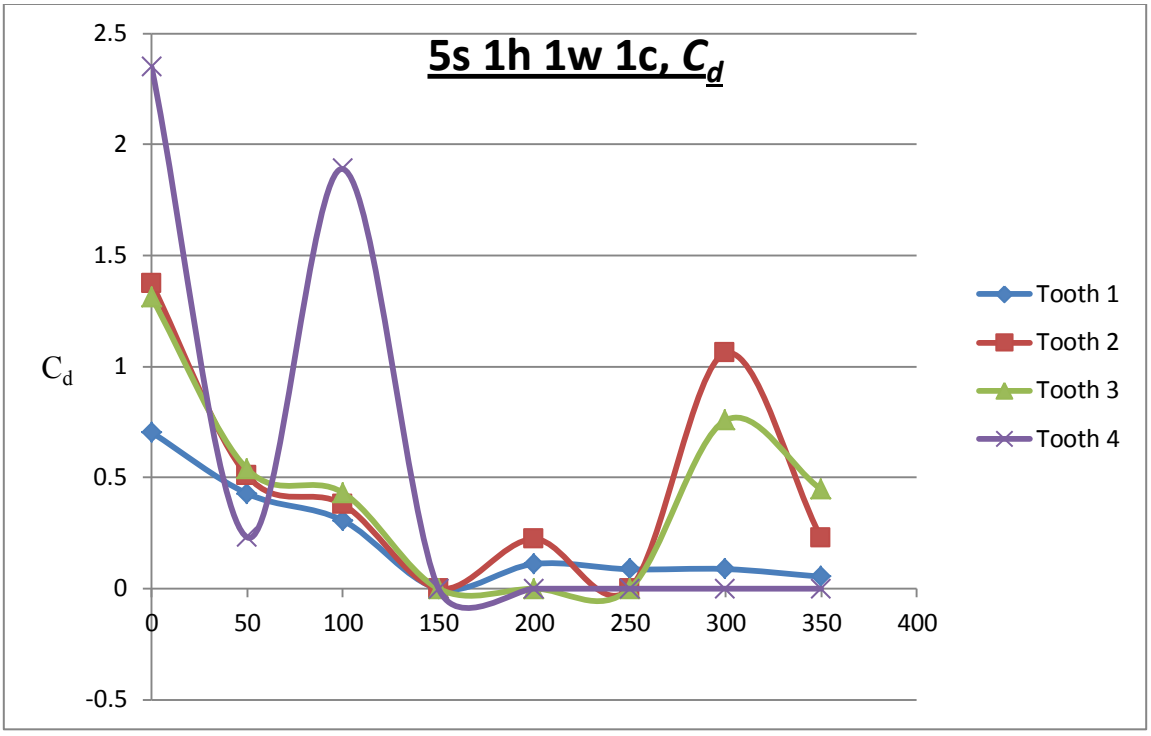

Figure 55. Effect of clearance on C_d on seal with tooth on stator with water.

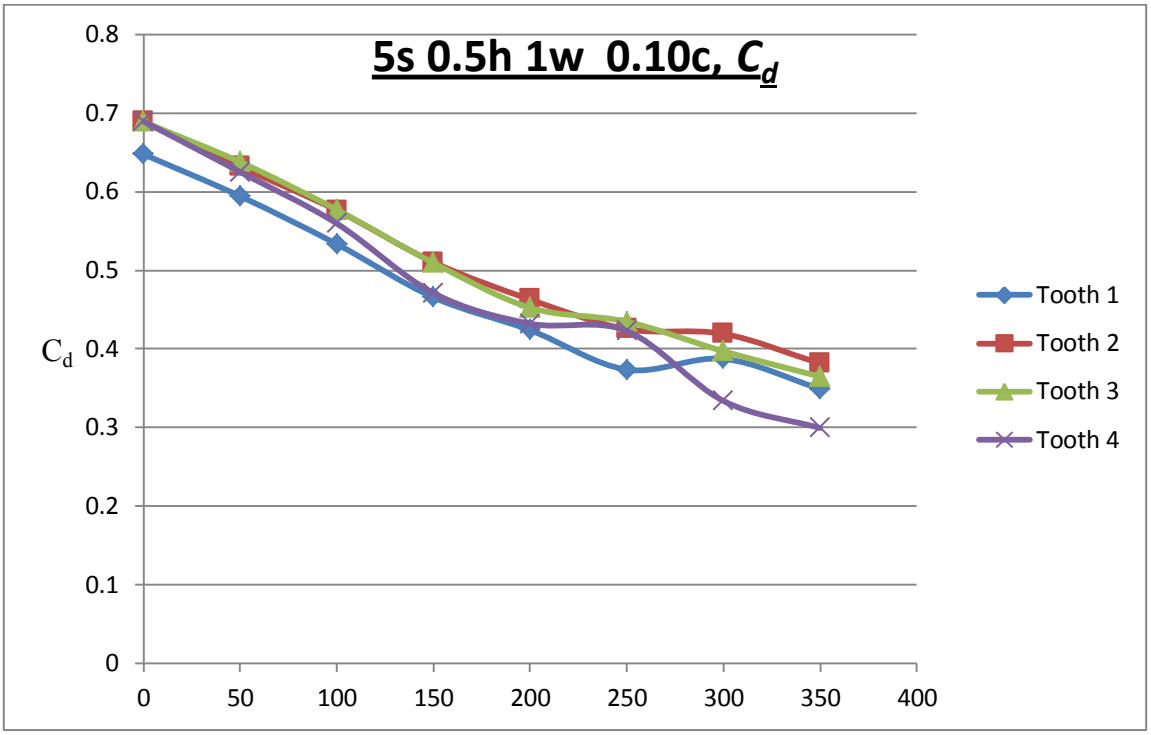

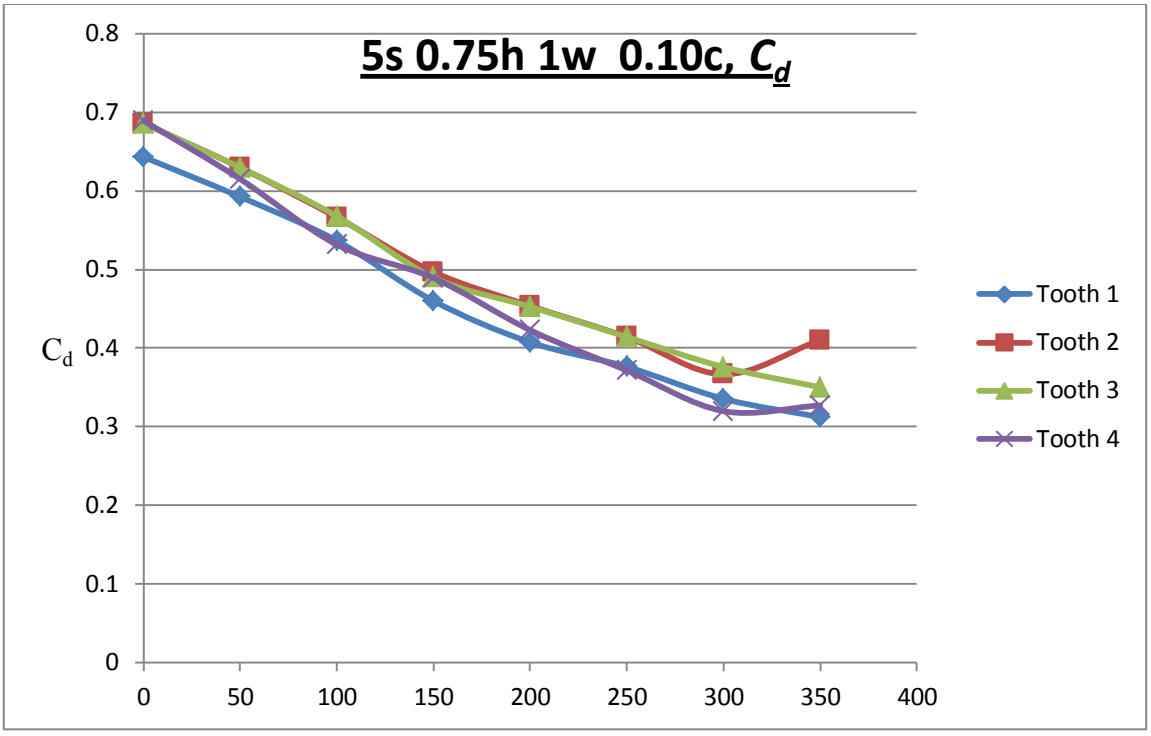
5s 0.75h 1w 0.10c, C_d
C_d
0.8
0.7
0.6
0.5
0.4
0.3
0.2
0.1
0
0
50
100
150
200
250
300
350
400
Tooth 1
Tooth 2
Tooth 3
Tooth 4

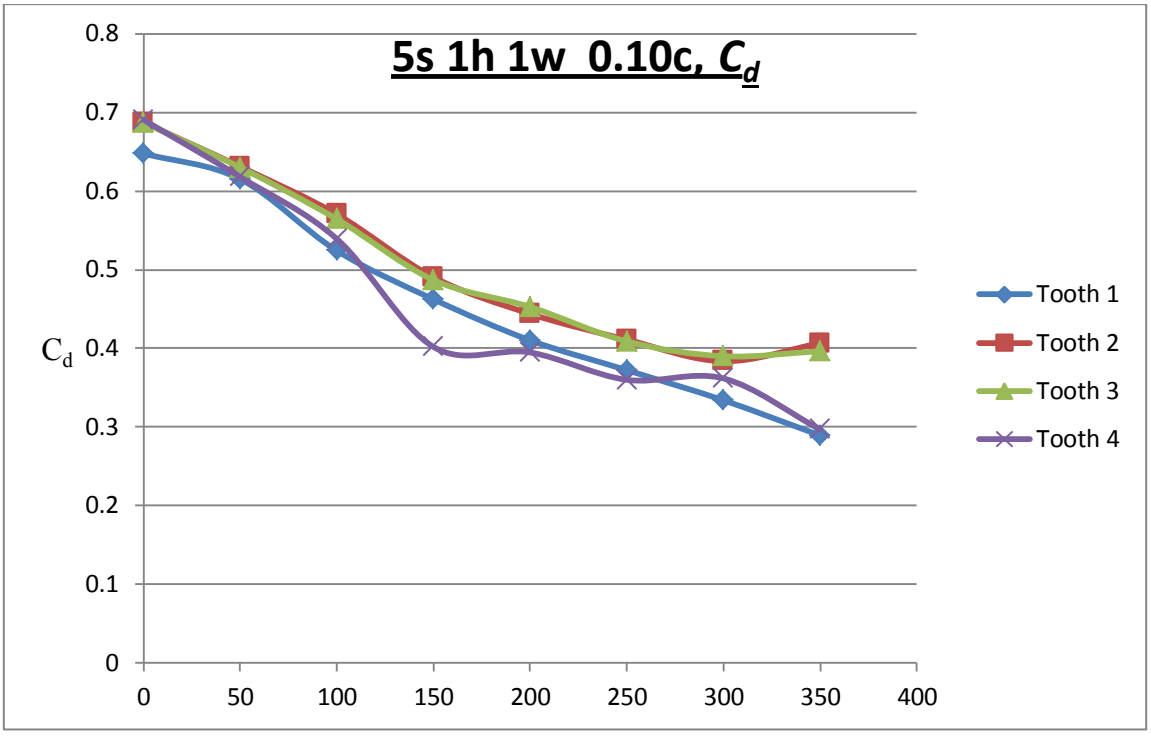
5s 1h 1w 0.10c, C_d
C_d
0.8
0.7
0.6
0.5
0.4
0.3
0.2
0.1
0
0
50
100
150
200
250
300
350
400
Tooth 1
Tooth 2
Tooth 3
Tooth 4

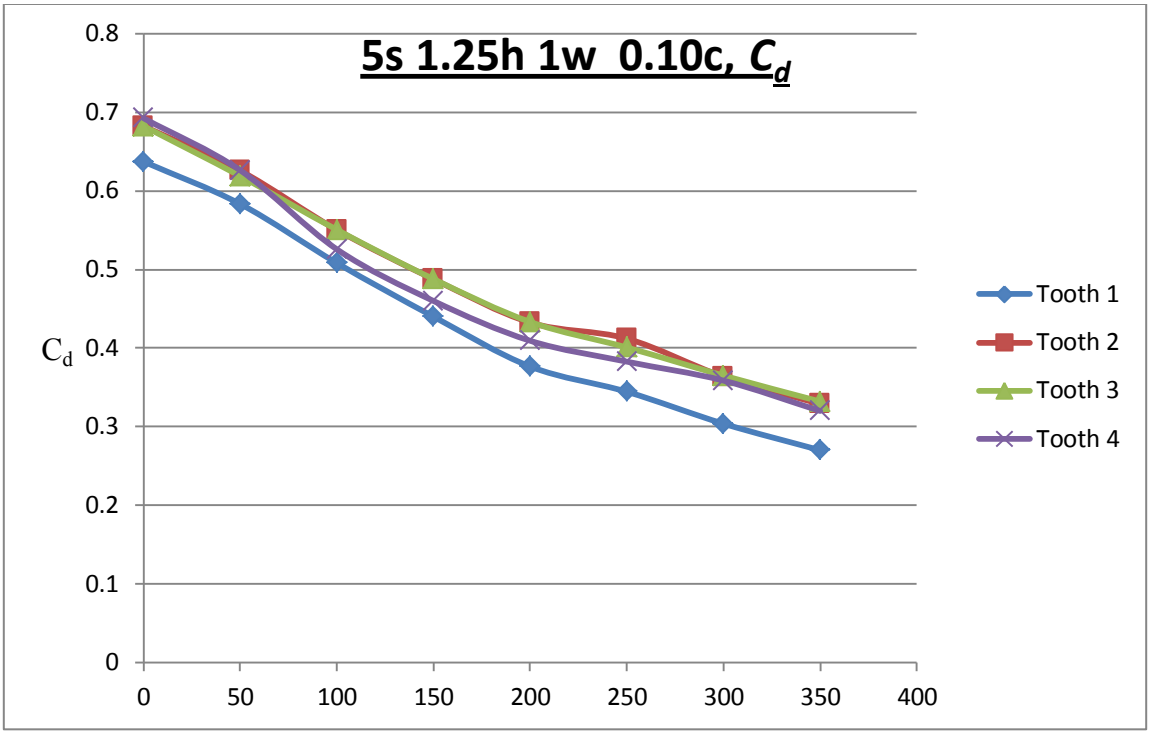
5s 1.25h 1w 0.10c, C_d
C_d
0.8
0.7
0.6
0.5
0.4
0.3
0.2
0.1
0
0
50
100
150
200
250
300
350
400
Tooth 1
Tooth 2
Tooth 3
Tooth 4

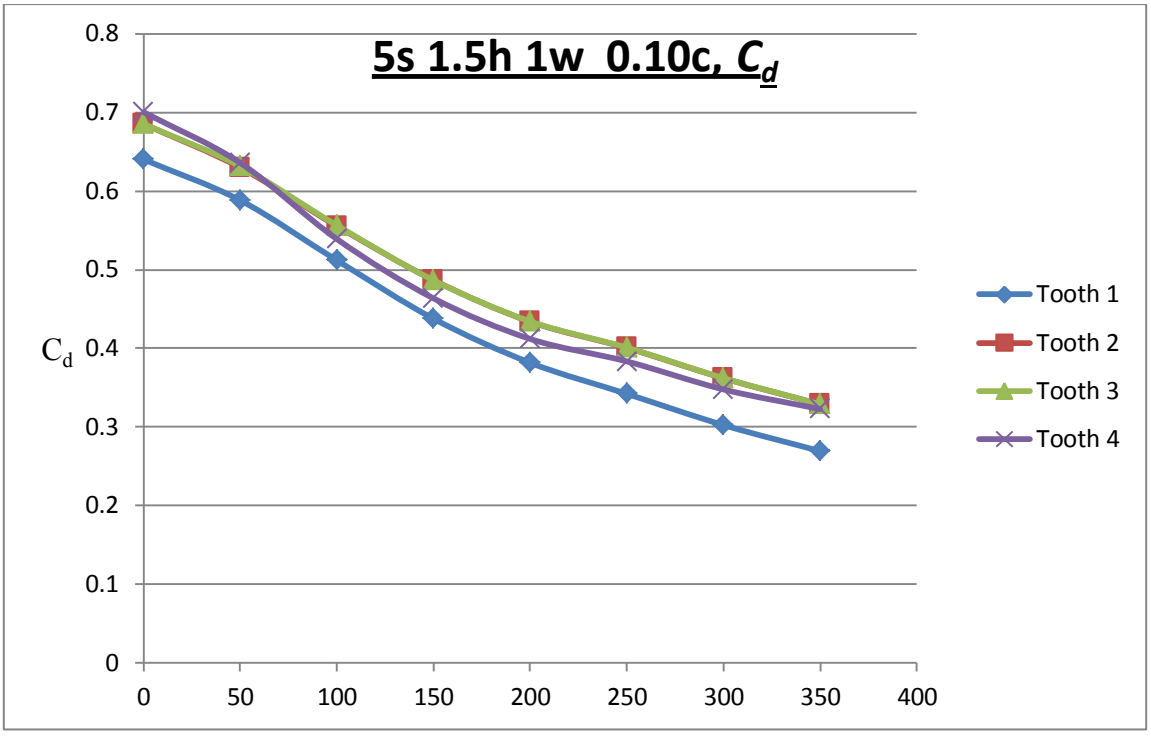
5s 1.5h 1w 0.10c, C_d
C_d
0.8
0.7
0.6
0.5
0.4
0.3
0.2
0.1
0
0
50
100
150
200
250
300
350
400
Tooth 1
Tooth 2
Tooth 3
Tooth 4

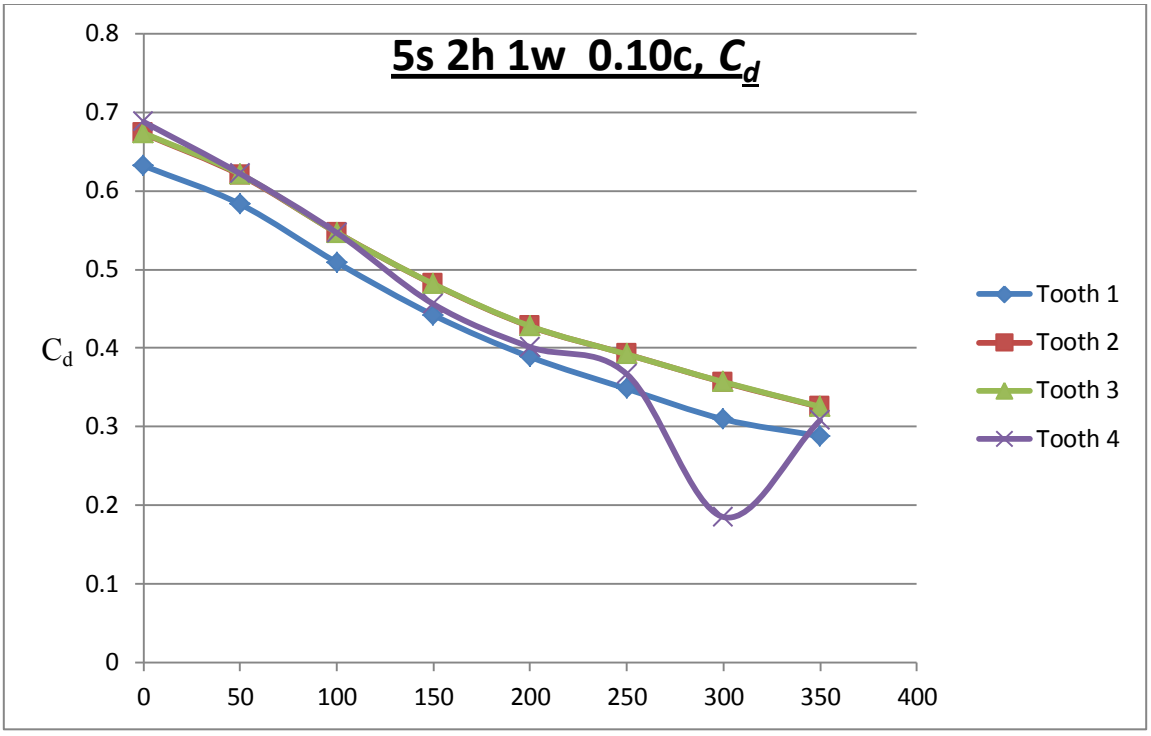

Figure 56. Effect of pitch-height ratio on C_d with tooth on stator for a seal with water.

APPENDIX F

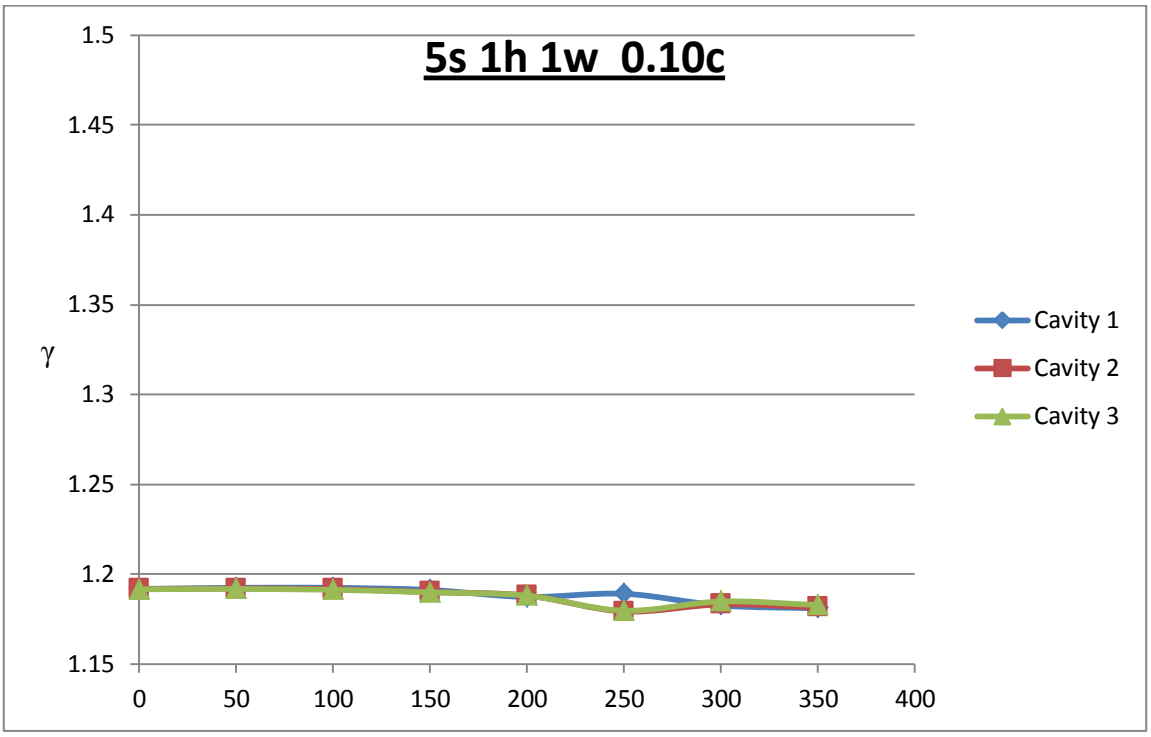
5s 1h 1w 0.10c
1.5
1.45
1.4
1.35
γ
1.3
1.25
1.2
1.15
0
50
100
150
200
250
300
350
400
Cavity 1
Cavity 2
Cavity 3

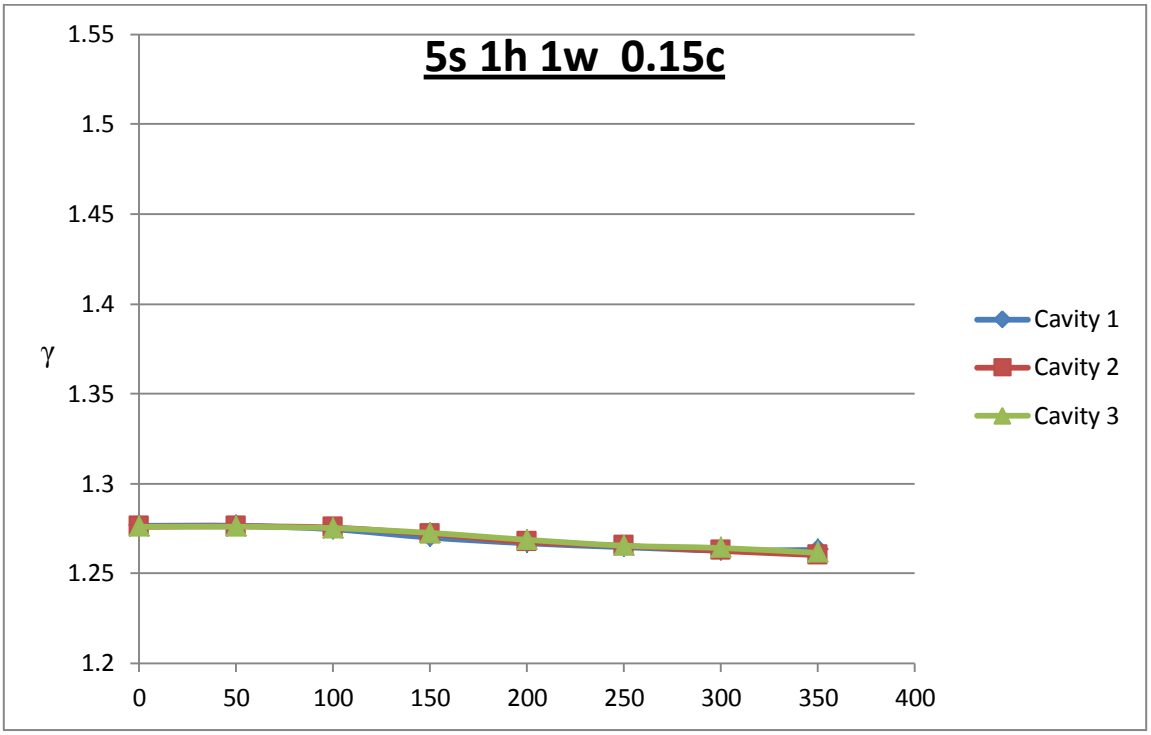
5s 1h 1w 0.15c
1.55
1.5
1.45
1.4
γ
1.35
1.3
1.25
1.2
0
50
100
150
200
250
300
350
400
Cavity 1
Cavity 2
Cavity 3

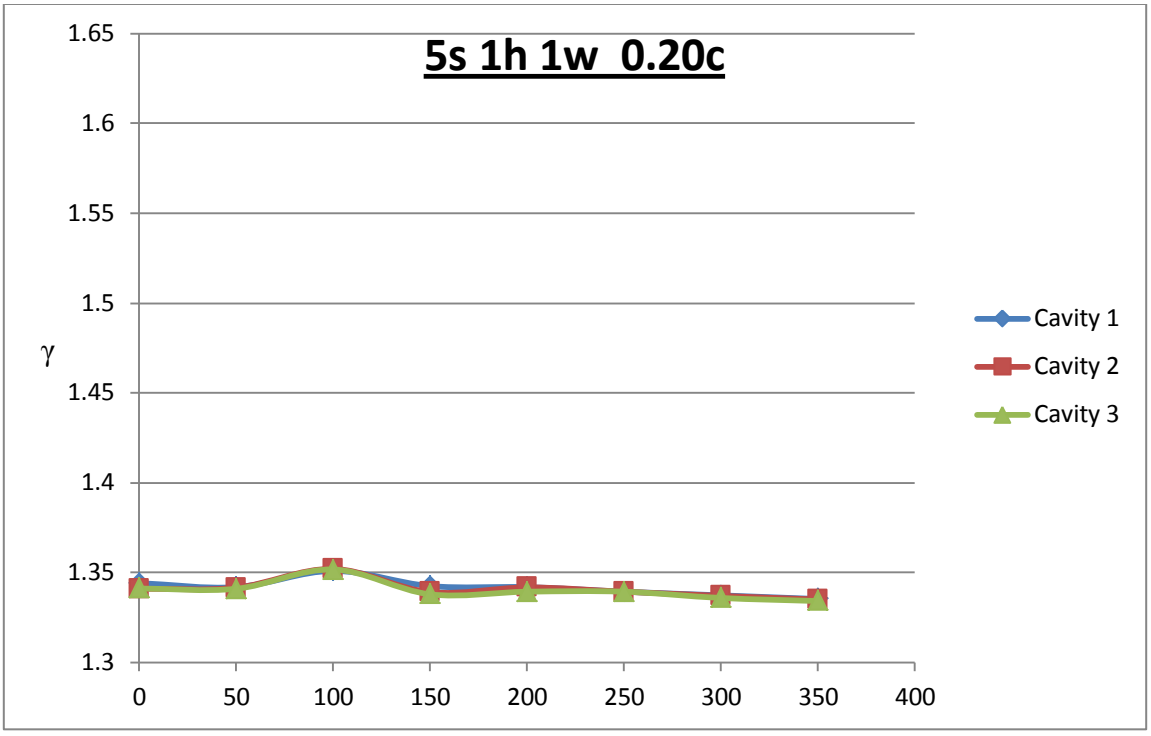
5s 1h 1w 0.20c
γ
1.65
1.6
1.55
1.5
1.45
1.4
1.35
1.3
0
50
100
150
200
250
300
350
400
Cavity 1
Cavity 2
Cavity 3

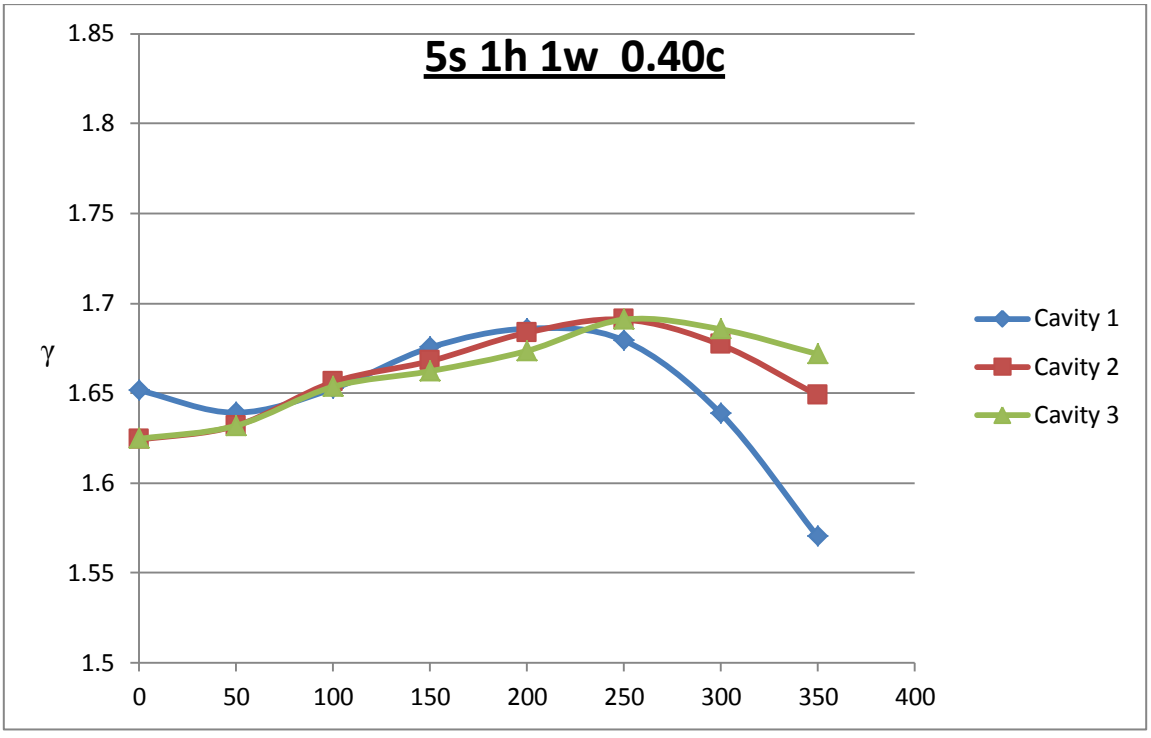
5s 1h 1w 0.40c
γ
1.85
1.8
1.75
1.7
1.65
1.6
1.55
1.5
0
50
100
150
200
250
300
350
400
Cavity 1
Cavity 2
Cavity 3

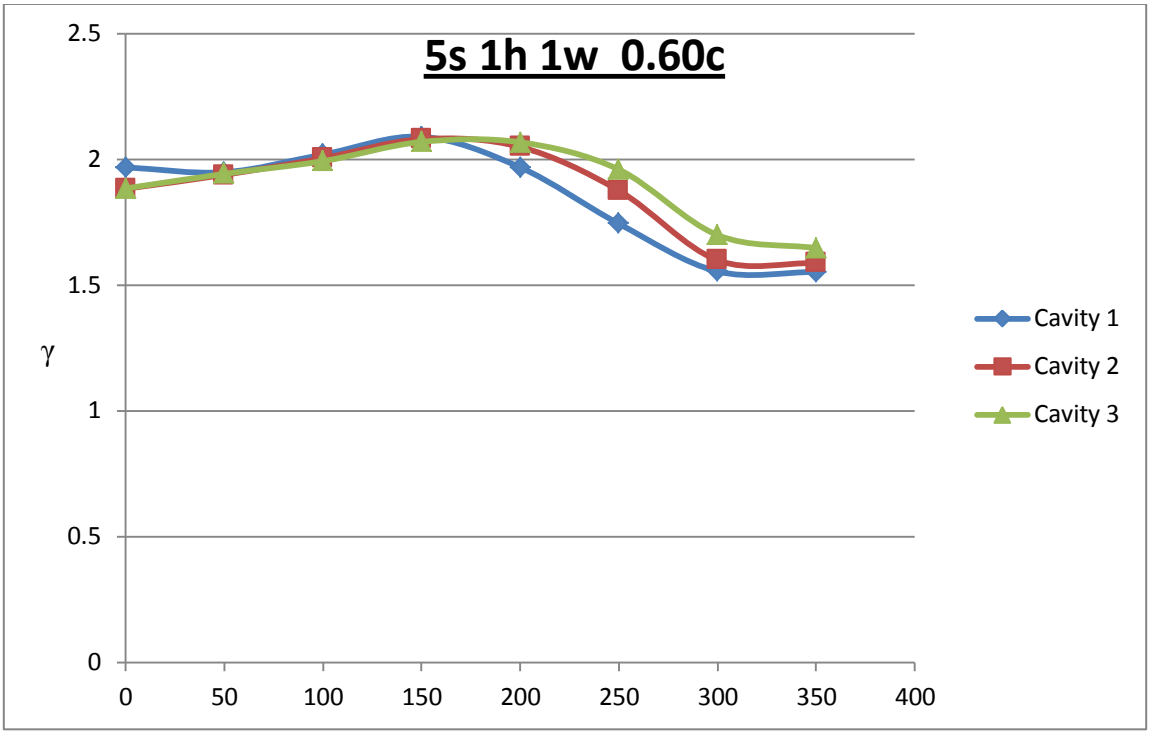
5s 1h 1w 0.60c
2.5
2
1.5
1
0.5
0
γ
0
50
100
150
200
250
300
350
400
Cavity 1
Cavity 2
Cavity 3

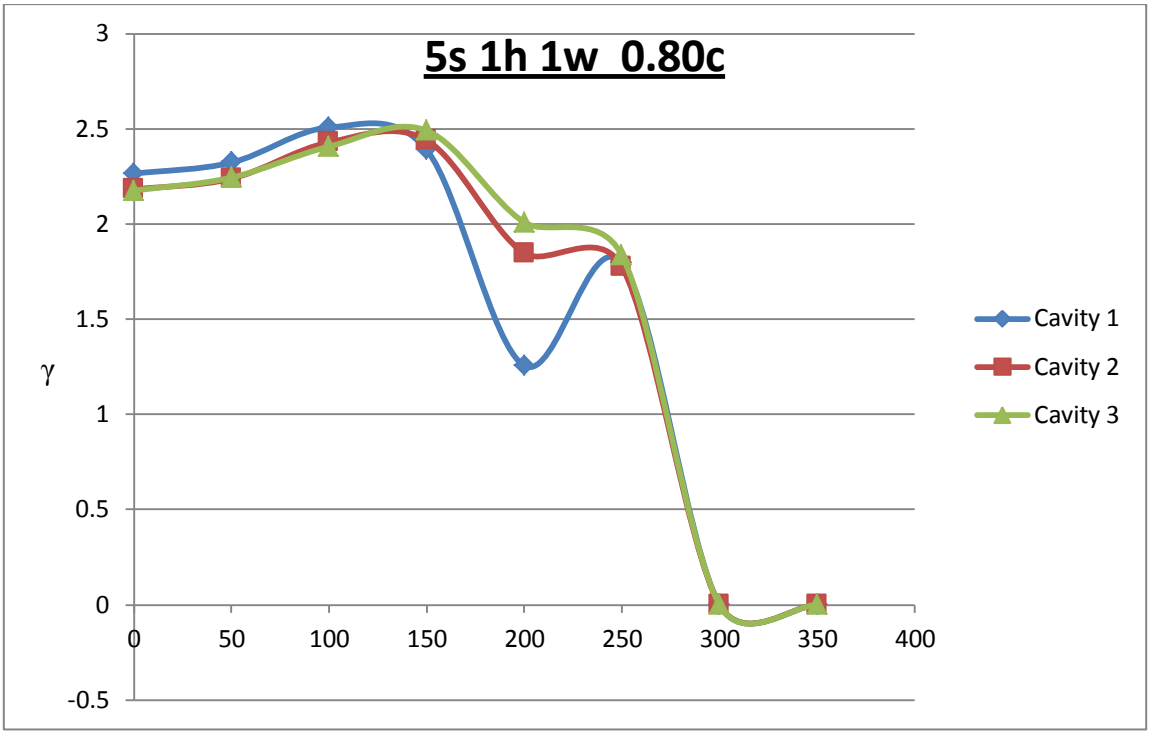
5s 1h 1w 0.80c
3
2.5
2
1.5
1
0.5
0
-0.5
γ
0
50
100
150
200
250
300
350
400
Cavity 1
Cavity 2
Cavity 3

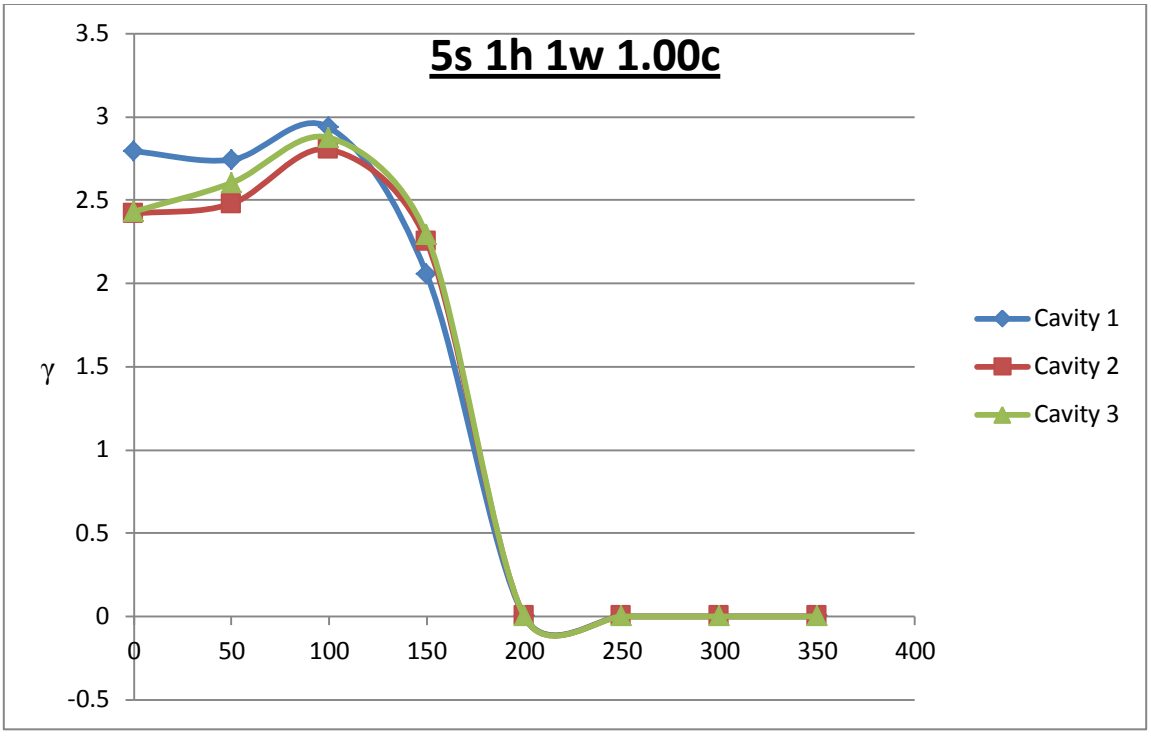

Figure 57. Effect of clearance on γ on seal with teeth on rotor with air.

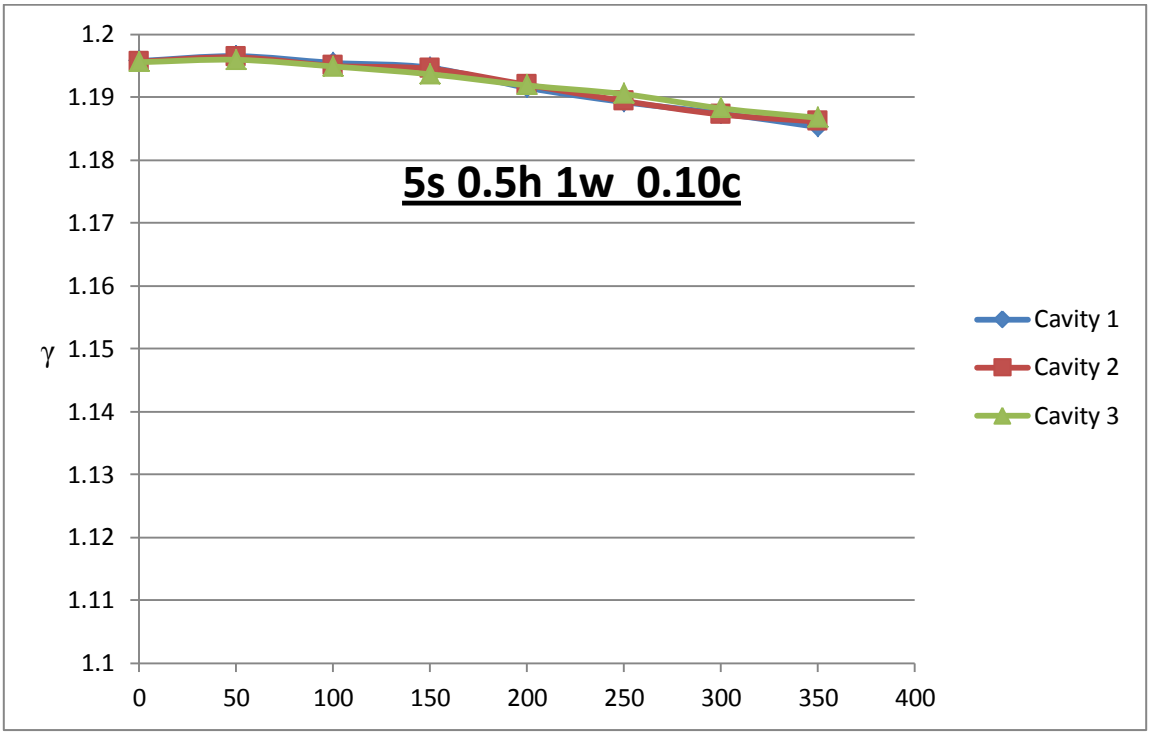

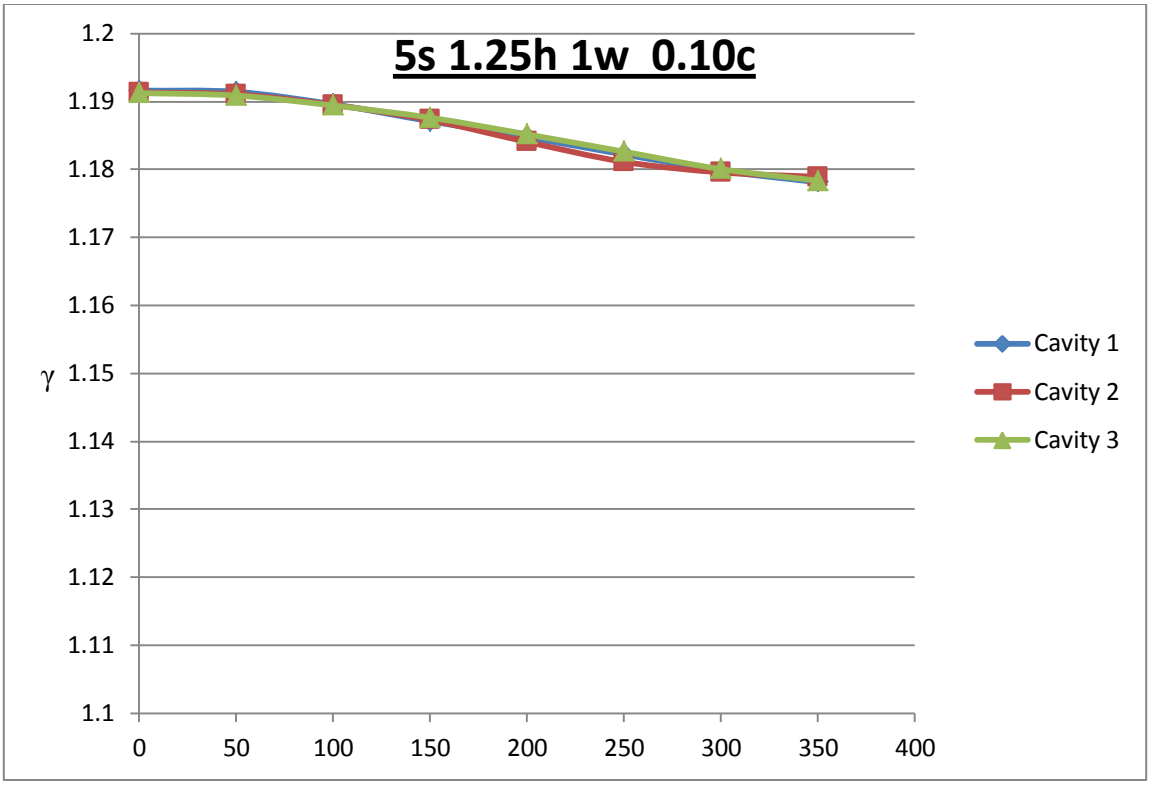

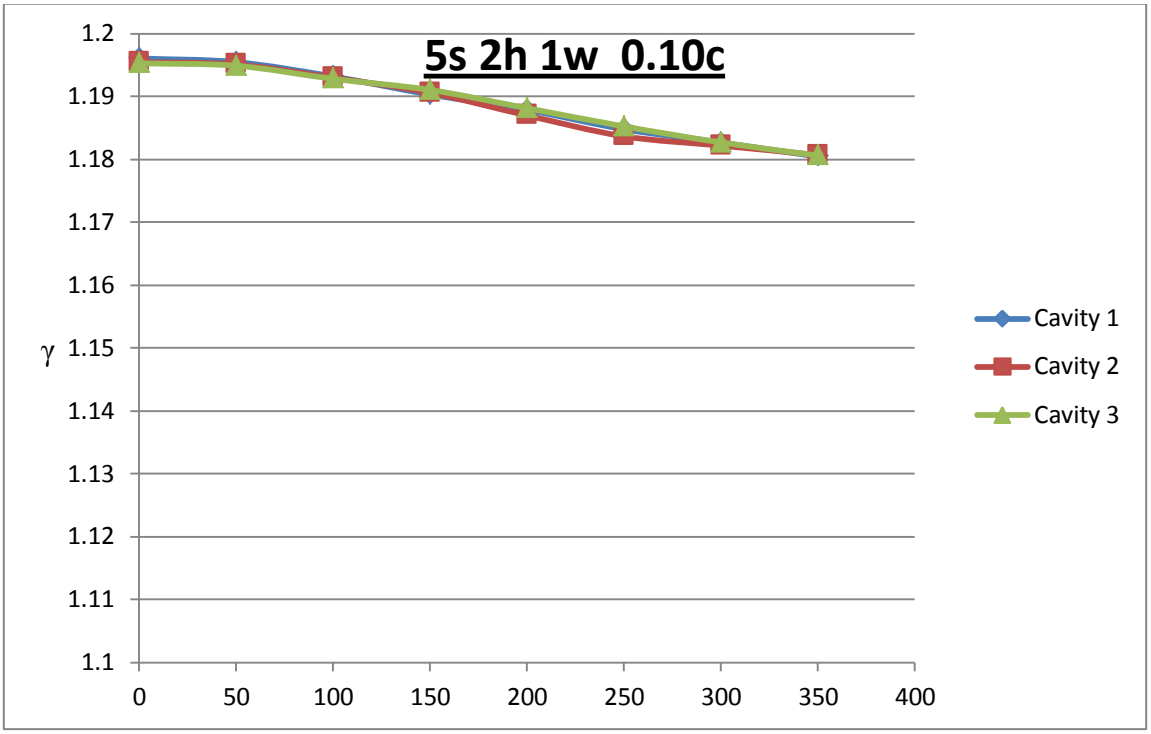

Figure 58. Effect of pitch-height ratio on γ on seal with teeth on rotor with air.

VITA

Vamshi Krishna Yamsani has received his Bachelor of Technology from the Indian Institute of Technology Guwahati in chemical engineering. He pursued graduate studies in mechanical engineering at Texas A&M University, College Station and graduated in August 2011 with a Master of Science degree. Previously, he interned at Max Planck Institute for Dynamics of Complex Technical Systems in Magdeburg, Germany and, also, at Hokkaido University in Sapporo, Japan.

Vamshi may be reached at yamsanis@gmail.com. His physical contact address is at the Department of Mechanical Engineering, 3123 TAMU, College Station, TX 77843-3123.